



Title Page

From Physics to AI: A Multidisciplinary Review of Contrail Prediction Models

Meiyin Zhu^a, Najeeb Ullah^a, Hongwei Deng^b, Shengnan Yang^{b,c}, Aman Ullah^a, Jiaqi Yin^a, Muhammad Owais Ghani^a, Tianxu Huang^a, Liuyong Chang^{a}*

^a International Innovation Institute, Beihang University, Hangzhou 311115, China

^b AECC Shenyang Engine Research Institute, Shenyang 110015, China

^c Institute for Aero Engine, Tsinghua University, Beijing 100084, China

Declaration of competing interest

The authors declare that they have no known competing financial interests or personal relationships that could have appeared to influence the work reported in this paper.

Acknowledgments

This work was supported by the National Natural Science Foundation of China (52306208 & U2433215 & 52306184) and by Beijing Natural Science Foundation (3262018). This work was also supported by the National Key Lab of Aerospace Power System and Plasma Technology (Grant No.110329JC36025060002) and by the Research Start-up Funds of Hangzhou International Innovation Institute of Beihang University (Grant No. 2024KQ004).

Corresponding author

*Liuyong Chang (changliuyong@buaa.edu.cn)

During the peer review process, author Longfei Chen has officially taken up a full-time position at the National Natural Science Foundation of China (NSFC).



22 In accordance with the official regulations and conflict-of-interest policies for NSFC staff, he is not permitted to be listed as
23 an author on any academic papers during his term of service.

24 Therefore, we respectfully request to remove Longfei Chen from the author list in the revised version of this manuscript.

25 All other authors agree to this change, and the scientific content and conclusions of the paper remain unchanged.

26



27 From Physics to AI: A Multidisciplinary Review of Contrail 28 Prediction Models

29 Meiyin Zhu¹, Najeeb Ullah¹, Hongwei Deng², Shengnan Yang^{2,3}, Aman Ullah¹, Jiaqi Yin¹, Muhammad
30 Owais Ghani¹, Tianxu Huang¹, Liuyong Chan^{1*}

31 ¹ International Innovation Institute, Beihang University, Hangzhou 311115, China

32 ² AECC Shenyang Engine Research Institute, Shenyang 110015, China

33 ³ Institute for Aero Engine, Tsinghua University, Beijing 100084, China

34

35 *Correspondence to:* Liuyong Chang (changliuyong@buaa.edu.cn)

36 **Abstract:** Aviation-induced condensation trails (contrails) and contrail cirrus represent a dominant yet uncertain component
37 of effective radiative forcing (ERF), potentially exceeding the warming impact of accumulated carbon dioxide. As the aviation
38 sector targets climate-optimal operations by 2030, the demand for scalable, real-time contrail forecasting has driven a
39 fundamental paradigm shift in modeling strategies. This review provides a comprehensive analysis of contrail prediction
40 methodologies spanning eight decades, classifying the evolution into five distinct epochs: (1) Thermodynamic and Analytical
41 Foundations (1940s–1990s), rooted in the Schmidt-Appleman Criterion (SAC) for binary formation thresholds; (2)
42 Microphysical Simulation (1990s–2010s), exemplified by the Contrail Cirrus Prediction (CoCiP) and APCEMM models,
43 which resolve complex particle dynamics and lifecycle evolution; (3) NWP-Integrated Frameworks (2000s–Present), such as
44 ECMWF IFS and WRF-Chem, which embed contrail parameterizations into global weather systems; (4) Satellite-Empirical
45 Models, leveraging AVHRR, MODIS, and CALIOP data to establish climatological baselines and validate physical
46 assumptions; and (5) AI-Driven and Hybrid Frontiers (2020–2026), where deep learning architectures, including U-Net
47 segmentation, Physics-Informed Neural Networks (PINNs), and the Google-DLR hybrid system, are revolutionizing real-time
48 detection and flight attribution. By critically evaluating the trade-offs between physical interpretability and computational
49 scalability, this paper identifies the emerging consensus that future operational systems must adopt hybrid architectures—
50 merging the robust constraints of first-principles physics with the adaptive precision of artificial intelligence—to enable
51 verifiable contrail avoidance and sustainable flight planning.

52 1 Introduction

53 Aviation has become an increasingly important focus in climate policy due to its growing share of global greenhouse gas
54 emissions and high-altitude impacts. Organizations such as the International Civil Aviation Organization (ICAO), The
55 Intergovernmental Panel on Climate Change (IPCC), the European Union Aviation Safety Agency (EASA) and national bodies
56 like National Aeronautics and Space Administration (NASA) ([Li et al., 2025](#)) and the U.S. Federal Aviation Administration
57 (FAA) ([Brasseur et al., 2016](#)) are actively engaged in monitoring, modeling, and mitigating aviation-induced climate effects.



58 In 2025, these agencies have taken concrete steps to address contrail-related warming: ICAO introduced contrail avoidance
 59 guidelines into its global environmental strategy; NASA and the FAA expanded operational trials of real-time flight rerouting
 60 algorithms targeting ice-supersaturated layers; and the EU’s Clean Aviation program launched funding initiatives for
 61 developing AI-based contrail forecasting tools aimed at integration by 2030. Aircraft emit a complex mixture of gases and
 62 particles—including Carbon Dioxide (CO₂), Water / Water Vapor (H₂O), Nitrogen Oxides (NO_x), Sulfur Oxides (SO_x),
 63 particulate matter (PM), and hydrocarbons (HC) ([Lee et al., 2009](#)).

64 **Table 1 List of Aviation Emissions, their source and effects on climate**

Emission	Source / Mechanism	Climate Effect	Residence Time	Altitude Sensitivity	Ref
CO ₂	Complete combustion of jet fuel	Long-term warming (GHG)	~100 years	Global (not altitude-dependent)	(Aamaas et al., 2025)
H ₂ O	Combustion product	Contrail & cirrus formation	Days to weeks	Strong effect at high altitudes	(Gaillot et al., 2023)
NO _x	High-temp combustion	Forms ozone (warming) & reduces CH ₄ (cooling) → net warming	Days to weeks	Amplified at high altitudes	(Lee et al., 2021)
SO _x	Sulfur in fuel	Sulfate aerosols (cooling)	Days	Moderate	(Lu et al., 2011)
PM	Incomplete combustion, soot	Ice nuclei for contrails, some warming	Days	High at cruise altitude	(Whitby, 1977)
H ₂ Cs	Incomplete combustion	Minor ozone formation	Hours to days	Minor at high altitude	(Oh, 2020)
CO	Incomplete combustion	Minor indirect effect	Weeks	Mostly low-altitude	(Ning et al., 2024)
N ₂ O	Trace from combustion	Strong long-lived GHG	~120 years	Global	(Filonchik et al., 2024)
Short Contrails	H ₂ O vapor condensing on soot	Short-lived warming	Minutes to <1 hour	Requires cold/moist conditions	(Kärcher et al., 2015)
Persistent Contrails	Sustained formation under specific conditions	Net warming (trap IR, reflect sun)	Hours to day(s)	Strong high-altitude dependency	(Schumann et al., 2017)
Contrail Cirrus Clouds	Spread & evolution of persistent contrails	Significant net warming	Hours to days	Only at cruise altitude	(Minnis et al., 2004)
Chemions	Ion emission from hot exhaust	Enhance aerosol nucleation, may affect contrail microphysics	Seconds to minutes	High at cruise altitude	(Yu and Turco, 1997)
Volatile particles	Homogeneous nucleation of H ₂ SO ₄ -H ₂ O	Provide additional ice nuclei, influence contrail onset	Minutes to hours	Strong at high altitude	(Yu and Turco, 1998)
Organic compounds	Unburned hydrocarbons / lubricants	May coat soot, alter ice-nucleating efficiency	Hours to days	Cruise altitude	(Yu et al., 1999)

65 Each of these emissions influences the Earth’s climate through distinct physical mechanisms and atmospheric interactions.
 66 Their impact varies significantly depending on altitude, chemical reactivity, and residence time in the atmosphere([Lee et al., 2009](#);
 67 [Lee et al., 2021](#)). Table 1 provides a list of aviation emissions and their effects on climate, including their sources,
 68 climate mechanisms, and altitude sensitivities as shown Figure 1 which highlight the roles of different compounds in warming
 69 or cooling, and their interactions with cloud processes.

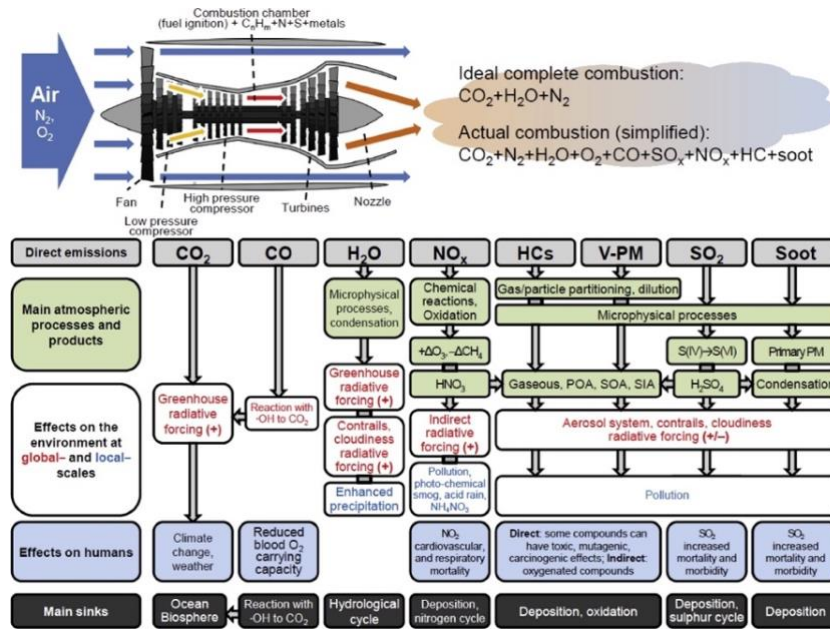


Figure 1 Complex mixture of gases and particles emits from aircraft turbofan engine (Lee et al., 2009)

A more quantitative picture of aviation’s climate impact is illustrated in Figure 2, showing effective radiative forcing (ERF) components from 1940 to 2018. Contrail cirrus (CC) dominates the non-CO₂ contribution with an estimated Radiative Forcing (RF) of 111.4 mW/m², exceeding that of CO₂ itself (34.3 mW/m²) (Lee et al., 2021).

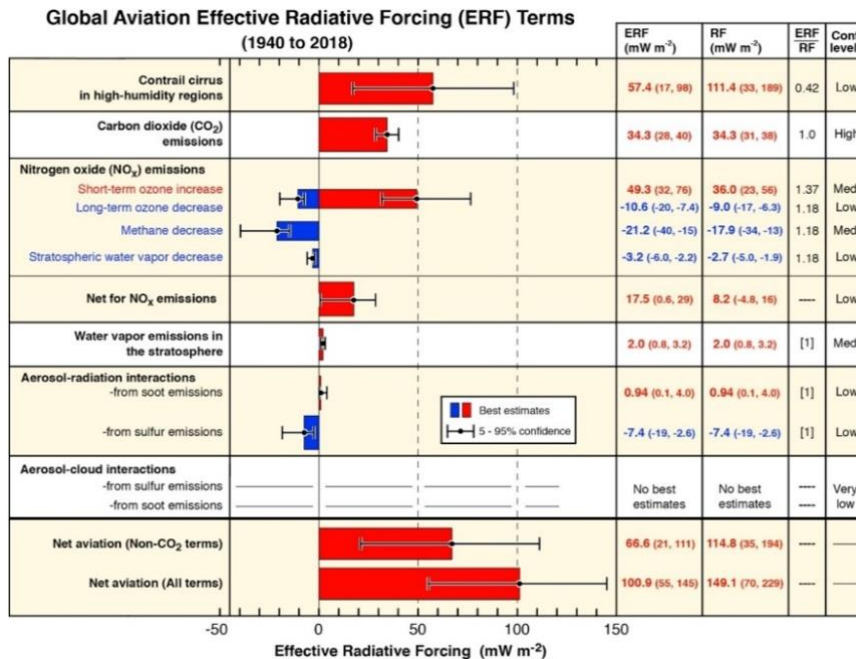
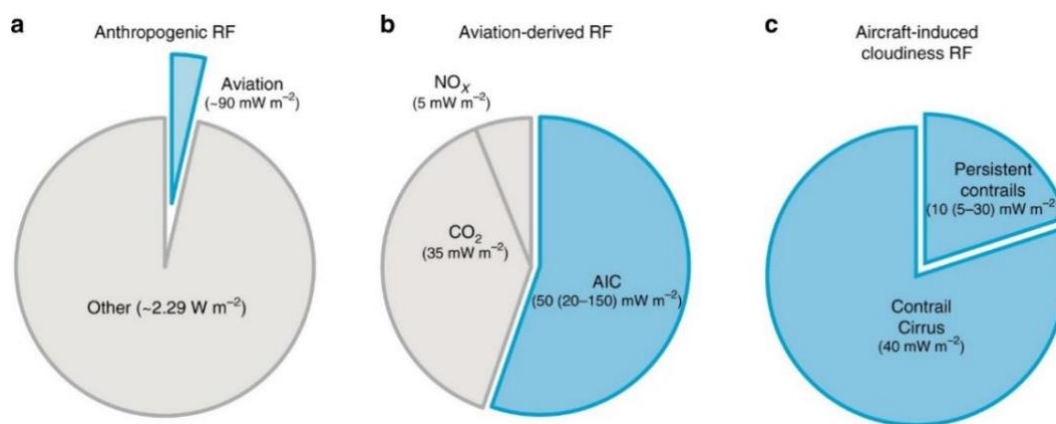


Figure 2 Global Aviation Effective Radiative Forcing (ERF) Terms (1940 to 2018) (Lee et al., 2021)



77 To contextualize aviation within global emissions, Figure 3a show that it contributes $\sim 90 \text{ mW/m}^2$ of the total $\sim 2.29 \text{ W/m}^2$
 78 anthropogenic RF. However, Figure 3b reveals that aircraft-induced cloudiness (AIC)—primarily persistent contrails and CC
 79 accounts for more than half of aviation’s total RF ($50\text{--}150 \text{ mW/m}^2$). A breakdown in Figure 3c shows that CC contributes ~ 40
 80 mW/m^2 , while persistent contrails add $\sim 10 \text{ mW/m}^2$, highlighting their disproportionate role in aviation-related climate effects
 81 ([Karcher, 2018](#)).



82
 83 **Figure 3 Aviation RF (a) Aviation's contribution to global RF in 2011 relative to pre-industrial times. (b) Forcing components**
 84 **within aviation, with AIC accounting for over half. (c) Breakdown of AIC RF into contrail cirrus and persistent contrails**
 85 **([Karcher, 2018](#)).**

86 The European airspace represents one of the most critical geographical focal points for contrail research due to its extreme
 87 traffic density. Data from EUROCONTROL indicates that the region sustained an average of approximately 28,000 flights per
 88 day throughout 2023, creating a near-constant saturation of aircraft within the upper troposphere. This high volume of traffic,
 89 as visualized in Figure 4, underscores the significant challenge of managing climate impacts. Europe serves as a primary "living
 90 laboratory" for validating advanced prediction models—ranging from thermodynamic criteria to AI-driven avoidance
 91 strategies as even minor tactical rerouting to avoid Ice supersaturated regions (ISSRs) ([Raumfahrt, 2023a](#)).



92
 93 **Figure 4 The airspace over Europe is one of the busiest. According to EUROCONTROL, there were an average of around 28,000**
 94 **flights per day in 2023 ([Raumfahrt, 2023b](#)).**



95 Contrails form when aircraft engines emit hot, moist exhaust into cold, supersaturated air at cruise altitudes, creating linear ice
96 clouds that may persist and spread, forming optically thin but radiatively significant ([Petzold et al., 2025](#)). These clouds trap
97 outgoing longwave radiation more effectively than they reflect incoming solar radiation, leading to a net warming effect,
98 particularly at night. Unlike CO₂, contrails exert a short-lived but intense radiative forcing, making their prediction and
99 mitigation a high-priority research area ([Singh et al., 2024](#)).

100 Over the decades, contrail modeling has evolved through five distinct categories, as depicted in Figure 5. The earliest are
101 thermodynamic or analytical models, based on the Schmidt–Appleman Criterion (SAC) developed in the 1940s–1950s
102 ([M.Bjormson, 1992](#); [Ernst 1941](#)), which assess whether atmospheric conditions favor contrail formation. These include plume
103 mixing models, Eulerian models, and threshold-based maps, including variants for alternative fuels. While computationally
104 efficient, these models offer only binary outputs and limited physical realism. Building on this, microphysical models emerged
105 in the 1980s and 1990s, simulating the lifecycle of ice particles nucleation, growth, sublimation, and deposition through tools
106 like Large Eddy Simulation (LES) models, the Unterstrasser-Gierens model, and Lagrangian cloud modules. The Contrail
107 cirrus prediction (CoCiP) model, developed by ([Schumann, 2012](#)), became widely used for its integration of microphysics
108 with global meteorological fields, offering more realistic simulations of contrail evolution and radiative effects. A more recent
109 advancement in this category is the Aviation Particle and Chemical Emissions Model (APCEMM), developed at Massachusetts
110 Institute of Technology (MIT), which provides plume-resolved simulations of gas-phase chemistry, aerosol dynamics, and
111 contrail ice formation. APCEMM models the near-field evolution of aircraft exhaust, capturing sub-grid chemical and
112 microphysical processes critical for accurate radiative forcing estimation ([Fritz et al., 2020](#)). As meteorological data and
113 computing resources advanced, Numerical Weather Prediction (NWP) integrated models developed during the 1990s and
114 2000s began embedding contrail parameterizations into operational weather forecasting systems. These include European
115 Centre Hamburg General Circulation Model (ECHAM) Series ([Stevens et al., 2013](#)), Global Forecast System (GFS) + SAC
116 ([M.Bjormson, 1992](#)), Series of Community Earth System Model (CESM) ([Hurrell et al., 2013](#)), Weather Research and Forecast
117 (WRF) and SAC ([Mazon and Pino, 2016](#)), and UK Met Office Unified Model (UKMO) contrail layers ([Zhang, 2025](#)), providing
118 global or mesoscale forecasts that consider vertical motion, wind shear, and humidity fields, though often limited by the
119 accuracy of upper-tropospheric humidity. Parallel to this, the rise of satellite-based models in the late 1990s and 2000s enabled
120 large-scale detection of contrails using sensors such as Advanced Very High Resolution Radiometer (AVHRR) ([Kalluri et al.,](#)
121 [2021](#)), Moderate Resolution Imaging Spectroradiometer (MODIS) ([Patrick Minnis, 2013](#)), Geostationary Operational
122 Environmental Satellite (GOES) ([Euchenhofer et al., 2025](#)), and Cloud-Aerosol Lidar with Orthogonal Polarization (CALIOP)
123 ([Winker et al., 2004](#)), employing techniques like split-window algorithms and optical thickness thresholds. Although excellent
124 for retrospective climatology and monitoring, these models are observational, not predictive and depend on overpass timing
125 and clear sky conditions. The most recent generation includes hybrid AI models, which integrate physical knowledge with
126 machine learning to deliver high-resolution, near-real-time predictions. Starting in the late 2010s, models such as Predictive
127 Real-time Emissions Technologies Reducing Aircraft Induced Lines in the Sky (PRE-TRAILS) ([Bock, 2024](#)), Global Aviation



128 emissions Inventory (GAIA) (Teoh et al., 2024a), and Convolutional Neural Network (CNN)-AVHRR have applied deep
 129 learning to satellite and meteorological data (Zhang et al., 2018). A major leap came in 2024, when Google AI, in collaboration
 130 with Breakthrough Energy and Deutsches Zentrum für Luft- und Raumfahrt (DLR) a German aerospace Center, released an
 131 enhanced hybrid contrail prediction system that combined CoCiP with satellite detection and aircraft routing algorithms,
 132 enabling real-time contrail avoidance strategy development (Zebediah Engberg, 2025). Additionally, Physics-Informed Neural
 133 Networks (PINNs), introduced in the early 2020s, such as those by (Raphael Alamu, 2025), embed thermodynamic constraints
 134 directly into neural architectures to ensure physically consistent predictions—offering a promising solution to the "black box"
 135 challenge in AI systems.

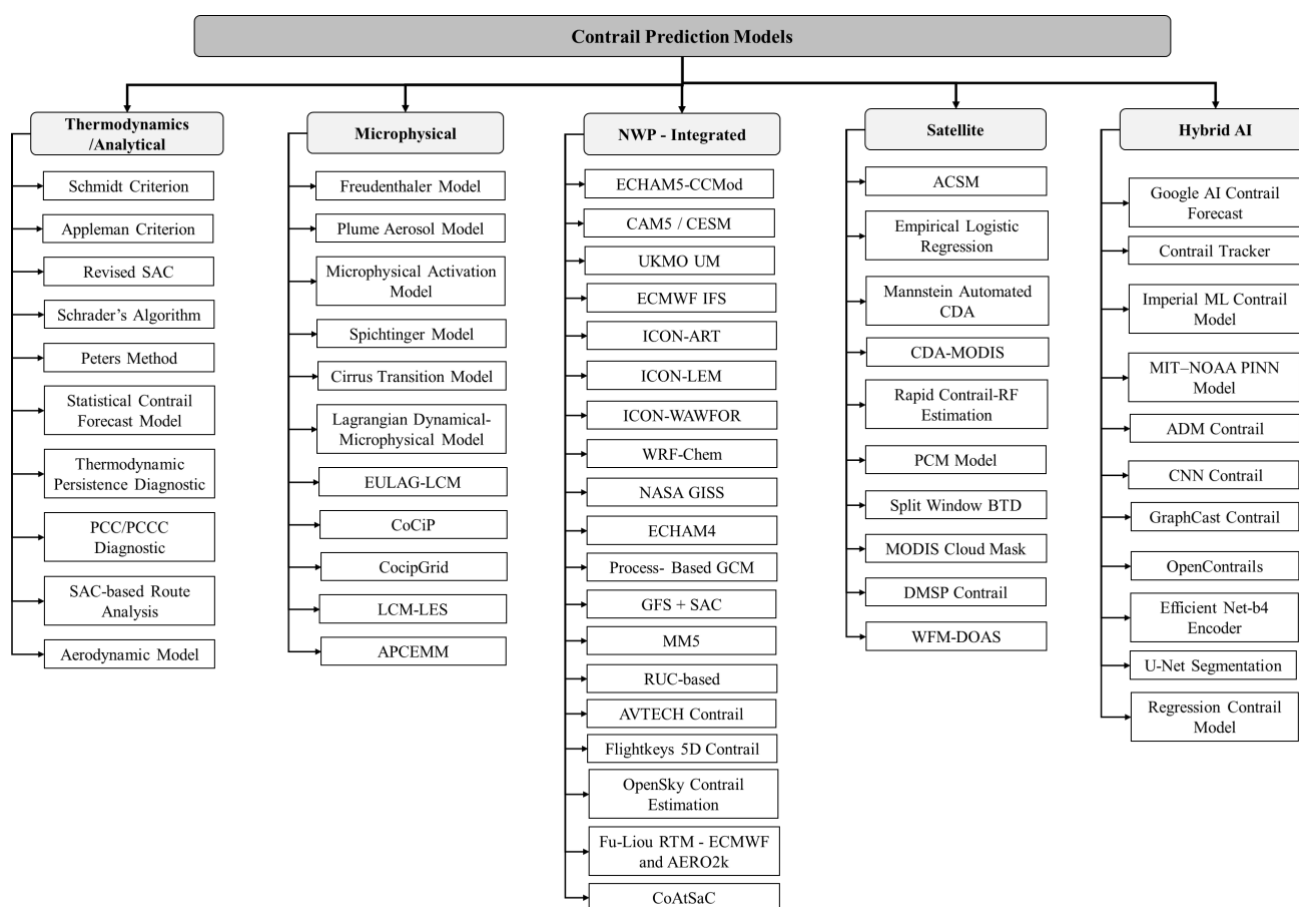


Figure 5 Tree diagram of contrail prediction models

136
 137 In summary, the development of contrail prediction models spans five major categories, which are illustrated in Figure 5.
 138 Thermodynamic/analytical, microphysical, NWP-integrated, satellite-empirical, and AI-driven—each characterized by
 139 distinct methodologies and trade-offs. Thermodynamic models are computationally efficient but overly simplistic;
 140 microphysical models provide high accuracy and process-level detail but are computationally intensive; NWP-integrated
 141 models offer realistic meteorological integration but are limited by data resolution and forecast uncertainty; satellite-based
 142



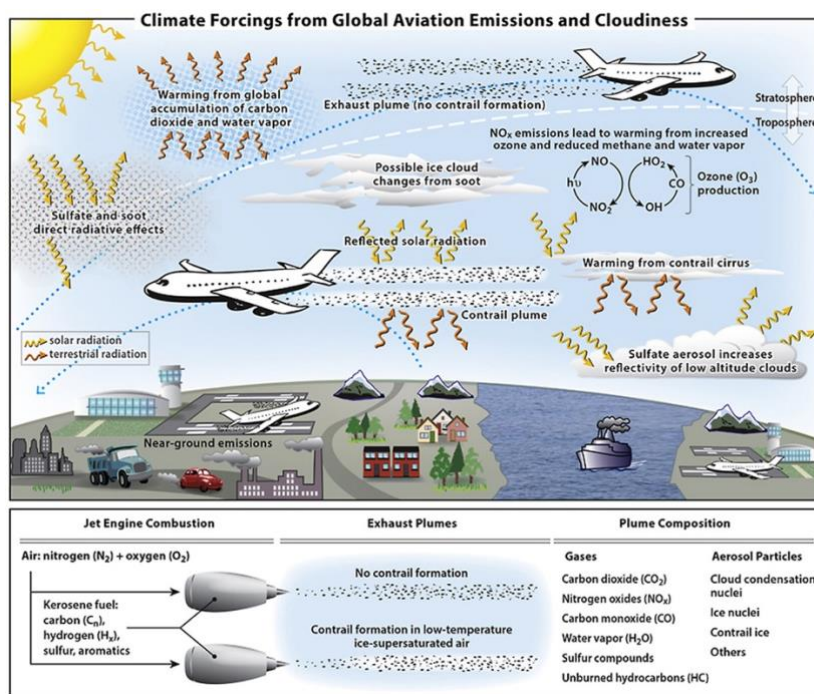
143 models enable large-scale observational insight but lack forward-looking predictive capability; and AI-driven models deliver
 144 rapid, high-resolution forecasts but depend heavily on large training datasets and robust validation. Understanding the strengths
 145 and limitations of each model type is essential for their effective use in climate assessments, aviation regulation, and
 146 operational strategy. This review systematically evaluates these modeling approaches, comparing their architectures,
 147 predictive performance, and roles within the broader context of climate mitigation—especially as the aviation sector moves
 148 toward AI-integrated environmental forecasting systems and next-generation sustainable flight planning.

149 2 Fundamentals of Contrail

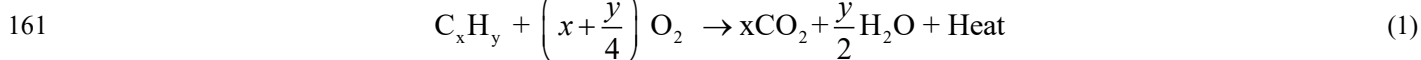
150 Contrails are the visible by-products of aircraft engine emissions interacting with the ambient conditions of the upper
 151 troposphere. Their formation, evolution, and eventual impact on climate are governed by a combination of atmospheric
 152 thermodynamics, microphysical processes, and operational parameters. This section reviews the fundamental mechanisms
 153 underlying contrail formation and sets the stage for subsequent discussions on predictive modeling.

154 2.1 Mechanism of contrail

155 Contrail formation is a thermodynamic and microphysical process initiated by the combustion of hydrocarbon jet fuels
 156 (typically Jet A-1), which react with atmospheric oxygen to produce CO₂, H₂O, NO_x, soot, and heat ([Gierens and Schumann, 1996](#)).
 157



158
 159 **Figure 6 Schematic overview of the processes by which aviation emissions and increased cirrus cloudiness affect the**
 160 **climate system ([Lee et al., 2021](#)).**



162 For every kilogram of fuel burned, approximately 1.2–1.3 kg of water vapor is emitted ([Steven L. Baughcum, 1994](#)). At cruise
 163 altitudes (~8–12 km), ambient temperatures are extremely low (often below -40°C), and the air may be supersaturated with
 164 respect to ice ($\text{RH}_i > 100\%$). As the hot, moist exhaust mixes with this cold ambient air, conditions favorable for ice nucleation
 165 may be achieved, particularly if the SAC is satisfied, which defines the threshold temperature below which contrail formation
 166 is thermodynamically possible.

167
$$T < T_{crit} = T_\infty - \frac{(1-\eta)Q}{C_p} \quad (2)$$

168 The critical temperature for contrail formation (T_{crit}) is calculated by taking the ambient air temperature (T_∞) and subtracting
 169 a term that represents the warming effect of the engine's waste heat. That term is $(1-\eta)Q/C_p$, where η is the engine's
 170 propulsion efficiency (the fraction of fuel energy converted to thrust), Q is the specific combustion heat of the fuel (about 43
 171 MJ/kg for kerosene), and C_p is the specific heat capacity of air at constant pressure (approximately $1005 \text{ J}\cdot\text{kg}^{-1}\cdot\text{K}^{-1}$). Thus,
 172 the waste heat fraction $(1-\eta)$ times the fuel energy Q gives the waste heat per unit mass, and dividing by C_p converts that
 173 energy into a temperature increase. The ambient air must be colder than T_{crit} for the mixed exhaust to reach ice supersaturation
 174 ([U.Schumann, 1996](#)).

175 Soot particles within the exhaust serve as effective ice nuclei, triggering heterogeneous nucleation, wherein water vapor
 176 deposits directly onto particulate surfaces and freezes into ice crystals ([Testa et al., 2024](#)). Volatile particles formed in the
 177 plume can also contribute to contrail ice particles, especially when fuel sulfur content is high ([Yu and Turco, 1998](#)) or soot
 178 concentrations are low ([Kärcher and Yu, 2009](#)). These initial ice particles grow via vapor deposition if ambient supersaturation
 179 is sustained, forming line-shaped contrails that may persist and spread under the influence of atmospheric shear and turbulence.
 180 In such conditions, contrails evolve into contrail cirrus extensive, optically thin ice clouds that can trap outgoing longwave
 181 radiation, contributing significantly to short-term positive radiative forcing. The net climatic impact of contrails depends on
 182 multiple factors, including ambient humidity, particle number concentration, and the vertical structure of the atmosphere,
 183 making accurate prediction a complex yet critical component of aviation climate impact assessments ([Singh et al., 2024](#)).
 184 Figure 5 illustrates the overall effect of climate forcing from global aviation emission and cloudiness, including the formation
 185 mechanism of contrails.

186 2.2 Atmospheric Conditions

187 The likelihood of contrail formation depends on several atmospheric parameters, with the most important being temperature
 188 and humidity. For a contrail to form, the atmosphere must be cold enough to allow the water vapor in the exhaust to condense
 189 and freeze. The ambient temperature typically needs to be below -40°C at the altitude of the aircraft for contrail formation to
 190 occur, as the water vapor needs to reach its frost point to transition into ice ([Kameníková et al., 2024](#)).

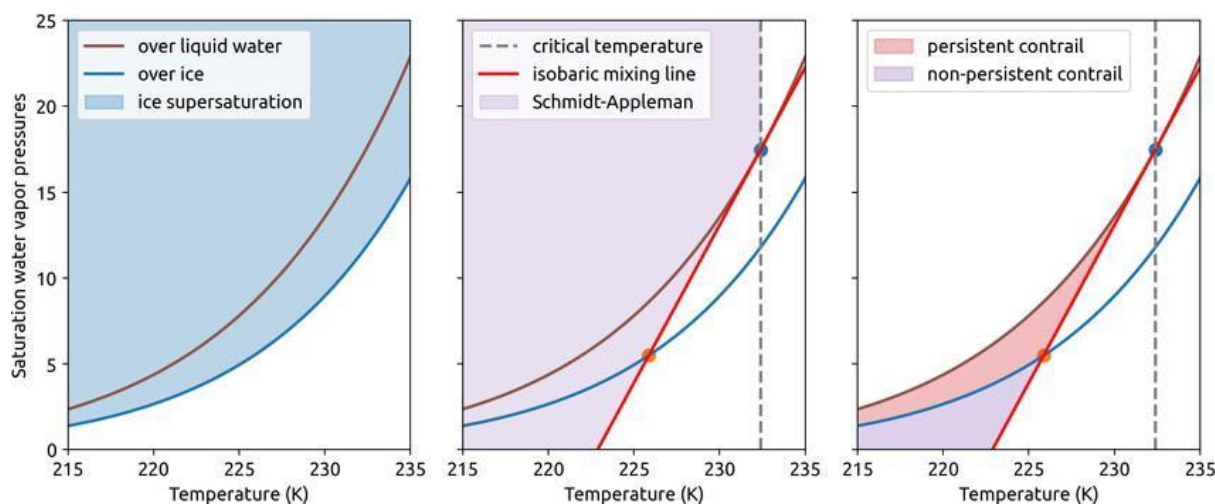


191 Equally important is the RH_{ice} , which measures how much water vapor is present in the atmosphere compared to the maximum
 192 amount the air can hold at a given temperature. Contrails will only form if the surrounding air is sufficiently supersaturated
 193 with respect to ice (i.e., $RH_i > 100\%$), which allows the water vapor to condense onto ice nuclei. This is why contrails tend to
 194 form at altitudes where the air is both cold and saturated or supersaturated with respect to ice.

195 The Schmidt-Appleman Criterion illustrated in Figure 7, developed in 1953, provides an empirical model for predicting when
 196 contrails will form based on the temperature and relative humidity with respect to ice. According to this criterion, contrails are
 197 most likely to form when the ambient temperature is below -39°C and the relative humidity with respect to ice exceeds a
 198 certain threshold. This criterion is widely used in contrail prediction models to estimate when and where contrails are likely to
 199 form under various atmospheric conditions.

$$200 \quad RH_i > RH_{i,threshold} \cdot T_{ambient} \leq -39^\circ\text{C} \quad (3)$$

201 According to Appleman's criterion, contrails could form when the ambient temperature was below -39°C and the RH_i
 202 exceeded a certain threshold, typically around 100% supersaturation. This criterion was revolutionary, providing a fundamental
 203 understanding of the basic conditions necessary for contrail formation. Figure 7 shows the dependence of contrail formation
 204 on altitude, temperature, and RH_i . It divides the atmosphere into three zones: "Always Contrails," "Possible Contrails," and
 205 "Never Contrails." Contrails always form in cold, high-altitude conditions and never form in warmer, low-altitude areas. The
 206 contour lines represent different RH_i levels, indicating that higher humidity allows contrails to form at higher temperatures.
 207 The dashed gray line shows the standard atmospheric temperature profile, helping identify where contrails are likely to occur
 208 under typical conditions.



209
210

Figure 7 Schmidt-Appleman criterion (Sun and Roosenbrand, 2023)

211 2.3 Microphysical Processes

212 The microphysical processes that govern the evolution of contrails are crucial for understanding their formation, persistence,
 213 and eventual climatic effects (Singh et al., 2024). These processes are driven by the interaction between the aircraft exhaust,



214 which contains water vapor, soot, and aerosols, and the surrounding atmosphere at high altitudes (Alsante and Cheng, 2024).
 215 Once the contrail forms, a series of nucleation, crystal growth, and sedimentation processes take place, shaping the
 216 characteristics of the contrail and determining its lifetime and radiative impact (Rubin-Zuzic et al., 2025). Below, we delve
 217 into the key microphysical processes that contribute to the formation and evolution of contrails. As shown in Table 2, the
 218 evolution of a contrail is categorized by distinct chronological stages, from initial engine emission to its final impact on the
 219 global climate.

220 **Table 2 In depth Microphysical process**

Stage	Process	Main Mechanism	Key Controls	Impact on Contrail
Emission & mixing	Exhaust dilution	Turbulent mixing and rapid cooling	Engine efficiency, ambient T, pressure	Determines supersaturation
Supersaturation	Water supersaturation	Schmidt–Appleman criterion	Ambient T, humidity	Enables contrail formation
Droplet Activation	Condensation	Heterogeneous condensation on soot/acid aerosols	Aerosol number, supersaturation	High droplet number density
Ice Nucleation	Freezing	Immersion freezing of soot-containing droplets	T < −38 °C, particle properties	Formation of ice crystals
Volatile Particle Formation	Homogeneous / ion-induced nucleation	Gas-to-particle conversion of H ₂ SO ₄ -H ₂ O or organics	Fuel sulfur content, soot concentration, ion emissions	Provides additional ice nuclei, especially when soot is low or sulfur high
Initial Growth	Deposition growth	Vapor diffusion onto ice	Ice supersaturation, T	Controls early crystal size
Persistence Check	Growth vs sublimation	Deposition (ISSR) or sublimation	RH with respect to ice	Short-lived or persistent
Crystal Evolution	Habit change & aggregation	Shape transitions, collisions	Supersaturation, turbulence	Alters optical properties
Sedimentation	Gravitational settling	Size- and shape-dependent fall speed	Crystal mass, air density	Vertical spreading, decay
Spreading & Aging	Contrail → cirrus	Wind shear and dilution	Wind gradients, stability	Long-lived contrail cirrus
Radiative Effect	Cloud–radiation interaction	SW scattering, LW trapping	Crystal size, optical depth	Net warming effect

221 2.3.1 Ice Nucleation

222 Governed by the Schmidt-Appleman criterion, contrail ice formation is a thermodynamic process that occurs when hot engine
 223 exhaust mixes with cold ambient air, leading to ice supersaturation. This supersaturation drives nucleation, which requires soot
 224 or metallic aerosols emitted by the engine to act as condensation nuclei. The process follows a condensation-freezing
 225 mechanism: water vapour first condenses onto the surfaces of these particles to form liquid droplets, which subsequently freeze
 226 as the plume rapidly cools.

227 The nucleation rate (J) can be described mathematically as:

$$228 \quad J = AS_x^n N_s \quad (4)$$

229 where A is constant related to the nucleation efficiency, S_x is the supersaturation with respect to ice. while N_s is the number of
 230 soot particle or nuclei per unit volume, n is an exponent typically around 1 for ice nucleation (Spichtinger et al., 2023).

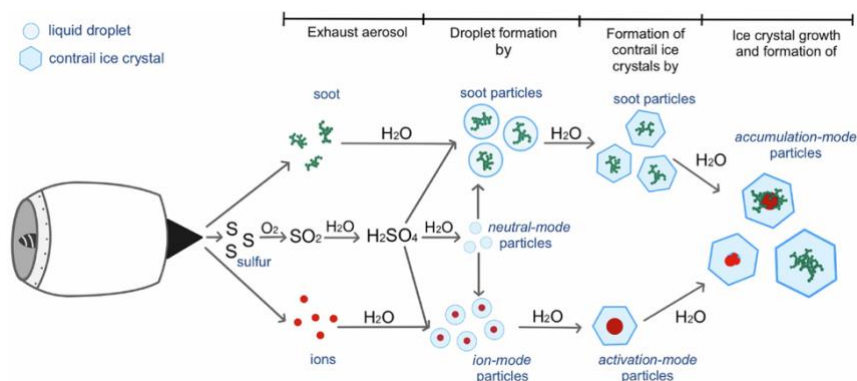


Figure 8 Formation of contrail ice particles for a fuel with medium to high sulfur content (Dischl et al., 2025)

Recent research has shown that this process is strongly modulated by fuel sulfur content, which influences nucleation in two distinct ways. Combustion converts fuel sulfur into SO_x and H_2SO_4 , which condense onto soot particles. This liquid coating enhances the hygroscopicity and effective size of the soot, rendering it a more efficient nucleus (Comstock et al., 2008). Under high-sulfur conditions (e.g., >500 ppm), excess sulfuric acid and water vapour can generate new volatile aerosol particles via homogeneous nucleation or heterogeneous nucleation on chemiions (Yu and Turco, 1997, 1998). These volatile particles can grow sufficiently to act as additional cloud condensation nuclei, producing a bimodal distribution of ice crystals. The competition between soot and volatile liquid plume particles is a key dynamic; for current engine emission levels, soot typically controls ice formation (Kärcher and Yu, 2009).

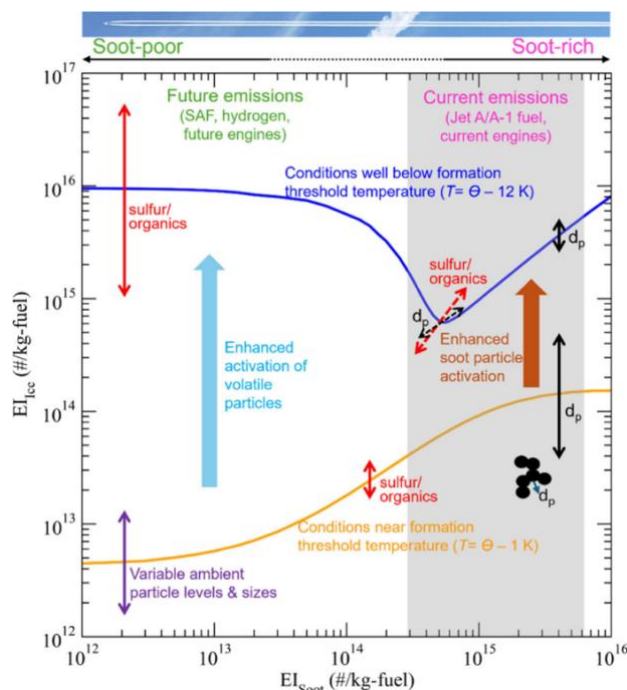


Figure 9 Nucleation of ice crystals in jet aircraft exhaust plumes (Yu et al., 2024a).



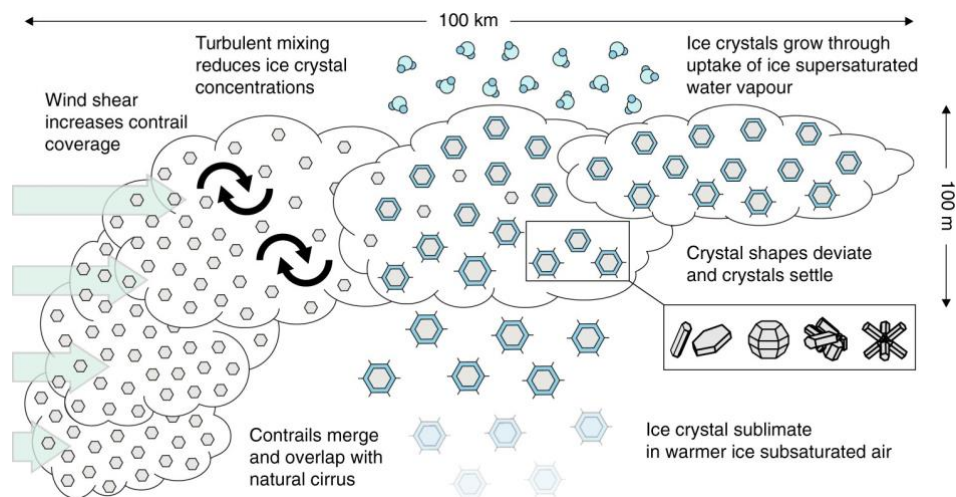
243 However, a transition to sustainable aviation fuels, which often emit smaller primary soot particles, may increase
 244 supersaturation within the plume and render the contribution of volatile particles more significant (Yu et al., 2024a). As the
 245 exhaust plume mixes with ambient air (typically between 8–12 km), the density of soot determines the nucleation regime
 246 (Ponsonby et al., 2024). Abundant soot particles serve as effective nucleation sites, leading to efficient ice crystal formation
 247 where crystal counts can reach 10^{16} (Mahrt et al., 2018). In these conditions, ice crystal numbers correlate linearly with soot
 248 emissions. When soot is scarce, ice nucleation becomes less efficient and is driven partially by ultrafine aqueous particles,
 249 depending strongly on ambient temperature and aerosol levels, resulting in lower crystal concentrations of around 10^{12} .
 250 Nevertheless, high fuel sulfur content can offset the lack of soot: volatile particles may then cause ice crystal numbers to
 251 exceed the number of emitted soot particles (Yu et al., 2024a).

252 2.3.2 Crystal Growth

253 The growth of ice crystals in contrails begins after nucleation, when the ice crystals grow through the deposition of water
 254 vapor from the surrounding supersaturated air (Laaksonen and Malila, 2022). This growth is driven by the degree of
 255 supersaturation with respect to ice (S_x), where water vapor condenses onto the crystals, causing them to grow larger (Verma
 256 and Burkhardt, 2022). The rate of crystal growth depends on the supersaturation level and is typically expressed as:

$$257 \quad G = K_1 (S_x - 1) \quad (5)$$

258 where, G is the growth rate of ice crystals (m/s), K_1 is the deposition coefficient (ranging from 10^{-8} to 10^{-7} m/s depending
 259 on atmospheric conditions (Libbrecht and Rickerby, 2011).



260
 261 **Figure 10 Factors affecting the development of aircraft-induced clouds (Karcher, 2018)**

262 In conditions of high supersaturation, ice crystals grow rapidly, typically at a rate of 10–100 nm per second, and can reach
 263 sizes around 1000 nm (1 micron) in 1–10 seconds as shown in Figure 11 (Wex et al., 2015). As the crystals grow, they begin
 264 to deviate from simple hexagonal shapes, transitioning into more complex forms such as droxtals, columns, and bullet rosettes,
 265 depending on the level of supersaturation and the surrounding temperature (Wolf et al., 2023). The optical properties of the



266 contrail are influenced by these growth processes, as larger ice crystals scatter more solar radiation and absorb more longwave
 267 radiation ([Rubin-Zuzic et al., 2025](#)). Wind shear plays a key role in increasing the lateral spread of the contrail, which enhances
 268 contrail coverage ([Kärcher et al., 2009](#)). This spread is due to horizontal movement, and as the contrail mixes with the ambient
 269 air, turbulent mixing occurs, which reduces the ice crystal concentrations ([Lewellen, 2014](#)). While mixing dilutes the contrail
 270 and reduces its density, it also causes it to spread, potentially merging with natural cirrus clouds, which increases the overall
 271 cloud coverage ([Lewellen, 2014](#)). Table 3 summarizes the four primary factors that dictate contrail crystal growth. It outlines
 272 how the soot emission index determines crystal size and density, how ambient temperature and humidity govern nucleation
 273 rates and long-term persistence, and how aircraft wake dynamics influence early crystal loss during the initial downwash.

274 **Table 3 Factors effecting crystal growth**

Factor	Influence on Growth
Soot Emission Index EI_{soot}	High soot = many nuclei = high competition = smaller, more numerous crystals . Low soot = fewer nuclei = larger, fewer crystals .
Ambient Temperature	Controls nucleation threshold and growth rate. Lower T = faster nucleation but slower diffusive growth dynamics.
Ambient Humidity RH_i	The fuel for growth. High RH_i leads to rapid growth and long persistence. $RH_i < 100\%$ causes immediate sublimation.
Aircraft Wake Dynamics	Determines the depth of the "downwash" and therefore how much adiabatic heating (and crystal loss) occurs in the first 2 minutes.

275 As the crystals grow larger, they experience sedimentation due to gravity. Larger crystals, typically those greater than 30 μm ,
 276 fall at speeds greater than 100 m/h, which is described by the fall speed equation ([Jensen et al., 2018](#)).

$$277 \quad v_f = \frac{2 (\rho_c - \rho_f) g r^2}{9 \mu} \quad (6)$$

278 Where, v_f is all speed of a crystal, where ρ_c the density of the crystal while ρ_f is the density of the fluid surrounding.

279 2.3.3 Sedimentation

280 As the ice crystals in contrails grow, they eventually reach a size where they begin to fall out of the contrail, a process known
 281 as sedimentation ([Singh et al., 2024](#)). Sedimentation is driven by the gravitational pull acting on the ice crystals, causing them
 282 to fall toward the Earth's surface. The rate of sedimentation depends on the size of the ice crystals and the surrounding
 283 atmospheric conditions. Larger crystals, typically those greater than 30 μm , settle more quickly due to their increased mass.
 284 The fall speed of these crystals can be described using the following equation ([Mahowald et al., 2014](#)).

$$285 \quad v_f = \frac{d^2 \left(\frac{g}{\eta} \right)}{\rho} \quad (7)$$

286 where V_f is fall speed, d is the diameter of the ice crystal, ρ is the density of ice and η is dynamic viscosity of air. Smaller
 287 crystals, with diameters typically less than 30 μm , experience slower fall speeds due to their lower mass and larger surface
 288 area-to-volume ratio ([Libbrecht, 2017](#)). These smaller crystals may remain suspended in the atmosphere for a longer period



289 unless the surrounding air is sufficiently supersaturated with water vapor to maintain their growth. The vertical wind shear in
290 the atmosphere can influence the rate and direction of sedimentation ([Podglajen et al., 2018](#)). Wind shear, which refers to the
291 variation in wind speed and direction at different altitudes, can alter the trajectory of the ice crystals ([Corbosiero and Molinari,
292 2002](#)). In turbulent conditions, vertical wind shear can cause the ice crystals to disperse more widely or remain aloft for a
293 longer duration. If the wind shear is weak, the contrail ice crystals are more likely to remain concentrated, leading to a more
294 persistent contrail. In areas with strong wind shear, the ice crystals may spread out or dissipate more quickly ([Jensen et al.,
295 2025](#)). In some cases, the ice crystals in a contrail may grow large enough to fall out and contribute to precipitation at the
296 Earth's surface ([Singh et al., 2024](#)). However, in most instances, especially in persistent contrails that evolve into contrail
297 cirrus, the ice crystals remain suspended in the atmosphere for an extended period ([Petzold et al., 2025](#)). The sublimation of
298 ice crystals in warmer, ice-sub-saturated air may also occur, further reducing their size. This process influences the persistence
299 and spatial extent of contrail cirrus clouds, which can significantly affect their optical properties and radiative forcing ([Bock
300 and Burkhardt, 2016](#)).

301 Sedimentation plays a key role in determining the lifetime, size distribution, and spatial spread of contrails and contrail cirrus,
302 influencing their eventual dissipation or expansion and their impact on the climate. The larger crystals fall at higher speeds
303 and can lead to the gradual dissipation of the contrail, while smaller crystals remain suspended, contributing to cloud
304 persistence and long-term radiative effects ([Kärcher and Corcos, 2025](#)).

305 2.4 Evolution of Contrail Cirrus

306 The evolution of contrail cirrus begins with the formation of contrails when jet aircraft exhaust, consisting of water vapor and
307 particulate matter, cools upon mixing with the ambient air at altitudes typically between 8–12 km ([Schumann and Heymsfield,
308 2017](#)). This cooling leads to ice nucleation on exhaust particles, forming ice crystals of approximately 1000 nm in size as
309 illustrated in Figure 11 ([Kärcher et al., 2018](#)). These crystals grow through sublimation and deposition, depending on the
310 surrounding supersaturation levels of water vapor, with growth rates of about 10–100 nm per second under favorable
311 conditions ([Magee et al., 2014](#)). Once the contrail forms, it may expand laterally due to wind shear, with horizontal spreading
312 rates of 0.1–1 km per hour depending on atmospheric turbulence and vertical wind profiles ([Unterstrasser, 2020](#)). However,
313 the evolution does not stop with this initial spreading; the subsequent vortex phase, occurring during the first seconds to
314 minutes after emission, plays a decisive role in dictating the contrail's vertical dispersion and ice crystal survival ([Saulgeot et
315 al., 2023](#)). During this phase, a pair of counter-rotating wingtip vortices descends and wraps around the exhaust plume, carrying
316 ice crystals several hundred meters below the flight altitude into warmer, drier air, which can cause substantial sublimation
317 and reduce the ice crystal number by up to 75 % compared to the initial emission ([Unterstrasser and Gierens, 2010b; Kleine et
318 al., 2018](#)). Large-eddy simulations show that when the ambient temperature exceeds 225 K or when the initial ice crystal
319 concentration is very high, adiabatic heating within the vortex core can evaporate most of the ice before the vortices break up
320 ([Bier et al., 2024](#)). After the vortex pair decays (≈ 30 –60 s), the remaining ice crystals enter the diffusion phase, where turbulent
321 mixing and wind shear broaden the contrail horizontally at rates that increase with vertical wind shear and decrease with



345 ([Peter et al., 2025](#)). This variability adds complexity to the prediction of contrail formation across different flight routes and
346 conditions.

347 **2.6 Implications for Predictive Modeling**

348 Advancing contrail prediction requires modeling approaches that not only reproduce the initial formation conditions but also
349 resolve the temporal and spatial evolution of contrail ice particles under realistic atmospheric variability ([Kärcher and Corcos,](#)
350 [2025](#)). Each class of model thermodynamic/analytical, microphysical, NWP-integrated, satellite-empirical, and AI-driven
351 carries specific implications for predictive accuracy, interpretability, and operational utility.

352 Thermodynamic and analytical models, based on closed-form criteria like the Schmidt-Appleman formulation, remain
353 valuable for rapid assessment of contrail formation thresholds. Their simplicity enables large-scale screening and
354 climatological mapping, but their binary logic and lack of temporal dynamics restrict their use in forecasting persistence or
355 radiative effects ([Cannon et al., 2024](#)).

356 Microphysical box models simulate particle-scale processes such as nucleation, coagulation, sublimation, and ice growth under
357 controlled thermodynamic conditions ([Pal et al., 2025](#)). These models offer fine-scale insights into contrail microstructure,
358 especially when parameterized with laboratory-derived aerosol properties. However, their reliance on high-resolution input
359 data and limited scalability reduce their practical application in real-time systems ([Bier et al., 2024](#)).

360 NWP-integrated models bridge physical realism with spatial coverage, embedding contrail schemes into regional or global
361 atmospheric simulations. Their ability to capture atmospheric heterogeneity including vertical motion, wind shear, and ambient
362 humidity makes them well-suited for studying contrail coverage and radiative forcing. However, uncertainties in upper
363 tropospheric humidity fields and the reliance on parameterizations for plume-scale processes introduce notable errors in
364 persistence estimation ([Randall et al., 2019](#)).

365 Satellite-based empirical models contribute observational validation and climatological baselines, essential for calibrating
366 physical and AI models. Their integration into machine learning workflows allows pattern recognition on a global scale. Still,
367 their passive nature and limitations in cloud-type discrimination reduce their standalone forecasting potential.

368 AI-driven models particularly those incorporating ensemble reanalysis, satellite data, and flight trajectories enable spatial
369 generalization and short-term forecasting ([Riggi-Carolo et al., 2023](#)). PINNs and hybrid frameworks combine
370 thermodynamic laws with learned patterns, improving robustness in data-sparse regions ([Hashemi et al., 2025](#)). These models
371 are increasingly being explored for optimizing flight paths to reduce climate impact. Their main limitations include reduced
372 interpretability, dependence on training data quality, and difficulties in propagating observational uncertainty through learned
373 parameters.

374 Effective contrail prediction in future frameworks will likely rely on hybrid systems that leverage the physical grounding of
375 first-principles models ([Di Giusto et al., 2024](#)), the scalability of NWP systems, the observational fidelity of satellites, and the
376 adaptive intelligence of AI ([U.Schumann, 1996](#)). Model coupling strategies that support uncertainty quantification, high-

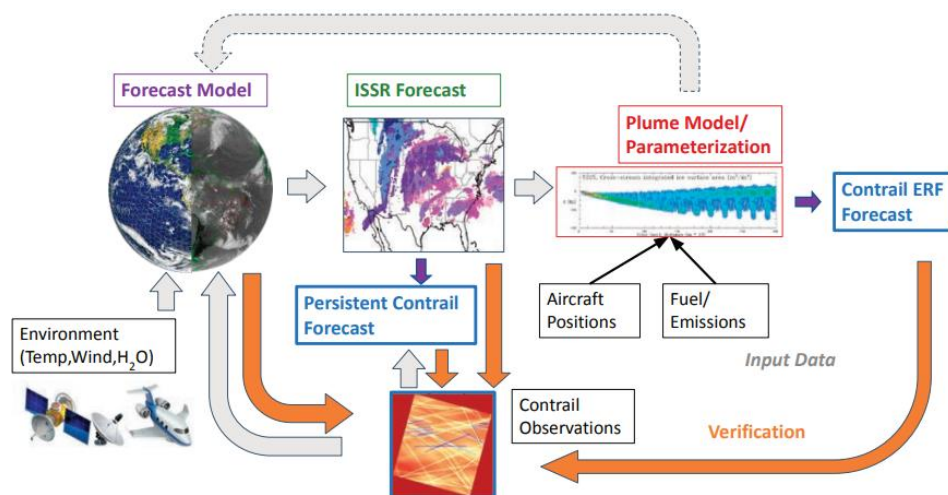


377 resolution inputs, and multi-objective optimization (e.g., fuel burn vs. radiative forcing) are critical for deployment in
 378 operational decision-making environments.

379 **3 Overview of Contrail Prediction Models**

380 Contrail prediction models have evolved along five major methodological lines, reflecting increasing sophistication in both
 381 atmospheric science and computational modeling (Engberg et al., 2025). Thermodynamic and analytical models, grounded in
 382 the Schmidt–Appleman Criterion, are among the earliest approaches used for predicting contrail formation (U.Schumann,
 383 1996). These models rely on threshold-based formulations involving ambient temperature, pressure, and aircraft exhaust
 384 characteristics to determine the likelihood of contrail initiation. While they are computationally efficient and valuable for rapid
 385 assessments, their simplified structure fails to account for spatial variability and offers limited insight into the dynamic
 386 evolution of contrails after formation.

387 Building on this foundation, microphysical box models provide a more detailed representation of contrail processes by
 388 simulating ice nucleation and growth within aircraft exhaust plumes (Ponsonby et al., 2025). These models incorporate aerosol
 389 microphysics and conservation equations as in Table 4. to capture particle behavior at high temporal and spatial resolution.
 390 Despite offering granular insights into the physical mechanisms of contrail development, they demand substantial
 391 computational power and high-resolution atmospheric data, which constrains their operational deployment.



392
 393 **Figure 12 Schematic elements of a contrail forecasting and verification system (Timothy C. Lieuwen (Nae), 2025)**

394 A further step in model complexity is represented by contrail schemes integrated into NWP systems. These models embed
 395 contrail-related processes within mesoscale or global circulation frameworks such as ECHAM4/5 or MM5 (P. Stier 2005).
 396 The advantage of this approach lies in its ability to provide spatially and temporally resolved forecasts under realistic
 397 meteorological conditions. However, model performance is sensitive to uncertainties in upper-tropospheric humidity fields
 398 and the simplifications inherent in parameterization schemes used to represent sub-grid scale processes (Peter et al., 2025).



399 In parallel, satellite-empirical models have emerged as a valuable tool for identifying contrail occurrence and building
 400 climatological datasets ([Jarry et al., 2026](#)). These models utilize remote sensing data from instruments such as AVHRR ([Yu
 401 et al., 2024b](#)), MODIS ([Duda et al., 2013](#)), and CALIPSO ([Singh et al., 2024](#)), often applying pattern recognition algorithms
 402 and statistical inference methods to detect linear contrail features. Although these approaches are highly effective for
 403 retrospective analysis and model validation, they lack forward predictive capabilities and are prone to misclassification,
 404 particularly under conditions of complex cloud backgrounds or low sensor resolution ([Yu et al., 2024b](#)).

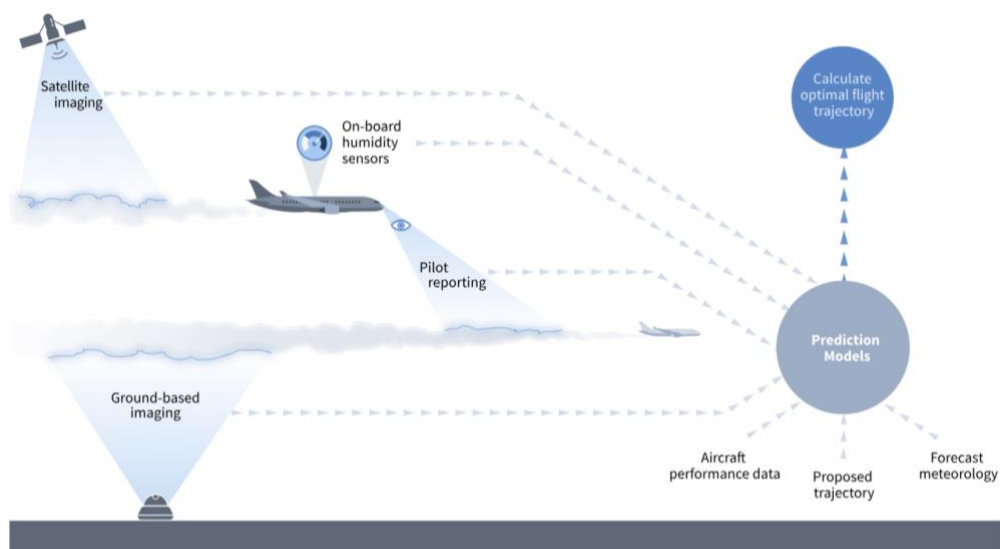
405 **Table 4 Core Aerosol Microphysics and Conservation Equations in Contrail Modeling**

S.No	Equation Type	Mathematical Expression	Eq.no	Ref
1	Mass Continuity (Air/Plume)	$\frac{\partial \rho}{\partial t} + \nabla \cdot (\rho u) = 0$	(8)	(Lewellen, 2014 ; R.Paoli, 2002)
2	Water Vapor Conservation	$\frac{Dq_v}{Dt} = S_{comb} - S_{cond} - S_{dep}$	(9)	(Schumann et al., 1996)
3	Energy (Thermodynamic) Conservation	$\rho c_p \frac{DT}{Dt} = -p(\nabla \cdot u) + L_{sub} \frac{Dq_i}{Dt} + Q_{rad}$	(10)	(Burkhardt and Kärcher, 2009 ; Chen and Gettelman, 2013)
4	Particle Number Conservation	$\frac{\partial n(r,t)}{\partial t} + \nabla \cdot (nu) = J_{nuc} + \frac{1}{r^2} \frac{\partial}{\partial r} (r^2 G(r)n) + S_{coag}$	(11)	(Jensen et al., 1998 ; Kärcher et al., 2018)
5	Condensational Growth of Ice Particles	$\frac{dr}{dt} = \frac{S_i - 1}{\frac{L_{sub}}{R_v T} + \frac{L_{sub} D_v}{kT} + \frac{R_v T}{p D_v}}$	(12)	(Huebsch et al., 2014)
6	Ice Mass Mixing Ratio	$M_i = \int_0^\infty \frac{4}{3} \pi \rho_i r^3 n(r) dr$	(13)	(Chen and Gettelman, 2013 ; Burkhardt and Kärcher, 2009)
7	Optical Depth of Contrail	$\tau = \int_0^\infty Q_{ext}(r) \pi r^2 n(r) dr$	(14)	(Chen and Gettelman, 2013 ; Teoh et al., 2024a)

406 More recently, AI-based models have gained prominence in the field. Leveraging techniques such as random forests
 407 ([Kameníková et al., 2024](#)), deep learning ([Lin et al., 2024](#)), and PINNs ([Raphael Alamu, 2025](#)), these models utilize large,
 408 multi-source datasets to forecast contrail formation and evolution with high spatial and temporal fidelity. They frequently
 409 outperform traditional models in predictive accuracy and operational feasibility, yet they introduce challenges in model
 410 interpretability, robustness under unseen conditions, and dependence on the quality and representativeness of training data. In
 411 response to these limitations, hybrid approaches that integrate physical modeling with machine learning have been increasingly
 412 proposed. These methods aim to combine the generalizability and physical interpretability of mechanistic models with the
 413 data-driven precision of AI, marking a significant frontier in current contrail prediction research ([Zebediah Engberg, 2025](#)).
 414 Figure 12 illustrates the architecture of a modern contrail prediction system that incorporates environmental data (e.g.,
 415 temperature, humidity, wind) sourced from satellite and reanalysis datasets. These inputs feed into weather forecast models,
 416 which in turn enable (ISSRs). The primary atmospheric condition supporting persistent contrail formation. This information,



417 combined with aircraft position data and engine emissions profiles, is processed through plume evolution models or
 418 parameterizations to estimate contrail characteristics and their ERF. The final outputs are compared against satellite-based
 419 contrail observations for model verification and performance evaluation, forming a feedback loop for continuous improvement.
 420 Complementing this structure,



RMI Graphic. Source: RMI analysis

421

422

Figure 13 Different technique used for contrail prediction (Grewe et al., 2017)

423

424

425

426

427

428

429

Figure 13 highlights various observational techniques that support contrail detection and prediction model refinement. Satellite imaging, ground-based instruments, and on-board humidity sensors contribute to real-time or retrospective identification of contrail events. Additionally, pilot reports serve as qualitative sources of observational input. These heterogeneous data streams are fed into prediction models that also ingest aircraft performance data, forecast meteorology, and proposed flight trajectories. The integration of these elements allows for the calculation of optimized flight paths that minimize contrail formation potential. Such predictive and prescriptive capabilities are central to emerging climate mitigation strategies aimed at reducing aviation-induced radiative forcing by avoiding contrail-prone airspaces.

430

3.1 Thermodynamic and analytical models

431

432

433

434

435

436

437

Thermodynamic and analytical models form the conceptual foundation of contrail prediction science. These models provide a physically grounded and mathematically tractable framework for identifying the atmospheric conditions under which contrails are expected to form. At their core lies the Schmidt Criterion (U.Schumann, 1996), the first theoretical formulation to describe contrail formation based on plume mixing and the derivation of a critical temperature threshold (Ulrich Schuman, 1997). This foundational work did not consider atmospheric humidity, limiting its predictive capacity. Building on this, the SAC introduced fuel efficiency and ambient pressure dependencies, enabling graphical representations of contrail formation potential under simplified conditions. These models gained popularity for operational forecasting due to their simplicity. However, they



438 retained core limitations such as assumption of a static atmosphere, homogeneous plume behavior, and a binary output
 439 (formation vs. no formation), without accounting for contrail persistence or radiative impacts. A concise summary of key
 440 models, their features, and limitations is provided in Table 5.

441 **Table 5 List of Thermodynamic and Analytical Contrail Prediction Models**

Model / Framework	Year / Developer	Key Features	Limitations	Ref
Schmidt Criterion	1941 / E. Schmidt	Established the mixing-line theory: exhaust and air mix isobarically to reach water saturation.	Lacked modern engine physics; did not account for pressure/altitude effects.	(Ernst 1941)
Appleman Criterion	1953 / H. Appleman	First graphical tool (Appleman Charts) used by pilots; introduced pressure/altitude as a variable.	Assumed fixed engine heat/water ratios; ignored modern propulsion efficiency η .	(N. 1953)
Revised SAC	1996 / U. Schumann	The Current Standard. Introduced η . Proved efficient engines (cooler exhaust) form contrails more easily.	Highly sensitive to humidity data errors in NWP models.	(U.Schumann, 1996)
Schrader's Algorithm	1997 / M. L. Schrader	The Gold Standard numerical solver used to find the tangent point (T_{crit}) on the vapor curve.	Iterative nature can be computationally slow for large-scale real-time simulations.	(Schrader, 1997)
Peters Method	1993 / Rich F. Coleman	A modified forecasting technique that used a different "Contrail Factor" for engine specific heat.	Criticized for errors in basic physics (requiring ice saturation instead of liquid for formation).	(Coleman, 1996)
Statistical Contrail Forecast Model	2001 / Jackson	Logistic regression relates contrail probability to radiosonde temperature/humidity	Small dataset (557 observations), limited geographically (New England) and seasonally	(Jackson, 2001)
Thermodynamic Persistence Diagnostic	2024 / Hofer - DLR	Validates thermodynamic contrail prediction using ERA5 vs. radiosondes	High false alarm rates due to unresolved humidity variability	(Hofer et al., 2024)
PCC/PCCC Diagnostic	2022 / Dischl - DLR	Diagnoses potential contrail/cirrus cover using ERA5 thermodynamic fields	Represents potential areas only, depends on reanalysis humidity accuracy	(Dischl et al., 2022)
SAC-based Route Analysis	2021 / Choi et al.	Applies SAC to sounding data for the Tokyo-Qingdao route to suggest altitude changes	Relies on sparse sounding data (low spatial resolution); limited to single route case study	(Choi et al., 2021)
Aerodynamic Model	2009 / K. Gierens et al.	Thermodynamic model for Aerodynamic Contrails ; based on pressure drop over wings, not exhaust.	Only applies to specific high-humidity conditions; often invisible or very short-lived.	(Jansen and Heymsfield, 2015)

442 In the following decades, analytical plume mixing models extended SAC through adiabatic cooling and isobaric mixing
 443 formulations, offering improved thermodynamic realism ([Khangaonkar et al., 2024](#)). Despite these advancements, they
 444 remained limited by their exclusion of microphysical processes such as ice nucleation, growth, and sublimation necessary for
 445 studying contrail evolutions.

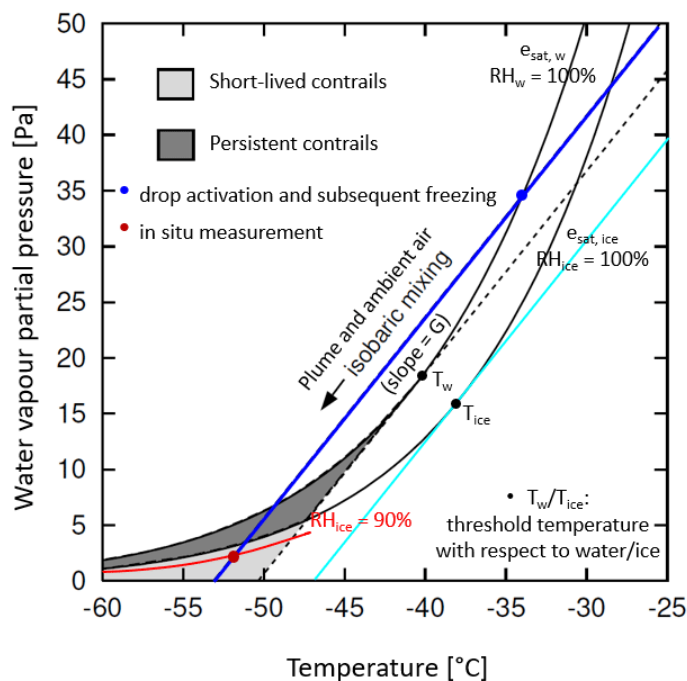


Figure 14 Schmidt-Appleman Criterion (Li et al., 2023b)

A significant step toward more dynamic modeling came with Lagrangian plume models (Anfossi et al., 2005) as shown in Figure 15. These models simulate the trajectory of aircraft exhaust as an evolving parcel, incorporating environmental factors such as wind shear, ambient humidity, and temperature gradients. By tracking plume dispersion over time, Lagrangian approaches capture spatial temporal variations and nucleation thresholds with greater fidelity. However, they are still constrained by computational complexity and a lack of full radiative feedback or comprehensive microphysics.

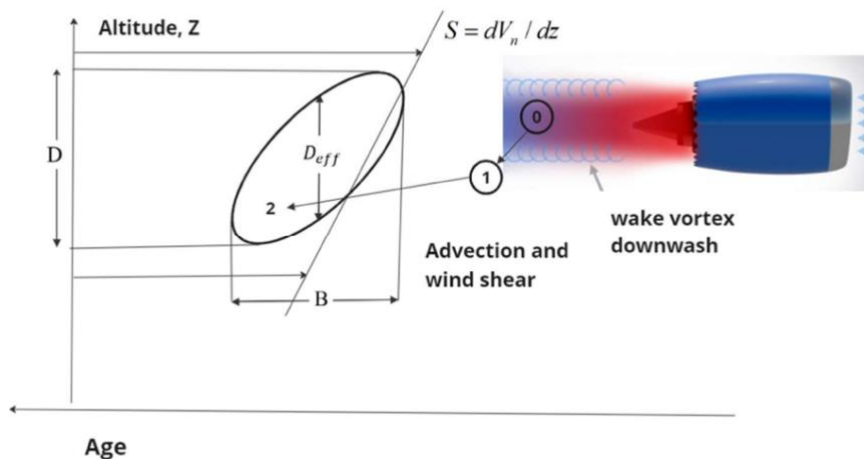


Figure 15 Lagrangian plume model

446
447
448
449
450
451
452

453
454



455 Parallel to these advancements, operational agencies such as FAA ([Brasseur et al., 2016](#)), DLR ([Raumfahrt, 2023a](#)), and ICAO
456 developed threshold-based formation maps (1990s–2020s), translating SAC outputs into global screening tools using standard
457 atmospheric profiles. These maps continue to support large-scale climatological assessments but struggle with mesoscale
458 resolution and real-time adaptability. With growing emphasis on sustainable aviation, modified SAC models emerged to
459 incorporate the effects of SAFs. Schumann proposed adjustments based on altered soot and water vapor emission indices,
460 reflecting new contrail behavior under SAF scenarios. These models, however, face uncertainties due to evolving fuel
461 chemistry and combustion characteristics. Finally, SAC-based diagnostics have been embedded in NWP models by institutions
462 like DLR, ECMWF, and NASA since the early 2000s. By integrating SAC into systems such as GFS, WRF, and CESM, these
463 frameworks enable large-scale contrail prediction. However, they rely heavily on the accuracy of upper-tropospheric humidity
464 data, and they function only as diagnostic modules not as standalone predictive models.

465 The statistical contrail forecast model was developed by Artie Jackson, Brian Newton, Doug Hahn, and Allan Bussey at the
466 Air Force Research Laboratory (Hanscom AFB, Massachusetts) in 2001. Moving away from purely thermodynamic
467 thresholds, the authors utilized logistic regression techniques to correlate specific atmospheric variables with the presence or
468 absence of contrails. The model was trained on a dataset from the "Contrail Field Program," which consisted of 557 coincident
469 aircraft observations and radiosonde measurements collected in eastern Massachusetts. By analyzing predictors such as
470 temperature and relative humidity, the model achieved a correct diagnosis rate of 85%, significantly outperforming the
471 standard Schrader (Appleman-based) algorithm, which had only 58% accuracy. The primary limitation of this model is that it
472 was developed using a relatively small dataset collected only during September in New England, which may restrict its
473 applicability to other geographic regions or seasons ([Jackson et al., 2001](#)).

474 A study was conducted by Sina Hofer, at the DLR and Forschungszentrum Jülich in 2024 about How well can persistent
475 contrails be predicted? The authors assessed the accuracy of predicting persistent contrails by applying the standard SAC and
476 Ice Supersaturation thresholds to ERA5 reanalysis data. The methodology involved comparing these diagnostic predictions
477 against high-resolution radiosonde measurements (treated as ground truth) to quantify performance metrics like the Probability
478 of Detection and False Alarm Rate. A primary limitation identified is that despite using state-of-the-art reanalysis ERA5, the
479 prediction of persistent contrails remains challenging because current models cannot sufficiently resolve the small-scale spatial
480 and temporal fluctuations of ice supersaturation, leading to significant uncertainties and high false alarm rates ([Hofer et al.,
481 2024](#)).

482 ERA5-based PCC/PCCC thermodynamic Diagnostic study was conducted by Rebecca Dischl, Stefan Kaufmann at DLR and
483 Johannes Gutenberg-Universität Mainz in 2022. The authors developed a methodology to quantify the Potential Contrail Cover
484 (PCC) and Potential Contrail Cirrus Cover (PCCC) over Europe and the North Atlantic by analyzing 10 years of ERA5
485 reanalysis data. The methodology applies the thermodynamic SAC to determine regions of formation and uses varying
486 thresholds of Relative Humidity over Ice to identify areas capable of supporting persistent contrail cirrus. By processing high-
487 resolution meteorological fields, the study establishes a climatology of favorable contrail conditions. A primary limitation of



488 this approach is that it calculates only the potential for coverage based on atmospheric state, ignoring actual air traffic density
489 and the microphysical lifecycle (advection, spreading, aging) of the contrails, and is ultimately constrained by the accuracy of
490 the moisture fields in the ERA5 reanalysis ([Dischl et al., 2022](#)).

491 The SAC Based route analysis study was conducted by Jun-Young Choi at the Korea National University of Transportation in
492 2021. The authors developed a basic contrail prediction model to support future aircraft certification for contrail reduction.
493 The methodology involves applying the SAC to atmospheric sounding data (temperature, pressure, and humidity profiles)
494 obtained from the University of Wyoming database. The study focused on the commercial flight route between Tokyo (Narita)
495 and Qingdao, analyzing vertical profiles to identify contrail-forming layers. The results demonstrated that adjusting flight
496 altitude—specifically descending or ascending by approximately 2,000 ft to 4,000 ft—could effectively move the aircraft out
497 of ice-supersaturated regions, thereby preventing persistent contrail formation. A primary limitation is the reliance on
498 radiosonde point data, which lacks the high spatial and temporal resolution of modern numerical weather prediction models
499 necessary for global trajectory optimization ([Choi et al., 2021](#)).

500 Collectively, these thermodynamic and analytical models define the parameter space within which all subsequent modeling
501 microphysical, satellite, and AI-based operates. While their simplifications limit predictive power, their physical
502 interpretability and computational efficiency make them valuable for screening, sensitivity testing, and as benchmarks for
503 advanced systems. As the field moves toward hybrid frameworks, there is growing interest in SAC-informed AI architectures,
504 where machine learning systems are constrained by physical laws to improve generalizability and transparency. Thus, these
505 models continue to serve as essential but increasingly complementary tools within the modern contrail modeling hierarchy.

506 3.2 Microphysical Box Models

507 Microphysical box models have evolved as a cornerstone of contrail modeling by providing detailed, process-level simulations
508 of ice nucleation, growth, and optical development within the aircraft exhaust plume. These models go far beyond threshold-
509 based frameworks like the SAC by resolving the fundamental microphysical processes that govern contrail life cycles. A
510 representative list of these microphysical models, including their approaches and primary foci, is provided in **Error! R
511 eference source not found.** Their development reflects increasing sophistication in how we understand the formation,
512 persistence, and climatic impacts of aircraft-induced clouds. Table 6 summarizes key microphysical contrail prediction models
513 developed primarily at DLR, MIT, and other institutes. These models resolve ice nucleation, growth, optical properties, and
514 lifecycle dynamics using Lagrangian, LES, or spectral bin approaches, enabling process-level simulations beyond simple
515 threshold-based formation criteria.

516 The Freudenthaler Model (optical parameterization), established through the extensive lidar research of Volker Freudenthaler
517 and colleagues serves as the definitive analytical framework for bridging the gap between microphysical simulation and remote
518 sensing observations. Unlike dynamic growth models, this parameterization solves the inverse scattering problem by
519 employing advanced geometric optics (ray-tracing) and T-matrix codes to correlate the physical morphology of ice crystals
520 specifically their aspect ratios and surface roughness—with their optical signatures, most notably the linear depolarization



521 ratio (δ). The model operates on the principle that non-spherical ice crystals scramble the polarization of incident laser light
 522 (unlike spherical liquid droplets which return linear depolarization ratio equal to zero, and it quantifies this effect by calculating
 523 the ratio of perpendicular to parallel backscatter intensity.

$$524 \quad \delta = P_{\perp} / P_{\parallel} \quad (15)$$

525 A critical contribution of this work is the definition of the "Freudenthaler Limit" or characteristic curves, which demonstrate
 526 that fresh contrails, composed of small, highly irregular, and randomly oriented crystals (e.g., droxtals or complex aggregates),
 527 exhibit significantly higher depolarization values $\delta \sim 0.4 - 0.5$ compared to the lower values $\delta < 0.3$ typical of aged, oriented
 528 crystals in natural cirrus; this optical distinction provides the essential validation metric for checking if the size distributions
 529 and habit assumptions in microphysical box models are physically consistent with real-world lidar measurements from
 530 platforms like CALIPSO or EARLINET.

531 **Table 6 List of Microphysical Contrail Prediction Models**

Model	Developer Institute	Approach	Primary Focus	Ref
Freudenthaler Model	LMU Munich / DLR	Lidar/Optical Theory	Optical properties & Lidar validation	(Freudenthaler et al., 1996)
Plume Aerosol Model	DLR	Near-field chemistry	Particle activation & soot-ice link	(Kärcher et al., 1998)
Microphysical Activation Model	DLR / Imperial College of London	Lagrangian parcel	Quantifying the contribution of volatile particles to contrail ice crystal numbers	(Ponsonby et al., 2025)
Microphysical Pyrcel	DLR / NASA	0D/1D Lagrangian	Jet-phase ice nucleation (<1s)	(Kärcher et al., 2015 ; Ponsonby et al., 2025)
Spichtinger Model	JGU Mainz / DLR	Advanced Microphysics	Competition between soot & ambient ice	(Spichtinger and Gierens, 2009)
Cirrus Transition Model	DLR	Cloud Dynamics	Linear-to-circular shape transition	(S. Unterstrasser, 2009 ; Unterstrasser and Gierens, 2010b)
Lagrangian Dynamical-Microphysical Model	DLR / NWRA	Lagrangian	Investigating physical controls on contrail lifetime statistics	(Bier et al., 2022)
EULAG-LCM	DLR	LES / Lagrangian	Vortex-phase crystal loss & survival	(S. Unterstrasser, 2009)
CoCiP	DLR	Lagrangian / Bulk	Life-cycle prediction & flight routing	(Schumann, 2012)
CocipGrid	Breakthrough Energy	4D spatiotemporal grid	Generate pre-computed global maps of Contrail Energy Forcing	(Engberg et al., 2025)
LCM-LES	DLR	High-Res Particle Tracking	Turbulence-microphysics interaction	(Unterstrasser and Sölch, 2010)
APCEMM	MIT	2-D Spectral Bin	Detailed chemistry & vertical advection	(Fritz et al., 2020)
ACM	DLR	Lagrangian parcel	Contrail ice formation on volatile particles	(Voigt et al., 2026)

532

533



534 Recent Advances have expanded these parameterizations to multi-wavelength applications (e.g., combining 355nm, 532nm,
535 and 1064nm) to retrieve crystal size distributions from spaceborne platforms like CALIPSO or EarthCARE. Its primary
536 Limitation is that it is non-predictive; it acts only as a translator between optical signals and physical shapes and cannot
537 simulate the time-evolution, formation, or atmospheric life cycle of the contrail itself ([Freudenthaler et al., 1996](#)).

538 The Plume Aerosol Model (frequently associated with the foundational work of Kärcher, Fahey, and Yu) functions as the
539 critical "initialization" module for contrail simulation, grounded in a Theoretical Foundation of Explicit Non-Equilibrium
540 Microphysics that governs the chaotic interaction between exhaust particulates and condensing vapors in the first few seconds
541 of plume evolution. This model captures the "Supersaturation Pulse," a violent transient event where the rapid mixing of hot
542 exhaust with cold ambient air drives the saturation ratios of water and sulfuric acid to extreme levels, forcing them to condense
543 onto hydrophobic soot particles. The model's Governing Equations couple the kinetic uptake rates of sulfuric acid (H_2SO_4)
544 and water vapor with the thermodynamic Kelvin Effect, calculating the precise energy barrier r_{crit} that a wetted soot particle
545 must overcome to "activate" into a freezing droplet; this determines the "Apparent Emission Index of Ice," or the fraction of
546 soot that successfully becomes a contrail. Recent Advances ([Yu et al., 2024a](#)) have adapted these schemes to account for
547 Sustainable Aviation Fuels (SAF) and hydrogen combustion, focusing on the formation of volatile particulate matter (vPM)
548 droplets in the absence of soot. However, the model is strictly bound by its Limitations, specifically its validity only within
549 the "jet regime" (0–100m behind the engine), as it neglects the macroscopic wake vortex dynamics and wind shear that
550 dominate the subsequent lifecycle of the contrail ([Kärcher et al., 1998](#)).

551 The Microphysical Parcel model simulate two distinct models specifically for particle activation in contrails: the extended K15
552 model, designed for efficient integration into global simulations, and the modified pyrce model, a high-fidelity benchmark
553 adapted from cloud physics to simulate isobaric mixing. The extended K15 model builds upon the framework by ([Kärcher et
554 al., 2015](#)) by introducing a third particle mode for vPM alongside soot and ambient particles and replacing analytical
555 approximations with exact numerical solutions ; however, because it omits the Kelvin effect in droplet growth equations, it
556 overestimates growth rates and systematically underpredicts peak plume supersaturations by 10%–70% compared to the
557 benchmark. In contrast, the modified pyrce model explicitly accounts for the Kelvin effect and homogeneous ice nucleation,
558 as well as kinetic vapor feedbacks like the Wegener-Bergeron-Findeisen process where growing ice crystals deplete moisture
559 from evaporating droplets which highlights the K15 model's inability to accurately simulate competition between particle types
560 in soot-rich regimes. While both models utilize Köhler theory ([Konopka and Vogelsberger, 1997](#)) to describe water saturation
561 , the authors caution that even the benchmark is limited by discretization errors of approximately $\pm 10\%$ and, more critically,
562 by the highly uncertain nature of prescribed volatile particle properties, necessitating urgent in situ validation to improve
563 accuracy ([Ponsonby et al., 2025](#)).

564 The Spichtinger Microphysics Scheme (developed by Peter Spichtinger and Klaus Gierens) is a specialized Double-Moment
565 ice nucleation code, built on a Theoretical Foundation of Competitive Nucleation Physics that rigorously models the
566 thermodynamic "tug-of-war" between Heterogeneous Nucleation (ice forming on soot) and Homogeneous Nucleation



567 (spontaneous freezing of liquid droplets below -38 C). The model simulates the "Supersaturation Pulse" as a competitive
568 event: as the air parcel cools, if soot-induced freezing occurs early and abundant crystals grow rapidly, they deplete the water
569 vapor—this "depletion effect" suppresses the supersaturation peak below the critical threshold ($S_{crit} \sim 1.5$) required for
570 homogeneous freezing. Its Governing Equations typically employ a two-moment approach, predicting both the Crystal
571 Number Density (N_c) and Ice Mass Mixing Ratio (q_c), while utilizing the Koop parameterization to calculate the stochastic
572 probability of liquid freezing based on water activity. Recent Advances have made this scheme central to Clean Aviation
573 research (e.g., hydrogen combustion), as it allows researchers to predict whether removing soot will eliminate contrails or
574 simply shift the formation mechanism to homogeneous freezing of background aerosols. However, its Limitations lie in its
575 high computational cost and complexity; it is rarely used as a standalone predictor but rather as an embedded microphysics
576 module within high-resolution LES codes like EULAG or COSMO ([Spichtinger and Gierens, 2009](#)).

577 The Cirrus Transition Model (often implemented via LES codes like *Méso-NH* or *EULAG*) addresses the critical Dispersion
578 Phase of contrail evolution, grounded in a Theoretical Foundation of Shear-Driven Turbulence and Radiative Transfer that
579 governs the transformation of a linear contrail into a diffuse cirrus cloud. Unlike early-stage models, it views the
580 Supersaturation Pulse not as a formation event, but as a maintenance mechanism driven by localized updrafts; as the ice crystals
581 absorb upwelling terrestrial infrared radiation, they heat the air inside the contrail, creating a "secondary circulation" or buoyant
582 rise that generates fresh supersaturation and sustains crystal growth against sublimation. Its Governing Equations couple the
583 Navier-Stokes equations for atmospheric turbulence with the Radiative Transfer Equation (RTE), explicitly solving for the
584 Optical Depth (τ) evolution and the vertical spread caused by wind shear (dU/dz). Advances by ([R.Paoli, 2002](#)) and
585 ([Unterstrasser and Sölch, 2010](#)) have incorporated synoptic-scale forcing"into these models, allowing researchers to simulate
586 how contrails originating in the same corridor merge into contrail outbreaks or homogeneous cirrus decks over hours. However,
587 the model faces significant Limitations due to its computational intensity; resolving the turbulent eddies across a domain large
588 enough to capture dispersion (10–50 km) requires massive resources, restricting its use to fundamental process studies rather
589 than operational global forecasting ([S. Unterstrasser, 2009](#); [Unterstrasser and Gierens, 2010b](#)).

590 This Lagrangian Dynamical-Microphysical Model microphysical model was developed by Bernd Kärcher at DLR and Milena
591 Corcos at NorthWest Research Associates (USA) in 2025. The authors devised a quasi-one-dimensional, Lagrangian
592 dynamical-microphysical model to investigate the lifetime statistics of persistent contrails. The methodology involves
593 initializing a contrail layer with a specific ice crystal size distribution and tracking the evolution of "Simulation Ice Particles"
594 (SIPs) as they undergo entrainment, dilution, depositional growth, sublimation, and gravitational settling. A key innovation is
595 the inclusion of stochastic vertical wind forcing to represent synoptic motions, mesoscale gravity waves, and microscale
596 turbulence, which drives rapid fluctuations in supersaturation. A primary limitation of this model is the assumption of a
597 vertically homogeneous layer, which neglects vertical variations in temperature and pressure, as well as the exclusion of wind
598 shear effects and internal radiative heating, which could potentially prolong contrail lifetimes ([Kärcher and Corcos, 2025](#)).



599 The Unterstrasser-Gierens Model (formally *EULAG-LCM*) represents the gold standard for the Vortex Phase of contrail
600 evolution, distinguished by a Theoretical Foundation of LES coupled with Lagrangian Particle Tracking that resolves the
601 complex 3D interaction between fluid dynamics and ice microphysics. Unlike simpler models that assume a static plume, this
602 model simulates the Supersaturation Pulse as a spatially heterogeneous event that is often violently reversed; it captures the
603 adiabatic compression caused by the aircraft's wake vortices dragging the exhaust plume downward (by 200–500m), which
604 generates localized heating that crushes the relative humidity and sublimates a significant portion of the ice crystals. Its
605 Governing Equations explicitly couple the anelastic or compressible Navier-Stokes equations (solved by the *EULAG* fluid
606 driver) with the Lagrangian trajectory equations for millions of individual simulation particles (SIPs), calculating the mass
607 evolution of each crystal based on its unique path through the turbulent, subsaturated vortex core. Recent Advances (e.g.,
608 Unterstrasser et al., 2020) have applied this framework to assess mitigation via formation flight (wake surfing) and the impact
609 of reduced soot emissions on crystal survival rates, fundamentally quantifying the Survival Fraction, the finding that up to
610 50% of crystals are destroyed in the first 3 minutes. However, the model is bound by Limitations of scale such as the extreme
611 computational cost of resolving fine-scale turbulence restricts its temporal scope to the first 5–10 minutes of flight, making it
612 unsuitable for simulating the hours-long dispersion or global radiative forcing of contrails ([S. Unterstrasser, 2009](#)).

613 The CoCiP Model, developed by DLR (Schumann et al.), stands as the operational standard for global-scale assessment, built
614 on a Theoretical Foundation of Lagrangian Particle Tracking coupled with a Gaussian Puff approximation that prioritizes
615 computational efficiency over microphysical granularity. Unlike explicit parcel models that resolve the initial Supersaturation
616 Pulse directly, CoCiP treats the formation event parametrically typically utilizing the SAC to trigger formation and relying on
617 sub-grid parameterizations (e.g., Kärcher et al.) to determine the initial ice crystal number thereby bypassing the millisecond
618 scale physics to focus on the macroscopic lifecycle. Its Governing Equations employ a bulk microphysics scheme that tracks
619 only two prognostic variables per flight segment. Total Ice Water Content (IWC) and Crystal Number (N_{ice})—evolving them
620 via simplified integral equations for depositional growth, sedimentation loss, and turbulent mixing, while the plume's spatial
621 extent is defined by analytically updating the Gaussian width (σ_y) and depth (σ_z). Recent Advances (e.g., Teoh et al., 2024;
622 Breakthrough Energy trials) have coupled CoCiP with real-time flight data and high-resolution reanalysis (ERA5) to validate
623 contrail avoidance strategies and estimate ERF for entire aviation fleets. However, the model is fundamentally constrained by
624 its Limitations, particularly the Gaussian assumption which enforces a simplified elliptical cross-section, rendering it incapable
625 of simulating complex internal structures like fall streaks, bi-modal size distributions, or the asymmetric shearing effects
626 critical for precise optical depth calculations ([Schumann, 2012](#)).

627 This CoCiP grid-based microphysical model was developed by Zebediah Engberg, and Roger Teoh, at Breakthrough Energy
628 (USA) and Imperial College London (UK) in 2025. The authors extended the existing Lagrangian CoCiP framework into a
629 grid-based forecasting tool (CocipGrid) to facilitate integration with air traffic management systems. The methodology
630 involves initializing infinitesimal contrail segments at every point in a 4D spatiotemporal grid and simulating their full
631 microphysical evolution including wake vortex dynamics, ice crystal survival, and radiative forcing using numerical weather



632 prediction inputs (e.g., ECMWF/ERA5). To maintain computational efficiency for operational use, the model categorizes
633 aircraft into simplified groups (e.g., N=3) based on mass and emissions. A primary limitation of this approach is that
634 simplifying the diverse global fleet into fewer aircraft-engine groups introduces prediction errors (approximately 13% for
635 N=3), and the model remains highly sensitive to biases in the forecast humidity fields ([Engberg et al., 2025](#)).

636 The Lagrangian Cloud Module (LCM-LES) (exemplified by codes like *EULAG-LCM* or the simpler LCM coupled to
637 COSMO) represents the theoretical pinnacle of microphysical fidelity, established on a Theoretical Foundation of Hybrid
638 Eulerian-Lagrangian Dynamics that discards the traditional grid-based approach for ice physics to instead track the individual
639 histories of millions of SIPs. Unlike bulk models that average the Supersaturation Pulse across a grid cell, the LCM resolves
640 the pulse as a unique, spatially heterogeneous experience for every crystal; it captures the stochastic nature of turbulent
641 fluctuations where two nearby particles might experience completely different growth histories due to sub-grid eddies. Its
642 Governing Equations are bifurcated: the 3D wind field is solved via the Eulerian Navier-Stokes equations, while the ice phase
643 is governed by Lagrangian trajectory equations and explicit mass growth equations calculated along these trajectories,
644 effectively eliminating the numerical diffusion errors that blur cloud edges in grid models.

645
$$\frac{d\vec{x}}{dt} = \vec{u} \quad (16)$$

646 Recent Advances (e.g., Sölch & Kärcher, Unterstrasser) have leveraged this method to resolve the entrainment interface, the
647 exact boundary where dry air mixes into the plume providing the first detailed quantification of how turbulence spectrums
648 influence crystal size distribution broadening and optical depth. However, this precision comes with severe Limitations in
649 computational scalability; the memory and processing power required to track millions of SIPs restrict its application to
650 fundamental process studies on supercomputers, rendering it infeasible for real-time forecasting or global climate simulations
651 ([Unterstrasser and Sölch, 2010](#)).

652 The APCEMM (Aircraft Plume Chemistry, Emissions, and Microphysics Model), developed by MIT (Fritz et al., 2020),
653 occupies a critical intermediate fidelity niche, distinguished by its Theoretical Foundation of 2-D Spectral Bin Microphysics
654 that bridges the gap between simple box models and expensive LES. Unlike 0-D models that homogenize the plume,
655 APCEMM simulates a cross-sectional slice perpendicular to the flight path, allowing it to resolve the "Supersaturation Pulse"
656 spatially; it captures how the pulse decays faster at the plume edges due to entrainment while persisting in the core, a gradient
657 essential for accurate crystal survival rates. Its Governing Equations explicitly solve the Smoluchowski Coagulation Equation
658 for roughly 40 discrete size bins (spanning from nanometers to 50+ microns), coupling this microphysics with a detailed
659 chemical solver that tracks the heterogeneous uptake of species like HNO₃ and SO₂ on ice surfaces. Recent Advances have
660 leveraged this structure to simulate precipitation plumes (fall-streaks) where large crystals settle out of the contrail core
661 providing the first computationally efficient method to quantify how these falling crystals dehydrate the upper troposphere and
662 alter local cirrus properties. However, the model retains specific Limitations tied to its dimensionality; by assuming the



663 atmosphere is uniform along the flight track (the infinite cylinder assumption), it cannot account for variations in weather
664 conditions, wind shear changes, or vortex instabilities that occur along the length of a single flight segment ([Fritz et al., 2020](#)).
665 Microphysical Activation Model study was published by Joel Ponsonby, Roger Teoh, Bernd Kärcher, and Marc E. J. Stettler
666 at Imperial College London and DLR Oberpfaffenhofen in 2025. The authors updated a microphysical model to challenge the
667 prevailing assumption in global simulations that only nvPM and ambient aerosols act as condensation nuclei for contrails. The
668 methodology involved extending the governing equations of particle activation to explicitly include vPM—ultrafine particles
669 formed from fuel sulfur and organic emissions—and benchmarking this updated framework against more complex detailed
670 microphysical simulations. The study demonstrated that vPM can contribute significantly to ice crystal numbers, particularly
671 in low-soot emission scenarios (e.g., using Sustainable Aviation Fuels), thereby altering the optical properties and radiative
672 forcing of the resulting contrails. A primary limitation is the increased complexity required to model the formation and growth
673 of these volatile modes, which depends heavily on accurate characterization of fuel sulfur content and organic emission indices
674 ([Ponsonby et al., 2025](#)).

675 The ACM (Aerosol and Contrail Microphysics) model, originally developed by Fangqun Yu and Richard Turco in the late
676 1990s ([Yu and Turco, 1997, 1998](#)) and substantially extended for the ([Voigt et al., 2026](#)) study, occupies a critical niche as a
677 Lagrangian parcel model that explicitly simulates the formation and activation of volatile particles in aircraft exhaust plumes,
678 particularly in the low-soot regime characteristic of modern lean-burn engines. Unlike models that assume ice nucleation
679 occurs solely on emitted soot particles, ACM's theoretical foundation includes ion-mediated nucleation, binary homogeneous
680 nucleation of H₂SO₄-H₂O, condensation of low-volatility organic vapours from unburned fuel, and nucleation of lubrication
681 oil vapours vented into the hot core flow. The governing equations track the evolution of particle number and size distributions
682 across multiple modes (soot, volatile sulfate, organics, and oil droplets) coupled to plume dilution, adiabatic cooling, and ice
683 nucleation via immersion freezing or homogeneous freezing of deliquesced volatile particles. A key recent advance, as reported
684 in ([Voigt et al., 2026](#)), was the ability of ACM to reproduce measured contrail ice number emission indices ($\approx 10^{15}$ kg⁻¹) behind
685 an A321 neo with LEAP-1A lean-burn engines, despite soot emissions being three orders of magnitude lower ($\approx 10^{12}$ kg⁻¹).
686 The model demonstrated that volatile particles formed from fuel sulfur (192 ppm) dominate ice nucleation in the low-soot
687 regime, and that for ultralow-sulfur fuels (2–3 ppm), lubrication oil and organic vapours become the primary ice-nucleating
688 sources. However, the model retains limitations tied to its zero-dimensional nature: it assumes homogeneous dilution of the
689 plume within a Lagrangian parcel, does not resolve spatial gradients such as vortex dynamics or entrainment at plume edges,
690 and its predictions depend heavily on uncertain emission indices for organic compounds and lubrication oil vapours, which
691 are not routinely measured in flight campaigns ([Voigt et al., 2026](#)).

692 3.3 NWP Integrated models

693 NWP integrated models form an essential category within the broader hierarchy of contrail prediction systems. These models
694 embed thermodynamic criteria and simplified microphysical processes into global and regional weather forecasting



695 frameworks. Unlike box or Lagrangian models which offer high-resolution but spatially limited simulations, NWP-based
696 systems operate over continental to global domains and exploit real-time meteorological inputs, enabling spatially and
697 temporally consistent evaluations of contrail formation across diverse atmospheric conditions. Table 7 provides a
698 representative list of these NWP-integrated systems, ranging from global climate models (ECHAM5, CAM5, UKMO UM) to
699 operational forecast models (ECMWF IFS, GFS, ICON) and commercial flight-planning tools (AVTECH, Flightkeys). Their
700 strengths lie in scalability, data assimilation capabilities, and compatibility with long-term climate modeling and operational
701 forecasting systems. Table 7 summarizes NWP-integrated contrail prediction models developed at DLR, ECMWF, NOAA,
702 NCAR, and other institutions. These systems embed SAC diagnostics or simplified microphysics into global/regional weather
703 models to enable large-scale contrail forecasting, climate impact assessment, and operational avoidance trials. The ECHAM5-
704 CCMod (ECHAM5-Cirrus), developed at DLR in collaboration with the Max Planck Institute for Meteorology (MPI-M)
705 (notably by [Burkhardt and Kärcher, 2011](#)), represents a paradigm shift in aviation climate modeling as the first GCM to treat
706 Contrail Cirrus not as a static parameter but as a fully prognostic cloud class distinct from natural cirrus. Methodologically,
707 the model modifies the standard ECHAM5 two-moment microphysics scheme (originally from MPI-M) to introduce a new
708 prognostic variable—the contrail cirrus fractional coverage (b_{cc}) which allows the model to simulate the complete lifecycle of
709 aviation-induced cloudiness, from initial linear formation via the SAC to the shear-driven spreading into aged cirrus decks.
710 Technically, it solves specific transport equations for contrail ice mass and crystal number density, enabling the simulated
711 clouds to compete with natural cirrus for water vapor and evolve independently based on local thermodynamic conditions.
712 This approach led to the critical scientific advancement of quantifying that the global net radiative forcing of aged contrail
713 cirrus (approx. 50 mW/m²) is roughly nine times larger than that of line-shaped contrails alone, fundamentally redefining the
714 scope of aviation's climate impact. However, the model is constrained by significant limitations, primarily its coarse global
715 resolution (typically T42 or T63, which necessitates heavy reliance on sub-grid parameterizations to estimate the initial plume
716 expansion and makes it incapable of resolving individual flight tracks or regional corridor dynamics with high precision
717 [Burkhardt and Kärcher, 2011](#)).

718 The CAM5 / CESM (+ Contrail Module), primarily developed by researchers at the National Center for Atmospheric Research
719 (NCAR) (notably [Chen and Gettelman, 2013](#)), with contributions from MIT), approaches contrail simulation through a distinct
720 Methodology of Source Term Injection rather than creating a separate cloud class. Unlike the ECHAM approach which
721 isolates contrail ice, this model directly modifies the standard Morrison-Gottelman two-moment microphysics scheme to inject
722 specific bursts of ice crystals into the grid cells where aircraft fly, based on global emissions datasets and thermodynamic
723 criteria. Technically, this allows the model to rigorously simulate the "Indirect Effect"—the complex aerosol-cloud interaction
724 where the high number density of contrail ice crystals (N_{ice}) competes with natural cirrus clouds for the available supersaturated
725 water vapor. A key scientific advancement from this framework was the revelation of a dehydration effect, where persistent
726 contrails effectively starve nearby natural clouds of moisture, potentially reducing their optical thickness—a negative feedback
727 loop that simpler models often miss. However, the model faces inherent limitations related to its grid scale; because it injects



728 the ice into large grid boxes, it artificially smears narrow contrails instantly across a vast area, leading to potential inaccuracies
 729 in calculating the local optical depth and radiative forcing of young, line-shaped plumes ([Chen and Gettelman, 2013](#)).

730

Table 7 List of NWP-Integrated Contrail Prediction Models

Model System	Developer Institute	Methodology	Primary Role	Ref
ECHAM5-CCMod	DLR / MPI-M	Prognostic Cloud Class	Global Climate Impact	(Burkhardt and Kärcher, 2011)
CAM5 / CESM	NCAR / MIT	Source Term Injection	Aerosol-Cloud Interaction	(Chen and Gettelman, 2013)
UKMO UM	UK Met Office	Contrail Sheet Parameterization	Radiative Forcing Efficacy	(Rap et al., 2010)
ECMWF IFS	ECMWF	Operational SAC Diagnostic	Real-time Avoidance Trials	(Gruber et al., 2018 ; Forbes et al., 2011)
ICON-ART	DWD / KIT / MPI-M	Icosahedral-Nonhydrostatic	Global Chemistry & Soot Tracking	(Gruber et al., 2018 ; Rieger et al., 2015)
ICON-LEM	MPI-M / DWD	Large-Eddy Simulation	High-Res Process Physics	(Verma and Burkhardt, 2022)
ICON-WAWFOR	DLR	Statistical Diagnostic Modeling	Probabilistic Contrail Forecasting	(Von Bonhorst et al., 2025)
WRF-Chem	NCAR / NOAA	Regional High-Res Eulerian	Local Corridor Dynamics	(S. Gruber, 2015)
NASA GISS	NASA GISS	Empirical/GCM Parameterization	US Climate Policy	(Hansen et al., 2005)
ECHAM4	DLR / MPI-M	Diagnostic Parameterization	Historic Climate Baseline	(M. Ponater, 1996)
Process- Based GCM	DLR	Prognostic simulation of contrail life cycle, spreading, and microphysics	Sensitive to optical depth thresholds and air traffic inventory quality	(Burkhardt and Kärcher, 2009)
GFS + SAC	NCEP (NOAA)	Global Diagnostic Post-process	Global Flight Planning	(Yoo and Li, 2012)
MM5	PSU / NCAR	Mesoscale Diagnostic	Regional Outbreak Studies	(Martin Stuffer, 2004 ; Carleton et al., 2008)
RUC-based	NASA	Estimates coverage (2005) and predicts probabilistic occurrence (2009)	diagnose and estimate regional persistent contrail coverage	(Duda et al., 2005 ; Duda and Minnis, 2009)
AVTECH Contrail Prediction	AVTECH/ KTH	Integrates SAC with real-time weather forecasts into a vertical trajectory optimize	operational tool for commercial airlines to minimize persistent contrails	(Kundgol et al., 2025)
Flightkeys 5D Contrail	Flightkeys / Breakthrough Energy	Integrates CoCiP and ECMWF into the Flightkeys 5D flight planning system	pre-tactical contrail avoidance	(Martin Frias et al., 2024)
OpenSky Contrail Estimation	TU Delft	SAC applied to interpolated ERA5 data	Rapid, scalable diagnostic tool for flight trajectory analysis	(Sun and Roosenbrand, 2023)
Fu-Liou RTM coupled with ECMWF and AERO2k data	University of Reading (UK)	Radiative transfer calculations applied to NWP-derived contrail maps	Assessing the climate impact of changing flight cruise altitude	(Rädel and Shine, 2008)
CoAtSaC	Google Research	Temporal clustering of advected tracks using RANSAC optimization	Automating the attribution of satellite-observed contrails to the specific flights that formed them	(Sarna et al., 2025)



731 The UKMO UM (Unified Model) with its contrail parameterization, developed primarily by the UK Met Office in
732 collaboration with the University of Leeds (notably ([Rap et al., 2010](#))), stands as a distinct Aerosol Climate approach to aviation
733 simulation. Methodologically, rather than simply injecting ice water like CESM, the model integrates a specialized "contrail
734 sheet" parameterization directly into its Edwards Slingo radiation scheme; it diagnoses the potential coverage of line-shaped
735 contrails based on the Schmidt-Appleman Criterion and traffic density, but crucially treats this coverage as a separate cloud
736 layer for radiative transfer calculations to avoid the overlap error common in other GCMs. Technically, the model is often
737 coupled with the UKCA (UK Chemistry and Aerosols) module, enabling it to rigorously simulate the microphysical link
738 between aviation soot emissions (number density) and the optical depth of the resulting ice crystals, using specific scaling
739 factors to account for the smaller crystal size of contrails compared to natural cirrus. A key scientific advancement from this
740 system was its robust quantification of the efficacy of contrail forcing demonstrating that a Watt of forcing from contrails
741 produces a different surface temperature response than a Watt of forcing from CO₂, largely due to the specific vertical profile
742 of heating. However, it is subject to limitations, particularly its reliance on diagnostic traffic inventories which are often static
743 time-slices, and the computational expense of the full UKCA chemistry package, which restricts the model's ability to run
744 high-resolution, multi-decadal simulations for rapid policy assessment ([Rap et al., 2010](#)).

745 The ECMWF IFS (Integrated Forecasting System), developed and operated by the ECMWF (Reading, UK / Bonn, Germany),
746 stands as the undisputed global standard for Operational Contrail Forecasting, serving as the meteorological engine behind
747 recent high-profile avoidance trials (e.g., with Breakthrough Energy and Google). Methodologically, the model distinguishes
748 itself by its superior handling of ISSR within its prognostic cloud scheme (originally based on Tiedtke/Tompkins); unlike
749 lower-fidelity models that immediately convert supersaturation into natural cirrus, the IFS is tuned to sustain high humidity
750 levels in clear air, enabling it to accurately map the Potential Contrail Cirrus Coverage that aircraft will encounter. Technically,
751 the operational implementation employs a diagnostic post-processing (or semi-prognostic) approach that applies the SAC to
752 high-resolution thermodynamic fields (HRES, currently ~9 km resolution), calculating the specific critical temperature at every
753 flight level to determine if exhaust plumes will persist. A major scientific advancement has been the recent integration of these
754 persistent contrail maps into real-time flight planning software, demonstrating the first viable climatological to operational
755 bridge for contrail mitigation. However, it faces limitations typical of operational constraints; the standard forecast output is
756 often diagnostic (a snapshot of potential formation) rather than fully prognostic (tracking the drift and aging of the contrail
757 over hours), and its bulk microphysics cannot resolve the specific optical depth variations caused by different engine soot
758 profiles without external parameterizations ([Forbes et al., 2011](#)).

759 The ICON-ART (ICOsahedral Nonhydrostatic model with Aerosols and Reactive Trace gases), developed through a
760 partnership between the German Weather Service (DWD), the MPI-M, and the Karlsruhe Institute of Technology (KIT),
761 represents the next generation of unified atmospheric modeling for both weather and climate. Methodologically, the system
762 replaces the traditional latitude-longitude grid with an icosahedral-triangular Arakawa-C grid, which provides exact local mass
763 conservation and eliminates the "pole problem" inherent in older global models. Technically, ICON-ART integrates the ART



764 module to resolve the lifecycle of aerosols (including aviation soot) and their chemical interactions online, utilizing a state of
765 the art two moment cloud ice microphysics scheme that explicitly predicts both ice mass and crystal number density to
766 skillfully resolve ISSRs. A significant scientific advancement of this model is its two-way coupling capability, where the
767 model can exchange variables with the CoCiP to account for direct contrail-weather interactions, such as the local warming of
768 ambient air and the butterfly effect where contrail-induced disturbances alter subsequent weather patterns. However, it faces
769 limitations related to computational complexity; the high numerical cost of its non-hydrostatic core and detailed aerosol-
770 chemistry modules often requires a trade-off between the length of the simulation and the horizontal resolution, and like other
771 NWP systems, it still relies on subgrid scale parameterizations for processes like homogeneous ice nucleation which can be
772 sensitive to unresolved vertical velocity fluctuations ([Rap et al., 2010](#)).

773 The ICON-LEM (ICOsahedral Non-hydrostatic Large-Eddy Model), developed by MPI-M and the DWD (with specialized
774 contrail implementations by Verma and Burkhardt, 2022), serves as a high-fidelity cloud-resolving atmospheric model. Unlike
775 coarse NWP models, it is built on a Theoretical Foundation of Resolved Large-Eddy Dynamics, where the most energy-
776 containing turbulent motions are explicitly calculated rather than parameterized. Methodologically, the system solves the non-
777 hydrostatic equations on a triangular icosahedral grid, typically at horizontal resolutions ranging from 156 m to 625 m. This
778 allows for the Scientific Advancement of simulating contrails within complex, heterogeneous environments, such as pre-
779 existing natural cirrus clouds. Technically, the model implements a specialized contrail parameterization that accounts for ice
780 nucleation in the jet phase and ice crystal survival during the vortex phase, while uniquely considering how "contrail-on-cirrus"
781 interactions (e.g., the sublimation of natural ice in the engine and competition for water vapor) alter the resulting cloud's optical
782 depth. However, its Limitations are centered on its massive computational demand; while it can be run in "weather forecasting
783 mode" for specific regional domains (e.g., over Germany), it is currently too resource-intensive to serve as a global operational
784 forecast tool or for multi-year climate assessments ([Verma and Burkhardt, 2022](#)).

785 The ICON-WAWFOR forecast evaluation study was conducted by Georg von Bonhorst, at DLR in 2025. The authors
786 investigated the reliability of contrail predictions under realistic operational conditions using the WAWFOR (World Aviation
787 Weather Forecast) dataset produced by the global ICON numerical weather prediction model. The methodology compared
788 two different cloud microphysics schemes—a standard one-moment scheme and a more complex two-moment scheme—to
789 assess their ability to forecast ISSR. By validating against high-resolution radiosonde data, the study demonstrated that even
790 advanced NWP models suffer from the Double Penalty problem, where predicted features are spatially or temporally shifted
791 from reality. Consequently, the authors conclude that precise, trajectory-based contrail avoidance is currently unrealistic due
792 to these non-linear forecast errors; instead, avoidance strategies should focus on broader zones of potential contrail formation
793 ([Von Bonhorst et al., 2025](#)).

794 The WRF-Chem (Weather Research and Forecasting with Chemistry) model, developed by a broad consortium led by the
795 National Center for Atmospheric Research (NCAR) and the National Oceanic and Atmospheric Administration (NOAA) (with
796 specific contrail implementations by researchers such as Gruber et al. and Unterstrasser), serves as the premier tool for



797 Regional Scale contrail assessment. Methodologically, unlike global models that must parameterize the entire world at coarse
798 resolution, WRF-Chem employs a high-resolution Eulerian grid (typically 1–5 km) to simulate specific high-traffic flight
799 corridors (e.g., Central Europe or the North Atlantic) with convection permitting fidelity. Technically, the model integrates
800 contrail physics by modifying advanced microphysics schemes such as the Morrison 2 moment scheme to include a prognostic
801 source term for aircraft ice; when a flight track intersects a grid cell satisfying the SAC, the model injects a precise mass and
802 number of ice crystals directly into the cloud variables, allowing them to interact online with local mesoscale dynamics like
803 gravity waves and frontal systems. A key scientific advancement of this framework is its ability to validate satellite
804 observations directly because it resolves the exact weather patterns at the time of flight, it allows researchers to perform point
805 to point comparisons with Lidar or camera data from campaigns like *ML-CIRRUS*, which is impossible with statistical global
806 models. However, it is constrained by limitations of scope; as a limited-area model, it relies on external global models for its
807 lateral boundary conditions and cannot capture the global climate feedback loops or the long-range inter-hemispheric transport
808 of aviation pollutants ([S. Gruber, 2015](#)).

809 The NASA GISS ModelE, developed by the NASA Goddard Institute for Space Studies (GISS) in New York, represents a
810 cornerstone of U.S. climate research, used extensively in IPCC assessments to quantify the global radiative forcing of aviation.
811 Methodologically, the model utilizes an Empirical Statistical Parameterization that differs from European prognostic
812 approaches; it defines the potential for contrail formation and persistence using the SAC but scales the resulting coverage and
813 optical depth based on high-resolution satellite correlations (e.g., from MODIS and CALIPSO data). Technically, the model
814 represents contrails as a diagnostic cloud fraction within its grid boxes, where the ice water content and effective radius are
815 constrained by local temperature and humidity fields, allowing the contrails to participate in the model's full radiative transfer
816 calculations. A major scientific advancement of ModelE has been its focus on Climate Sensitivity; by performing perturbed-
817 parameter ensemble runs, NASA researchers (notably Rind, Minnis, and Diederhoven) have been able to isolate the
818 hemispheric asymmetry of contrail warming, showing that the concentrated flight corridors of the Northern Hemisphere drive
819 a disproportionate surface temperature response compared to uniform greenhouse gas forcing. However, the model faces
820 inherent limitations, primarily its reliance on prescribed traffic inventories and its diagnostic nature, which means it cannot
821 fully simulate the dynamic "spreading" of a single contrail over multiple hours into a sprawling cirrus deck contrail cirrus
822 without simplified statistical scaling factors ([Hansen et al., 2005](#)).

823 The ECHAM4(+Contrail Parameterization), developed at the DLR (notably by Ponater et al., 2002) in conjunction with the
824 MPI-M, represents the foundational era of global contrail climate modeling. Methodologically, the model treats contrails
825 through a diagnostic parameterization rather than a separate cloud class; it calculates potential contrail coverage based on the
826 SAC and local humidity, then scales this by a time-dependent air traffic density inventory to estimate actual coverage.
827 Technically, the model introduces a sub-grid scale modification to the cloudiness parameterization, allowing a grid box to
828 contain both natural clouds and a linear contrail fraction, which influences the radiative transfer code. A major scientific
829 advancement provided by this system was the first comprehensive global estimate of Radiative Forcing (RF) from line-shaped



830 contrails, providing the baseline figure of approx. 3.5 to 10 mW/m² that served as the primary reference for the IPCC Special
831 Report on Aviation. However, the model is subject to significant limitations, specifically its memoryless nature; because it
832 lacks a prognostic variable for contrails, it cannot simulate the advection, spreading, or aging of contrails into cirrus clouds
833 effectively ignoring the vast majority of aviation's warming impact that occurs after the initial linear phase ([M. Ponater, 1996](#)).
834 The Process-based Contrail Cirrus Parameterization (ECHAM4 GCM) was developed by Ulrike Burkhardt and Bernd Kärcher
835 at the DLR in 2009. The authors developed a novel parameterization scheme within the ECHAM4 general circulation model
836 that introduces contrail cirrus as a separate, prognostic cloud class. The methodology simulates the entire life cycle of contrails,
837 initializing them based on thermodynamic formation criteria and calculating their evolution as they spread due to wind shear
838 and grow within fractional ice-supersaturated areas. This approach allows the model to capture the transition from young line-
839 shaped contrails to aged contrail cirrus and their interaction with the global water budget. A key limitation of this model is that
840 the global distribution of young contrail coverage tends to be smoothed out due to grid-scale transport, and the accuracy is
841 fundamentally limited by the host model's ability to represent upper-tropospheric humidity and sub-grid scale supersaturation
842 ([Burkhardt and Kärcher, 2009](#)).

843 The GFS+SAC (Global Forecast System+SAC) represents the primary operational diagnostic tool for the aviation industry,
844 developed and maintained by the National Centers for Environmental Prediction (NCEP) under the NOAA. Methodologically,
845 the system does not function as a standalone microphysical model but rather as a post processing algorithm that applies the
846 classic thermodynamic mixing equations of the SAC to the 3D output fields (temperature, pressure, and relative humidity) of
847 the GFS weather model. Technically, the model evaluates the mixing line between hot, moist engine exhaust and cold ambient
848 air to determine if liquid saturation is reached (the formation condition) and subsequently checks if the environment is
849 supersaturated with respect to ice to predict contrail persistence. A significant scientific advancement of this system has been
850 its evolution from a course 1.0° grid to the current high-resolution 0.25° (approx. 28 km) spectral grid, coupled with ensemble
851 forecasting techniques (GEFS) that allow airlines to calculate Contrail Frequency Indices (CFI) and assign a probability of
852 persistence for specific flight routes. However, the system faces critical limitations, primarily the persistent humidity bias
853 found in most global NWP models; the GFS often struggles to accurately resolve the vertical depth and horizontal extent of
854 the thin, ISSRs layer where contrails live. Furthermore, because it is a diagnostic tool, it cannot simulate the prognostic
855 lifecycle of the contrail—such as its drift, transition into a cirrus deck, or its complex radiative feedbacks making it useful for
856 immediate flight planning but insufficient for long-term climate impact assessments ([Yoo and Li, 2012](#)).

857 The MM5+SAC (Fifth-Generation Penn State/NCAR Mesoscale Model + SAC) represents the foundational era of regional
858 NWP for aviation. Developed primarily by Pennsylvania State NCAR, this system was among the first to move contrail
859 prediction from simple global averages to high-resolution regional grids. Methodologically, the system functions as a
860 diagnostic tool where the MM5 serves as the atmospheric engine, providing high resolution 3D fields of temperature and
861 relative humidity. The SAC is then applied as a post-processing algorithm to these fields to calculate the thermodynamic
862 mixing of aircraft exhaust with the environment. Technically, the model solves non-hydrostatic, terrain-following equations



863 that allow it to resolve mesoscale features (like mountain waves or local fronts) which dictate the formation of ISSRs. A
864 significant scientific advancement was the application of Arctic MM5 and other regional versions to study specific contrail
865 outbreaks over areas like Alaska and the contiguous US, proving that regional NWP could achieve a high probability of
866 detection (over 80% in some studies) by accurately capturing synoptic-scale humidity variations. However, the system faces
867 notable limitations: as a precursor to the modern WRF model, its microphysics are less sophisticated, often leading to threshold
868 errors where small inaccuracies in humidity lead to binary (yes/no) failures in predicting persistence. Furthermore, in its
869 standard SAC diagnostic form, it does not track the life cycle of the contrail (drift, spreading, or sublimation) but rather
870 provides a "snapshot" of potential formation at a single point in time ([Martin Stuffer, 2004](#); [Carleton et al., 2008](#)).

871 The Rapid Update Cycle (RUC) NWP-integrated diagnostic model was developed by David P. Duda at the NASA Langley
872 Research Center in 2005. The authors developed a method to estimate persistent contrail coverage over the United States by
873 integrating commercial air traffic data with hourly meteorological analyses from the RUC numerical weather prediction model.
874 The methodology calculates Potential Contrail Frequency based on modified Appleman thermodynamic criteria within the
875 RUC model grid, and then converts this to contrail coverage using air traffic density data. The model was tuned empirically
876 by comparing the results against satellite-derived contrail coverage from NOAA-16 AVHRR data, leading the authors to
877 conclude that a fourth root relationship between flight path length and contrail coverage provided the most accurate results. A
878 primary limitation of this model is its dependence on the accuracy of the underlying NWP humidity fields, which suffer from
879 a known dry bias, as well as uncertainties inherent in the satellite observations used for tuning and the lack of military air
880 traffic data ([Duda et al., 2005](#)).

881 The evolving body of diagnostic modeling was developed by David P. Duda at NASA Langley Research Center and the
882 National Institute of Aerospace between 2005 and 2009. The initial 2005 methodology integrated commercial air traffic data
883 with hourly Rapid Update Cycle (RUC) meteorological analyses to estimate persistent contrail coverage, utilizing a modified
884 Appleman criterion. This model was empirically tuned against NOAA-16 AVHRR satellite data, establishing a fourth root
885 relationship between flight path length and contrail coverage ([Duda et al., 2005](#)). In 2009, the authors refined this into a
886 probabilistic forecasting methodology by applying logistic regression to high-resolution RUC and Advanced Regional
887 Prediction System (ARPS) analyses. This study derived distinct "SURFACE" (ground-observation based) and "OUTBREAK"
888 (satellite-observation based) models, identifying upper-tropospheric temperature, humidity, and wind direction as key
889 predictors. A primary limitation of this collective framework is its purely diagnostic nature—predicting occurrence at fixed
890 locations without explicitly modeling physical advection or spreading—and its sensitivity to known dry biases in the
891 underlying NWP humidity fields ([Duda and Minnis, 2009](#)).

892 This AVTECH prediction and optimization Model was developed by Chirag Bipinchandra Kundgol, and David Rytter, at KTH
893 Royal Institute of Technology and AVTECH Sweden AB in 2025. The authors presented a real-time contrail management tool
894 designed for commercial airline fleets. The methodology calculates the critical temperature for contrail formation using the
895 SAC Criteria applied to high-resolution weather forecasts from the UK Met Office. These predictions are integrated into a



896 Dynamic Programming (DP) algorithm that optimizes the aircraft's vertical flight profile to minimize a combined cost function
897 of fuel, time, and contrail persistence. A primary limitation of this model is its direct dependence on the accuracy of the
898 underlying weather forecast data (particularly relative humidity). additionally, the current iteration focuses only on avoiding
899 persistent contrails without calculating their specific radiative forcing or climate impact ([Kundgol et al., 2025](#)).

900 The Flightkeys 5D Contrail operational analysis was conducted by Alejandra Martin Frias and Marc Shapiro, at Flightkeys
901 (Austria) and Breakthrough Energy (USA) in 2024. The authors integrated the CoCiP model (via the Contrails API) into the
902 Flightkeys 5D (FK5D) commercial flight planning system to evaluate the feasibility and cost of contrail avoidance. The
903 methodology involved simulating 84,839 American Airlines flights from June 2023 and January 2024 using ECMWF HRES
904 weather forecasts to identify regions of high contrail energy forcing. Flights predicted to form warming contrails were re-
905 optimized using *Dijkstra's and A algorithms** to navigate around these regions (defined as hard constraints). The study found
906 that navigational avoidance could reduce contrail energy forcing by approximately 73% with a minimal increase in fuel
907 (0.11%) and total cost (0.08%). A primary limitation of this study was the use of simplified "hard" avoidance polygons, which
908 may be less efficient than a continuous cost-based optimization approach ([Martin Frias et al., 2024](#)).

909 OpenSky Contrail Estimation is a data-driven diagnostic study which was conducted by Junzi Sun and Esther J. Roosenbrand
910 at Delft University of Technology (TU Delft) in 2024. The authors presented a computationally efficient framework to estimate
911 persistent contrail formation by integrating open-source flight trajectories from the OpenSky Network with meteorological
912 reanalysis data from ERA5. The methodology applies the SAC implemented via the pycontrails Python library to high-
913 resolution ADS-B data, enabling large-scale assessments of contrail coverage without relying on proprietary airline flight
914 recorders. A primary limitation of this approach is its reliance on the spatiotemporal resolution and humidity accuracy of the
915 ERA5 dataset, which limits the precision of individual flight-level predictions compared to models using higher-fidelity
916 weather inputs ([Sun and Roosenbrand, 2023](#)).

917 The radiative forcing assessment was conducted by Gaby Rädcl and Keith P. Shine at the Department of Meteorology,
918 University of Reading (UK) in 2008. The authors developed a framework to quantify the global RF of persistent contrails and
919 its sensitivity to cruise altitude changes. The methodology involved deriving global contrail coverage by combining the
920 AERO2k aviation emissions inventory (2002) with meteorological data from ECMWF analyses, using thermodynamic criteria
921 tuned to match independent satellite observations. These coverage maps were then processed through the Fu-Liou delta-4-
922 stream radiative transfer model to calculate Shortwave and Longwave effects. The study performed perturbation experiments,
923 increasing air traffic in 2,000 ft vertical layers and found that contrails formed at approximately 10 km (33,000 ft) altitude
924 produce the largest net radiative forcing per kilometer flown. A primary limitation of this model is the high uncertainty
925 (estimated at ~60%) resulting from the necessary assumptions regarding constant contrail optical depth and the scarcity of
926 global observational data for validation ([Rädcl and Shine, 2008](#)).

927 CoAtSaC (Contrail Attribution Sample Consensus) & SynthOpenContrails is a methodological study was conducted by Aaron
928 Sarna and Vincent Meijer at Google Research, TU Delft, and ONERA in 2025. The authors addressed the lack of ground truth



929 for contrail attribution by developing SynthOpenContrails, a large-scale synthetic dataset generated by filtering CoCiP
930 microphysical simulations to match the statistical properties of satellite observations. Furthermore, they introduced CoAtSaC,
931 a highly scalable attribution algorithm that employs RANSAC (Random Sample Consensus) to robustly identify physical
932 contrails by analyzing the temporal evolution of the "W" parameter (cross-track advection error). By grouping single-frame
933 matches that form coherent linear structures over time, the algorithm effectively distinguishes true flight sources from
934 coincidental overlaps. A primary limitation of this approach is its inability to attribute contrails detected in only a single
935 satellite frame (resulting in lower recall for short-lived contrails) and its inherent dependence on the accuracy of the ERA5
936 wind fields used for advection ([Sarna et al., 2025](#)).

937 **3.4 Satellite-Based and Empirical Models**

938 Satellite-based and empirical contrail prediction models have played a foundational role in mapping contrail occurrence,
939 validating physical simulations, and generating training datasets for AI development. Early efforts used thermal infrared
940 channels to detect linear contrails against natural cloud backgrounds, enabling the first contrail climatologies over North
941 America and Europe. Subsequent models incorporated automated detection algorithms, statistical regression methods, and
942 radiative transfer calculations to estimate contrail properties and their climate impacts. Despite their utility for large-scale and
943 long-term studies, these models generally lack vertical resolution, struggle to distinguish contrails from thin cirrus, and depend
944 heavily on manual validation or training data quality. Table 8 summarizes representative satellite-based and empirical contrail
945 models, including automated detection systems (Mannstein CDA, MODIS), empirical logistic regression, radiative forcing
946 estimators (Rapid Contrail-RF), multi-sensor cloud masks, and historical climatology products (DMSP, ACSM).

947 One of the earliest large-scale efforts was led by ([Minnis et al., 1998](#)), who used NOAA's AVHRR split-window infrared
948 channels to detect contrails based on brightness temperature differences (BTD) between 10.8 μm and 12.0 μm bands. These
949 models enabled the construction of contrail climatologies over North America and Europe but lacked vertical resolution and
950 struggled to distinguish contrails from overlapping cirrus. A similar approach was extended through AVHRR split-window
951 threshold algorithms, forming the basis for multiple empirical detection frameworks used during the 1980s and 1990s.

952 The MODIS-based contrail detection system developed by NASA Ames improved spatial and spectral resolution by
953 incorporating aircraft trajectory overlays and cloud phase information, supporting event-based analysis and radiative forcing
954 estimates. MODIS cirrus optical thickness algorithms, while not contrail-specific, have been adapted to estimate the
955 microphysical properties of persistent contrail cirrus. In geostationary orbit, GOES-based systems like the NASA GOES split-
956 window tracker and studies by ([Li et al., 2023a](#)), offered temporal continuity, enabling lifecycle monitoring of contrail
957 persistence and spreading, though resolution constraints and variable background conditions limit their reliability in tropical
958 and polar regions ([Li et al., 2023a](#)).

959 For vertical profiling, CALIOP lidar aboard CALIPSO introduced a major advancement by detecting contrails using
960 backscatter and depolarization ratio signatures. These measurements enabled studies like ([Burkhardt et al., 2010](#)) to compare
961 modeled contrail cirrus with observed vertical structures, thereby informing global climate models. However, CALIOP's low



962 temporal coverage (1–2 overpasses/day) and narrow swath limit real-time applications. More recently, VIIRS-based
963 experimental models and MISR angular radiance techniques have expanded detection capabilities through multi-angle and
964 multispectral sensing, providing improved estimates of contrail shape, albedo, and radiative impact ([Meyer et al., 2025](#)).
965 Similarly, SCIAMACHY contributed early spectral insights into cirrus-aerosol overlap, though not specifically optimized for
966 contrail analysis.

967 Operationally, NOAA and DoD have employed empirical contrail forecast products based on vertical profiles of RH_i and
968 temperature, derived from radiosonde and satellite data, to support aviation planning. These empirical forecasts remain in
969 limited use for military and strategic purposes. Importantly, many of these satellite-based models are now integrated into AI
970 workflows—MODIS and AVHRR data feed into neural networks developed by Teoh et al. and Zhang & Li, while CALIOP
971 vertical profiles have been used to benchmark CoCiP and PINN-based models. Additionally, synthetic datasets derived from
972 these satellite products are often used to validate hybrid AI-physics architectures such as GAIA and Google's recent
973 transformer-based platforms.

974 The Ames Contrail Simulation Model (ACSM) was developed by ([Li et al., 2023a](#)) at NASA Ames and Langley Research
975 Centers in 2023 . The authors designed the ACSM to support Strategic Traffic Flow Management (STFM) by providing a
976 computationally efficient tool to estimate the global climate impact of aviation. The methodology integrates the Schmidt-
977 Appleman Criterion for formation with Lagrangian particle advection equations to track contrail position and evolution driven
978 by RUC, RAP, or MERRA meteorological data. The model adapts the physics from the DLR CoCiP model but introduces
979 significant simplifications for speed: it models the contrail cross-section as a rectangle with uniform ice density (rather than a
980 Gaussian ellipsoid) and assumes all ice particles are spherical throughout their lifecycle. A primary limitation of ACSM is the
981 exclusion of explicit wake vortex downwash modeling; instead, it initializes contrails with fixed average dimensions and
982 neglects the specific sinking dynamics that affect early-stage ice crystal survival, while also relying on the inherent accuracy
983 of the input NWP humidity fields ([Li et al., 2023a](#)).

984 The empirical model to predict widespread occurrences of contrails was developed by lead author ([Travis et al., 1997](#)) from
985 the Department of Geography at the University of Wisconsin-Whitewater. This logistic regression model is designed to
986 forecast the probability of widespread contrail clusters outbreaks rather than individual plumes by analyzing specific
987 atmospheric conditions. The model calculates persistence probability using three statistically significant variables: the column-
988 integrated water vapor counts (WV) for the 700–100-mb layer derived from GOES 6.7 μ m satellite imagery, the interaction
989 between this moisture count and the mean 300–100-mb temperature (WVT) from NWS rawinsondes, and WVT² to account
990 for the non-linear middle range of conditions where contrails thrive. However, the model has several limitations. It becomes
991 less reliable for predicting small outbreaks (under 100 km), struggles with accuracy when contrails are located near or within
992 multilayered natural clouds, is highly sensitive to the low spatial density of rawinsonde temperature data, and cannot be easily
993 applied to regions lacking consistent data, such as coastal waters or outside national borders ([Travis et al., 1997](#)).



994 Mannstein Automated Contrail Detection Algorithm (CDA) is classical satellite detection algorithm was developed by
995 ([Mannstein et al., 2010](#)) at DLR in 1999. The authors presented a fully automated scheme to detect linear contrails using
996 infrared data from the Advanced Very High-Resolution Radiometer (AVHRR). The methodology utilizes the "split-window"
997 technique, exploiting the brightness temperature difference between the 11 μm and 12 μm channels to identify thin ice clouds,
998 followed by morphological filtering to isolate linear structures with specific width and length criteria. This algorithm was
999 applied to derive the first diurnal and seasonal climatologies of contrail coverage over Central Europe. A primary limitation
1000 of this approach is its deliberate tuning for a low false-alarm rate, which significantly reduces detection efficiency (missing
1001 optically very thin or non-linear aged contrails) and makes the derived coverage values lower bound estimates ([Mannstein et](#)
1002 [al., 2010](#)).

1003 CDA-MODIS is satellite-based observational study was conducted by ([Minnis et al., 2013](#)) at the NASA Langley Research
1004 Center in 2013. The authors sought to reduce the uncertainty in contrail climate forcing by quantifying the properties of contrail
1005 cirrus. the spreading, aged phase of contrails that is often missed by standard linear detection algorithms. The methodology
1006 involved analyzing 21 cases of spreading contrails using Terra and Aqua MODIS data; they applied a standard CDA to identify
1007 linear segments and manually tracked their evolution into irregular cirrus shapes. By retrieving microphysical properties from
1008 the satellite radiances, the study established that contrail cirrus has significantly higher optical depths (2–3 times) and larger
1009 effective particle sizes (20% larger) than the adjacent linear contrails, and that accounting for this spreading phase increases
1010 calculated contrail coverage by a factor of 2.4 to 7.6. A primary limitation of this method is the difficulty in automating the
1011 detection of these older, shapeless contrails, particularly in regions of dense air traffic where overlapping plumes reduce the
1012 sensitivity of current detection algorithms ([Minnis et al., 2013](#)).

1013 Rapid Contrail - RF is satellite based observational study which was conducted by ([Dimitropoulou et al., 2026](#)) at the Royal
1014 Meteorological Institute of Belgium in 2025. The authors developed a Rapid Contrail-RF Estimation Approach to quantify the
1015 radiative forcing of contrail cirrus using geostationary Meteosat Second Generation (MSG/SEVIRI) data. The methodology
1016 involved visually identifying days with intense contrail activity and utilizing the Optimal Cloud Analysis (OCA) product
1017 provided by EUMETSAT to retrieve ice cloud properties (optical thickness, effective radius, pressure). These observed
1018 properties were processed through Look-Up Tables (LUTs)—constructed using the libRadtran radiative transfer model—to
1019 compute Shortwave and Longwave fluxes, while a separation scheme was applied to isolate the specific radiative contribution
1020 of the contrails from natural cirrus. A primary limitation of this approach is its reliance on visual identification to select analysis
1021 days, which limits automation and global scalability, as well as the dependency on the accuracy of the OCA retrieval product
1022 which can have uncertainties for multi-layer or optically thin clouds([Dimitropoulou et al., 2026](#)) .

1023 The probabilistic detection model was developed by ([Musial et al., 2014](#)) at the University of Bern in 2014. The authors
1024 designed the Probabilistic Cloud Mask (PCM) to resolve the ambiguity of binary cloud masks by employing a
1025 multidimensional information space. The methodology involves constructing extensive Look-Up Tables (LUTs) where
1026 spectral features enhanced by an Invariant Coordinate System (ICS) transformation to improve thin cirrus and snow separation



1027 are binned alongside ancillary data (solar angles, texture, and land cover). Probabilities are derived by analyzing the frequency
1028 of cloud/snow occurrences within these bins based on a training dataset composed of PPS and MODIS masks. A primary
1029 limitation of this approach is the subjectivity involved in selecting binning intervals and the computational constraint on LUT
1030 size, which limits the resolution of the probability estimates, as well as the fact that the model's maximum accuracy is inherently
1031 capped by the quality of the reference masks used for training ([Musial et al., 2014](#)).

1032 Split Window Brightness Temperature Difference (BTD) is a satellite detection methodology developed by ([Lee, 1988](#)) at the
1033 Naval Environmental Prediction Research Facility (Monterey, California) in 1989. The author addressed the difficulty of
1034 detecting thin, narrow contrails in standard infrared imagery by utilizing the "Split Window" technique applied to AVHRR
1035 (Advanced Very High-Resolution Radiometer) data. The methodology involves co-registering digital data from Channel 4
1036 ($11\mu\text{m}$) and Channel 5 ($12\mu\text{m}$), converting raw gray shades to calibrated brightness temperatures, and subtracting the Channel
1037 5 value from the Channel 4 value to create a difference image. The study demonstrated that while the Earth's surface and thick
1038 clouds exhibit small temperature differences (+1 to +2 K), newly formed contrails and thin ice clouds show significantly larger
1039 positive differences (+2 to +6 K) due to the differential transmissivity of ice particles, making them appear bright against a
1040 dark background. A primary limitation of this technique is that natural thin cirrus clouds share similar spectral properties with
1041 contrails, making it difficult to distinguish anthropogenic plumes from natural high clouds solely based on brightness
1042 temperature differences without additional geometric analysis ([Lee, 1988](#)).

1043 MODIS Cloud Mask All Tests Consolidation (ATC) satellite validation study was conducted by Z̄aneta Nguyen Huu, at the
1044 Institute of Geography and Spatial Management, Jagiellonian University (Poland) in 2025. The authors evaluated the utility
1045 of the MODIS operational Cloud Mask (MYD35 Collection 6.1) for creating a global cirrus mask by validating it against 136
1046 million observations from the CALIOP lidar. To improve detection reliability, they introduced the ATC approach, which
1047 aggregates results from six standard spectral tests (including the $1.38\mu\text{m}$ "cirrus band" and $11\text{--}12\mu\text{m}$ split-window) into a
1048 unified boolean flag. The study established that while ATC achieves a Probability of Detection (POD) of roughly 81% during
1049 the daytime, it suffers from a high False Alarm Rate (FAR) of ~35% and performs significantly worse at night (POD ~25%)
1050 due to the unavailability of solar channels. A primary limitation of this framework is its inability to reliably detect optically
1051 thin cirrus ($\text{COT} < 0.4$), which active sensors like CALIOP easily identify, leading to a substantial underestimation of global
1052 nighttime cirrus coverage compared to lidar climatologies ([Nguyen Huu et al., 2025](#)).

1053 Defense Meteorological Satellite Program (DMSP) Contrail is an extensive climatological analysis conducted by James Q.
1054 DeGrand et al. at The Ohio State University, Pennsylvania State University, University of Wisconsin-Whitewater, and the
1055 University of Oklahoma in 2000. The authors developed a satellite-based climatic description of jet contrails over the
1056 contiguous United States by manually analyzing very high resolution (0.6 km) thermal-infrared imagery from the DMSP polar
1057 orbiters. The methodology involved the visual identification of contrails on hard-copy film strips for the midseason months
1058 (January, April, July, October) of the period 1977–1979, validating these observations against ground-based records to
1059 establish spatial distribution patterns. A primary limitation of this study is the inherent subjectivity of the manual identification



1060 technique and the restricted temporal coverage (limited to specific months and satellite overpass times), which prevents a
 1061 continuous assessment of diurnal or long-term trends ([Degrand et al., 2000](#)).
 1062 WFM-DOAS (Weighting Function Modified Differential Optical Absorption Spectroscopy) v2.1 is a satellite retrieval
 1063 validation study conducted by J. Heymann et al. at the Institute of Environmental Physics (IUP), University of Bremen in
 1064 2012. The authors assessed the global quality of the WFM-DOAS retrieval algorithm (version 2.1), which determines
 1065 atmospheric CO₂ columns from SCIAMACHY near-infrared spectra. The methodology involved minimizing the difference
 1066 between the logarithm of the measured sun-normalized radiance and a linearized radiative transfer model to retrieve vertical
 1067 column densities. These retrievals were then compared globally against the CarbonTracker model to quantify systematic
 1068 biases. The study found that while the retrieval captures the seasonal cycle well, it suffers from significant systematic errors
 1069 (typically underestimations) due to light path shortening by thin cirrus clouds and aerosols, necessitating rigorous filtering to
 1070 achieve sufficient accuracy for surface flux inversion.

1071 **Table 8 List of Satellite-Based and Empirical Contrail Prediction Models**

Model System	Developer Institute	Key Features	Limitations	Ref
ACSM	NASA	Full lifecycle simulation optimized for Strategic Traffic Flow Management	simplified rectangular cross-section; no wake vortex downwash modeling	(Li et al., 2023a)
Empirical Logistic Regression	1996/ David J. Travis	Predicts outbreak probability using GOES water vapor counts and rawinsonde temperatures via a non-linear equation.	Unreliable for small areas (<100 km), obscured by natural clouds, and sensitive to input data density	(Travis et al., 1997)
Mannstein Automated CDA	1999 / - DLR	Uses infrared brightness temperature difference (T ₄ - T ₅) and morphological line filters	Tuned for low false alarms resulting in low detection efficiency; misses wide/aged contrails	(Mannstein et al., 2010)
CDA-MODIS	2013 - NASA	Quantifies optical depth and particle size of spreading contrail cirrus	Reduced detection sensitivity in dense air traffic or overlapping cirrus	(Minnis et al., 2013)
Rapid Contrail-RF Estimation	2025 -RMI Belgium	Quantifies RF using geostationary OCA products and radiative transfer LUTs	Relies on manual visual identification; limited to specific case studies	(Dimitropoulou et al., 2026)
PCM Model	2014 / University of Bern	Provides continuous probability estimates for cloud, snow, and clear-sky	Accuracy limited by training data quality; LUT size constraints	(Musial et al., 2014)
Split Window BTD	1989 / Thomas F. Lee	Enhances contrail visibility by subtracting 12μm from 11μm radiances	Difficult to distinguish contrails from natural thin cirrus clouds	(Lee, 1988)
MODIS Cloud Mask	2025 / Nguyen Huu et al.	Validates passive cirrus detection using active lidar (CALIOP) ground truth	Low nighttime reliability; misses optically thin cirrus ($\tau < 0.4$)	(Nguyen Huu et al., 2025)
DMSP Contrail	2000 / DeGrand et al.	High-resolution (0.6 km) mid-season contrail climatology over the US	subjective manual identification; limited to 1977-79 mid-season months	(Degrand et al., 2000)
WFM-DOAS	2012 / Heymann et al.	Retrieves XCO ₂ from NIR spectra; assesses aerosol/cloud induced bias	Significant systematic errors (~1%) caused by thin cirrus and aerosols	(Heymann et al., 2012)



3.5 AI-Driven Contrail Prediction Models

In recent years, AI has emerged as a transformative paradigm for contrail prediction, enabling scalable, high-resolution, and near real-time modeling capabilities that extend beyond the limitations of traditional physics-based approaches. AI-driven models are particularly well suited to handling large, heterogeneous datasets—combining meteorological fields, flight trajectories, and satellite observations—while offering new pathways for operational contrail mitigation. These models range from computer vision systems for contrail detection in satellite imagery to random forest classifiers for formation probability, physics-informed neural networks that embed thermodynamic constraints, and deep learning architectures for altitude estimation and flight attribution. Table 9 summarizes representative AI-driven contrail models, including Google’s contrail forecast system, Eurocontrol’s Contrail Tracker, Imperial College’s random forest model, MIT–NOAA’s PINN, and various deep learning segmentation approaches (U-Net, EfficientNet, OpenContrails).

One of the earliest operational AI-based contrail prediction systems was introduced by (Engberg et al., 2025) who developed a Random Forest classifier trained on ERA5 meteorological reanalysis, aircraft trajectory data, and satellite-derived contrail labels. The model demonstrated practical applicability in real-time contrail avoidance strategies by identifying contrail-favorable atmospheric regions. Similarly, (Heni et al., 2025) proposed a feedforward neural network using ERA5 data and satellite observations to predict global contrail-prone regions. While effective at large scales, this approach remains constrained by its reliance on historical datasets and limited physical interpretability. A significant advance toward improving physical consistency in AI models was achieved through the introduction PINNs by (Raphael Alamu, 2025). By embedding thermodynamic constraints most notably the SAC directly into the learning architecture, these models reduced prediction errors relative to unconstrained deep networks while maintaining adherence to established contrail formation physics. However, PINNs introduce increased training complexity and sensitivity to hyperparameter selection, which remain active challenges. It is notable that many AI-driven contrail prediction frameworks including those developed by (Engberg et al., 2025), and Google rely heavily on global reanalysis datasets such as ERA5 or MERRA-2 as their meteorological backbones. Furthermore, established physical models, particularly the CoCiP, continue to serve as critical benchmarks and are frequently used to generate synthetic training data. As hybrid AI–physics frameworks mature, they offer a promising route to combining the interpretability of physical models with the scalability and adaptability of machine learning, enabling real-time contrail mitigation in next-generation flight management systems.

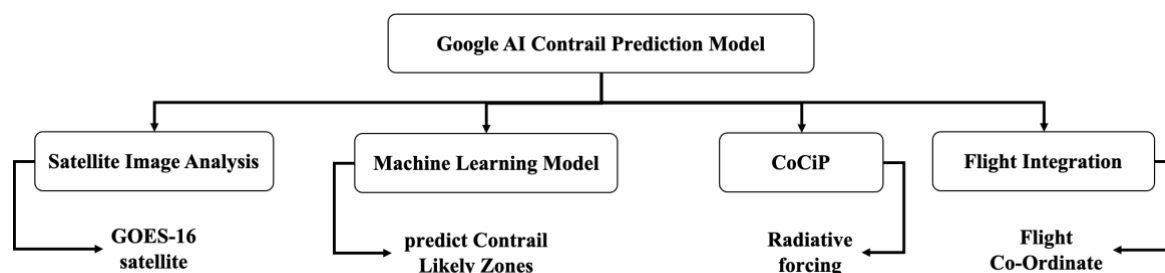


Figure 16 Google AI Contrail model framework



1100 The Google contrail framework emerged from a recent collaboration between Google Research, DLR, American Airlines, and
1101 Breakthrough Energy (2023–2024). To address the interpretability limitations of purely data-driven algorithms, the authors
1102 designed a hybrid, dual-component architecture that integrates a Machine Learning-based Contrail Likely Zone (CLZ) model
1103 with the physics-based CoCiP model. The CLZ model was trained on over 1.3 million flight tracks using high-resolution
1104 meteorological features from ECMWF HRES. Crucially, to mitigate observational blind spots and ensure rigorous validation,
1105 the system was calibrated against both passive geostationary data MODIS and independent active spaceborne lidar CALIPSO.
1106 The methodology calculates the final climate impact by multiplying the ML-derived formation probability by the CoCiP-
1107 simulated energy forcing, which is subsequently adjusted by a 0.42 conversion factor to estimate ERF. Furthermore, the
1108 framework introduced the Global AI Aviation model, a transformer-based architecture designed for multi-objective flight
1109 trajectory optimization. Despite its high predictive capability, critical limitations remain. The system is proprietary, limiting
1110 independent verification, and currently struggles to provide robust probabilistic uncertainty quantification. Consequently,
1111 managing the operational "regret factor"—ensuring that automated avoidance maneuvers do not incur a net climate penalty
1112 via excess CO₂ emissions due to deterministic false-positive forecasts—remains a primary challenge for real-world integration
1113 ([Zebediah Engberg, 2025](#)).

1114 To bridge the gap between theoretical forecasting and empirical validation, an AI-driven ADM system was introduced by
1115 ([Geraedts et al., 2024](#)). Unlike prognostic microphysical models, this scalable framework operates retrospectively, employing
1116 a computer vision algorithm to process passive infrared imagery from the GOES-16 ABI. By advecting historical ADS-B
1117 flight trajectories using numerical weather data, the system physically aligns individual flights with observed persistent
1118 contrails. This generated a massive empirical dataset of over 1.6 million flight segments, providing a critical baseline to directly
1119 benchmark predictive frameworks like CoCiP. However, significant observational constraints remain. The computer vision
1120 architecture exhibits a 30% error rate (false positive and negative) relative to human labeling. Furthermore, the reliance on
1121 passive geostationary sensors restricts detection to optically thick, horizontally expansive contrails. The system cannot resolve
1122 sub-pixel formations, optically thin cirrus, or precise vertical profiles, highlighting the necessity of integrating active
1123 spaceborne lidar (e.g., CALIOP) to mitigate these fundamental observational blind spots ([Geraedts et al., 2024](#)).

1124 Addressing the vertical placement errors frequently encountered in NWP-integrated models, an AI-driven Contrail Altitude
1125 Estimation framework was introduced by ([Meijer et al., 2024](#)) at MIT in 2024. Utilizing a CNN, this approach bypasses
1126 traditional thermodynamic parameterizations to estimate altitudes directly from passive thermal infrared imagery GOES-16
1127 ABI. Crucially, to overcome the inherent vertical resolution limits of geostationary sensors, the model was rigorously trained
1128 and validated against coincident, active spaceborne lidar CALIPSO to establish high-precision ground-truth labels. While the
1129 CNN efficiently generates pixel-wise altitude maps from spatial patches of brightness temperatures, critical operational
1130 constraints persist. The model's accuracy degrades significantly in complex, multi-layer cloud scenes, particularly where
1131 contrails overlap with underlying meteorological layers. Furthermore, the architecture is fundamentally restricted to
1132 identifying the visible contrail top rather than resolving the full vertical depth. For tactical flight avoidance, this lack of



1133 volumetric boundary data presents a severe limitation; aircraft require precise bottom-edge altitudes to execute minimal-
1134 descent rerouting without incurring unnecessary aerodynamic and fuel penalties ([Meijer et al., 2024](#)).

1135 GraphCast Contrail AI-integrated simulation framework was developed by Najrane Heni at the University of Stuttgart in 2025.
1136 The authors presented the first study integrating GraphCast, a deep learning-based weather forecasting model, with the CoCiP
1137 to estimate contrail formation and radiative forcing. The methodology involves a multi-source data pipeline that combines
1138 flight trajectories from OpenSky with meteorological data from both GraphCast and ERA5 reanalysis. By replacing traditional
1139 numerical weather prediction inputs with AI-generated forecasts, the study aims to enhance computational efficiency and
1140 prediction skill. A primary limitation of this approach is that GraphCast currently operates at a lower vertical resolution (13
1141 pressure levels) compared to ERA5 (37 levels), which can reduce the accuracy of detecting thin ice-supersaturated regions
1142 critical for persistent contrail formation ([Heni et al., 2025](#)).

1143 OpenContrails AI-based detection study was conducted by Joe Yue-Hei Ng, and Kevin McCloskey at Google Research and
1144 MIT in 2024. The authors introduced OpenContrails, a publicly available dataset of human-labeled contrails derived from
1145 GOES-16 ABI data. The methodology employs a deep learning model—specifically a U-Net architecture with a ResNet-18
1146 backbone—that utilizes a sequence of satellite images (temporal context) to distinguish persistent linear contrails from natural
1147 cirrus clouds and surface features. By training on over 40,000 labeled scenes and using hard-example mining, the model
1148 achieves significantly higher accuracy than single-frame approaches. A primary limitation is the inherent subjectivity and
1149 potential inconsistency of human annotations used for ground truth, as well as the restriction of the dataset to the geographical
1150 coverage of the GOES-16 satellite (primarily the Americas) ([Ng et al., 2024](#)).

1151 EfficientNet-b4 Encoder with Pseudo-Labeling study was conducted by Qunwei Lin from Trine University in 2024. The
1152 authors developed an optimized framework for contrail detection using the EfficientNet-b4 architecture as a feature extraction
1153 encoder, chosen for its balance of accuracy and efficiency using compound scaling. The methodology integrates three novel
1154 techniques to enhance performance: Misalignment Correction, which applies a 0.5-pixel shift to counteract errors introduced
1155 by polygon-to-mask conversions; Soft Labeling, which utilizes the average vote of multiple human annotators to provide
1156 confidence gradients rather than binary hard labels; and Pseudo-labeling, a two-phase training strategy that uses the model's
1157 own predictions on unlabeled data to enrich the training set. A primary limitation addressed by the authors is the model's high
1158 sensitivity to geometric inconsistencies (e.g., from flip/rotation augmentations), necessitating precise alignment corrections to
1159 maintain cross-validation performance ([Lin et al., 2024](#)).

1160 U-Net Segmentation combining Hough Transform Matching is an observational study conducted by Emmanuel Riggi-Carollo
1161 and Thomas Dubot at the French Civil Aviation Authority (DGAC) and ONERA (The French Aerospace Lab) in 2024. The
1162 authors developed a hybrid detection and identification pipeline designed to associate persistent contrails observed in GOES-
1163 16 satellite imagery with their specific source aircraft. The methodology first employs a U-Net deep neural network to segment
1164 contrail pixels from the satellite images, followed by a Hough Transform to extract linear features from these masks. To
1165 identify the source flight, the system utilizes ADS-B air traffic data and ERA5 meteorological reanalysis wind fields to advect



1166 potential candidate trajectories to the time of the satellite image, matching the geometric alignment of the flight path with the
 1167 detected contrail line. A primary limitation of this approach is the challenge of accurately distinguishing contrails from natural
 1168 cirrus clouds in the segmentation phase, as well as the dependence on precise wind data to correctly link the advected flight
 1169 path to the observed contrail position over time ([Riggi--Carrolo et al., 2023](#)).

1170 **Table 9 List of AI-Driven Contrail Prediction Models**

Model	Developer / Institution	Method	Input Data Sources	Key Feature	Ref
Google AI Contrail Forecast	DLR / Google Research / American Airlines	thermodynamic + microphysical simulation AI-assisted classification	Aircraft trajectory, temperature, relative humidity, soot emissions	Provides labeled contrail datasets and probabilistic forecasts; supports operational contrail avoidance	(Engberg et al., 2025; Geraedts et al., 2024)
Contrail Tracker	Eurocontrol	Computer Vision / AI (Multi-Modal)	Ground-based visible & IR cameras + MTG geostationary satellite data	Automates contrail-to-flight attribution for real-time validation of mitigation strategies	(Jarry et al., 2026)
Imperial ML Contrail Model	Imperial College London / DLR	Random Forest Classifier	ERA5 reanalysis + flight path data	Predicts contrail formation probability and persistence; used for eco-routing	(Teoh et al., 2024b)
MIT-NOAA PINN Model	MIT / NOAA	PINN	Atmospheric reanalysis + thermodynamic constraints	Embeds Schmidt-Appleman physics in neural nets; reduces forecast error by ~40%	(Di Giusto et al., 2024)
ADM Contrail	Google, MIT	Computer vision detects contrails in satellite images; physics-based algorithms match them to flights	GOES-16 infrared imagery, ADS-B flight paths, and ECMWF weather data	Created a massive 1.6-million-flight empirical dataset to benchmark contrail prediction models	(Geraedts et al., 2024)
CNN Contrail	MIT	CNN	GOES-16 ABI, CALIPSO/CALIOP, LIDAR)	Predict directly from geostationary satellite imagery	(Duda et al., 2005)
GraphCast Contrail	University of Stuttgart	Integrates AI weather forecasting (GraphCast) with CoCiP	OpenSky, GraphCast, ERA5	Integrates GraphCast with CoCiP	(Henl et al., 2025)
OpenContrails	Google Research & MIT	Spatio-Temporal Deep Learning	GOES-16 ABI, OpenContrails Dataset	Uses temporal context & OpenContrails	(Ng et al., 2024)
EfficientNet-b4 Encoder	Trine University	Deep learning segmentation with semi-supervised training	Satellite imagery with human-annotated polygon masks	EfficientNet-b4 backbone, misalignment correction, soft labeling	(Lin et al., 2024)
U-Net Segmentation	DGAC & ONERA	U-Net architecture for semantic segmentation	GOES-16 AB, ADS-B, ERA5	Automates the attribution of satellite-detected contrails to specific flights	(Riggi--Carrolo et al., 2023)
Regression Contrail Model	MIT	deep learning regression trained on geometric stereo-derived altitude labels	GOES-16 ABI	Estimates contrail altitude from single-view geostationary thermal imagery	(Meijer et al., 2024)



1171 Deep Learning Regression Model (GOES-16 ABI) is an AI-based retrieval study conducted by Vincent R. Meijer et al. at the
1172 MIT Laboratory for Aviation and the Environment in 2024. The authors developed a Deep Learning model designed to
1173 estimate the altitude of persistent contrails using only single-view multispectral data from the GOES-16 ABI. The methodology
1174 involved training a neural network to identify the spectral signatures associated with different cloud top heights, effectively
1175 overcoming the limitations of traditional thermal brightness temperature methods which struggle with optically thin contrails
1176 that transmit radiation from warmer lower layers. By learning from a dataset of accurate altitude labels (likely derived from
1177 geometric stereo methods or active lidar), the model can assign altitude values to contrail pixels in real-time. A primary
1178 limitation of this approach is its dependence on the quality and representativeness of the ground truth training data, as well as
1179 reduced performance in scenes with low thermal contrast between the contrail and the underlying surface or cloud layers
1180 ([Meijer et al., 2024](#)).

1181 **4 Key Findings**

1182 This multidisciplinary review of contrail prediction methodologies (1940–2026) synthesizes eight decades of research to
1183 highlight five critical insights that define the current state and future trajectory of aviation climate mitigation. First,
1184 microphysical box and plume models (e.g., APCEMM, LCM-LES) achieve high fidelity by resolving ice crystal growth,
1185 sedimentation, and spreading using either size-resolved sectional schemes APCEMM or particle-based stochastic nucleation
1186 LCM-LES, yet neither resolves nanometer-scale nucleation from first principles; APCEMM relies on a prescribed
1187 black-carbon activation parameterization, while LCM-LES uses empirical nucleation laws without explicit treatment of
1188 volatile species. By contrast, the ACM model explicitly simulates binary homogeneous and ion-mediated nucleation of H_2SO_4 –
1189 H_2O , condensation of organic vapors, and nucleation of lubrication oil droplets, and was validated against in-flight data from
1190 a lean-burn A321neo, proving that contrail ice crystals in low-soot regimes form predominantly on newly nucleated volatile
1191 particles rather than on emitted soot. All such microphysical models remain computationally prohibitive for global fleet
1192 forecasting, underscoring the need for hybrid architectures. Second, regardless of model sophistication, prediction accuracy is
1193 fundamentally capped by the quality of upper-tropospheric humidity data; the systematic “dry bias” in reanalyses like ERA5
1194 prevents reliable identification of ice-supersaturated regions, causing either underestimation of contrail persistence or high
1195 false-alarm rates. Even the ACM model’s success depended on accurate meteorological inputs, making improved humidity
1196 observations the primary bottleneck for real-time contrail avoidance. Third, the period 2020–2026 has seen a decisive shift
1197 toward hybrid AI systems that embed physical laws into neural networks (e.g., Google-DLR, PINNs, CoCiP Grid), overcoming
1198 the lack of thermodynamic consistency in purely data-driven models. ACM’s explicit nucleation schemes provide a physically
1199 grounded target for such hybrid AI, enabling machine learning to learn the mapping from fuel properties and meteorology to
1200 ice crystal numbers without sacrificing interpretability. Fourth, modern climate models (e.g., ECHAM5-CCMod) confirm that
1201 a strong Pareto distribution governs contrail forcing: approximately 2–10% of global flights cause 80% of the total energy
1202 forcing, because aged, spreading contrail cirrus dominate warming. Fleet-wide avoidance is therefore inefficient; operational
1203 systems must minimize the “regret factor” by targeting only high-impact flights. ACM’s finding that low-sulfur fuels greatly



1204 reduce ice crystal numbers adds a new lever to target those flights. Fifth, satellite validation has evolved from retrospective
1205 climatologies to active calibration for deep learning networks (e.g., OpenContrails), yet a “nighttime blind spot” persists.
1206 Transitioning from passive sensors to active spaceborne lidar (e.g., CALIOP, EarthCARE) is essential to benchmark vertical
1207 profiles and optical depths. ACM’s predictions of bimodal ice crystal size distributions under low-soot, high-sulfur conditions
1208 provide specific, testable hypotheses for such active sensors. Together, these insights chart a course toward accurate, scalable,
1209 and operationally viable contrail mitigation.

1210 **5 Future Research Directions**

1211 As the aviation sector transitions from theoretical climate assessment to operational mitigation, the focus of contrail prediction
1212 research must pivot from simple detection to actionable, high-confidence forecasting. The current reliance on purely
1213 data-driven, “black box” deep learning models presents a severe safety certification challenge for aviation authorities. When
1214 current AI networks encounter noisy training data, they frequently predict contrail formation in physically impossible
1215 conditions, such as warm or dry air masses. To overcome this, future research must prioritize “glass box” hybrid architectures
1216 where the AI component handles non-linear pattern recognition—such as satellite texture analysis—while a differentiable
1217 physics layer mathematically constrains the output. Specifically, the development of PINNs that strictly enforce
1218 thermodynamic laws, including mass conservation and the Clausius-Clapeyron relation, directly within the loss function will
1219 ensure that predictions always adhere to the physical reality of the Schmidt-Appleman criterion. However, even a perfectly
1220 constrained AI is ultimately limited by its meteorological inputs. The systematic underestimation of upper-tropospheric
1221 humidity in NWP models, such as the ECMWF and GFS, remains the single largest source of forecast error. Merely correcting
1222 this bias post-hoc is proving insufficient for tactical flight routing because current operational models do not effectively
1223 assimilate high-resolution water vapor radiances at flight levels. Moving forward, researchers must investigate machine
1224 learning techniques designed to assimilate real-time satellite radiances (from instruments like GOES-16 and Meteosat) directly
1225 into the initial conditions of weather models. The ultimate goal is to create a dynamic “humidity nowcasting” system capable
1226 of identifying ISSR with kilometre-scale precision before an aircraft ever enters them. Furthermore, predicting initial formation
1227 is no longer sufficient; the modeling focus must shift to lifetime prediction. Given that approximately 10 % of flights cause
1228 roughly 80 % of contrail-induced warming, the current binary focus on simply avoiding all contrails is operationally inefficient
1229 and potentially counterproductive due to the inherent CO₂ penalty of diversions. We currently lack robust tools to predict
1230 which specific contrails will harmlessly dissipate and which will spread into warming cirrus outbreaks. Future algorithms must
1231 be tailored to specifically identify “big hitter” flights—those traversing regions of deep supersaturation and high wind shear
1232 where contrails are predicted to persist for more than four hours. By shifting the focus in this way, operational trials can finally
1233 test “severity-based” avoidance rather than “frequency-based” avoidance. Validating these severity-based predictions requires
1234 overcoming the severe limitations of passive thermal imagery. The current reliance on passive sensors creates a significant
1235 “nighttime blind spot” and fails to resolve the vertical depth of contrails, which is critical for accurate radiative forcing
1236 calculations. Because passive sensors cannot accurately measure the optical depth of thin contrails or distinguish vertically



1237 overlapping layers, it is essential to integrate data from next-generation active spaceborne lidar, such as EarthCARE, to validate
1238 the vertical profiles in AI and NWP models. Simultaneously, research should focus on developing multispectral algorithms
1239 for geostationary satellites that can detect optically thin contrails at night, potentially utilizing machine learning to artificially
1240 enhance thermal contrast. ACM specifically call for additional targeted experiments: exploring how reductions in volatile
1241 particles (apart from soot) affect contrail ice formation, testing sulfur-free fuels to further reduce ice crystal numbers in
1242 lean-burn engines, better quantifying the role of organic fuel constituents and lubrication oil vapours, updating global fleet
1243 models that currently underestimate the climate impact of lean-burn aircraft, and addressing the complete data gap for emerging
1244 technologies such as hydrogen-powered aircraft. Finally, if these predictive tools are to be adopted by pilots and airline
1245 dispatchers, the output format must evolve. Operators require probabilistic risk assessments, not deterministic “yes/no”
1246 forecasts that are highly prone to false alarms. The community must transition toward ensemble prediction systems that replace
1247 single deterministic outputs with a clear “Probability of Persistence” and defined confidence intervals. Only with these
1248 probabilistic metrics can the industry define precise “Regret Factor” thresholds: determining the exact probability of formation
1249 at which the climate benefit of avoidance mathematically outweighs the fuel cost of the maneuver. Achieving this will require
1250 coupling advanced contrail prediction models directly with aerodynamic fuel-burn performance models to ensure every
1251 diversion results in a verifiable, optimized net climate benefit per flight.

1252 **6 Conclusion**

1253 The evolution of contrail prediction modeling from 1940 to 2026 represents a fundamental transition from theoretical
1254 atmospheric science to operational climate engineering. This review has critically examined the five dominant modeling
1255 paradigms Thermodynamic, Microphysical, NWP-Integrated, Satellite-Empirical, and AI-Driven revealing that no single
1256 approach suffices on its own. Instead, the field is converging toward a hybrid methodology that leverages the strengths of each
1257 era to solve the aviation climate challenge. For over half a century, the SAC provided the necessary thermodynamic boundary
1258 conditions for understanding formation, but it could not address the critical issue of persistence. The subsequent rise of
1259 Microphysical Box Models (e.g., CoCiP, APCEMM) successfully resolved the complex lifecycle of ice crystals, establishing
1260 that aged Contrail Cirrus—not the initial linear plume—is the primary driver of radiative forcing. However, the computational
1261 cost of these physical simulations rendered them impractical for global, real-time fleet management. The integration of NWP
1262 and Satellite Observation bridged this gap by enabling global climatologies, yet these systems hit a glass ceiling imposed by
1263 the Upper-Tropospheric Humidity dry bias and the observational blind spot" of passive sensors. Operational validation remains
1264 hindered by the difficulty of detecting optically thin plumes at night, creating a significant verification gap. The profound
1265 disruption of the 2020s driven by Artificial Intelligence—has fundamentally altered this landscape. AI and Deep Learning
1266 have surpassed traditional physical schemes in detection speed and pattern recognition, yet they face the Black Box
1267 interpretability challenge that limits their certification for safety-critical operations. Consequently, the most viable path
1268 forward, as demonstrated by recent breakthroughs from Google Research and DLR, lies in Physics-Informed Hybrid
1269 Architectures. By using satellite data to correct NWP biases and physical laws to constrain AI predictions, these systems offer



1270 the first scalable solution for operational contrail avoidance. Ultimately, the science of contrail prediction has matured from a
 1271 diagnostic discipline into a prescriptive one. The discovery that a mere 2–10% of Big Hitter flights drive 80% of the warming
 1272 has redefined the operational goal: we do not need to avoid all contrails, only the most damaging ones. The future of sustainable
 1273 aviation therefore depends on minimizing the Regret Factor deploying high-precision hybrid models that can surgically divert
 1274 these high-impact flights without incurring unnecessary carbon penalties. As aviation targets net-zero emissions, integrating
 1275 these intelligent forecasting tools into global Air Traffic Management will be as critical as the development of new fuels or
 1276 airframes.

1277 7 Appendices

1278 7.1 Appendix A: Model Comparison Tables

1279 **TABLE A1.** Comprehensive Comparison of Contrail Prediction Models

Model Name	Developer(s)	Model Type	Purpose/Contribution	Limitations
SAC	Schmidt & Appleman (1940s–50s)	Thermodynamic	Established threshold conditions for contrail formation	Binary output; ignores microphysics and plume evolution
Freudenthaler Model	Freudenthaler et al. (1995)	Microphysical Box	Simulated particle growth and lidar backscatter for early detection	Lacks full lifecycle modeling; optical only
Plume Aerosol Model	Kärcher et al. (1996, 1998)	Lagrangian Microphysical	Simulated soot–ice nucleation and aerosol microphysics	Assumes steady state; simple entrainment
Microphysical Parcel Model	Jensen et al. (1998)	Microphysical Box	Included supersaturation feedback; validated with SUCCESS campaign data	No turbulence modeling; simplified dispersion
Spichtinger Model	Spichtinger et al. (2005)	Microphysical Box	Simulated contrail–cirrus transition using relative humidity feedback	Less focused on young plume evolution
Cirrus Transition Model	Kärcher & Burkhardt (2008, 2010)	Time-Resolved Cirrus	Parameterized aged contrail cirrus in climate models (e.g., ECHAM)	Not plume-resolving; needs external initialization
Unterstrasser-Gierens	Unterstrasser & Gierens (2010)	Eulerian Microphysical	Captures coagulation, vertical structure, entrainment, and decay	Limited meteorological coupling
CoCiP	Schumann / DLR (2011–Present)	Global Lagrangian	Simulates contrail evolution with weather data; predicts radiative impact	Simplified particle physics; relies on global reanalysis
Lagrangian Cloud Module (LES)	Lewellen (2014)	LES-Coupled Microphysical	Resolves turbulence, shear, and anisotropic dispersion	High computational cost
APCEMM	MIT (Fritz et al., 2020)	Modular Plume-Scale	Simulates gas-phase chemistry, aerosol evolution, plume microphysics	Requires detailed input; high complexity
ECHAM4/5	MPI Hamburg	NWP-Integrated	Embeds contrail cirrus physics into global circulation model	Limited resolution; approximated humidity
MM5 + SAC	NCAR	NWP-Integrated	Mesoscale contrail forecasts under realistic conditions	Dependent on SAC thresholds
GFS + SAC	NOAA	NWP-Integrated	Operational-scale contrail prediction with global coverage	Simplistic contrail formation logic
CESM Contrail Layer	NCAR	Climate Model Integration	Enables contrail radiative forcing in Earth system model	Coarse resolution; assumes parameterized microphysics



WRF-SAC	NOAA/Community	NWP-Integrated	High-resolution contrail formation within mesoscale weather forecasts	Lacks full lifecycle evolution
UKMO Contrail Layer	UK Met Office	NWP-Integrated	Introduced climatological contrail layers in unified model	Static layers; lacks dynamic prediction
CNN-AVHRR	Zhang & Li (2021)	AI-Driven	Uses CNN to detect contrails in AVHRR imagery	Dependent on clear-sky imagery
PRE-TRAILS	Teoh et al. (2020)	AI-Driven Hybrid	Uses deep learning for contrail detection from multi-sensor data	Needs curated training datasets
GAIA	GAIA Consortium (2021–)	AI Hybrid Forecasting	Learns contrail patterns across spatial–temporal scales	Black box nature; explainability issues
Google AI + CoCiP	Google, Breakthrough Energy, DLR (2024)	Hybrid (AI + Physics)	Real-time contrail prediction & aircraft rerouting tool	Requires massive compute and integration
PINNs for Contrails	Wang et al. (2023)	Physics-Informed AI	Embeds SAC thermodynamics in neural architecture	Still under research; not widely validated

1280

1281

TABLE A2. Critical Synthesis and Comparative Matrix of Contrail Prediction Paradigms

Modeling Paradigm	Spatial Scale	Computational Cost	Prediction Accuracy & Lifecycle Evolution	Suitability for Operational Forecasting	Key Operational Limitations
Thermodynamic / Analytical (e.g., SAC)	Local to Global	Very Low	Low: Binary formation thresholds only. Cannot simulate lifecycle aging or persistence.	High for rapid climatological screening; Low for active flight routing.	Incapable of simulating advection, spreading, or the resulting radiative forcing.
Microphysical Box & Plume Models (e.g., APCEMM, LES)	Plume-scale (0–100 km)	Very High	Very High: Rigorously resolves nucleation, wake vortex dynamics, and long-term crystal survival.	Very Low: Computationally prohibitive for global fleet integration.	Requires massive supercomputing resources; highly sensitive to local boundary conditions.
NWP-Integrated (e.g., ECMWF IFS, WRF-Chem)	Regional to Global	Moderate to High	Moderate: Captures advection, wind shear, and weather interactions, but relies on bulk parameterizations.	Moderate: Currently used in pre-tactical flight planning and research trials.	Heavily constrained by persistent "dry biases" and resolution limits of upper-tropospheric humidity.
Satellite-Empirical (e.g., MODIS, CALIOP)	Global (Swath-dependent)	Low	None: Strictly observational and retrospective. Cannot simulate future evolution.	Low: Cannot forecast future atmospheric states for avoidance.	Plagued by "nighttime blind spots"; struggles to distinguish aged contrails from natural cirrus.
Hybrid AI-Driven (e.g., PINNs, Google/DLR)	Global	Low (Inference) / High (Training)	High: Combines physical constraints (like SAC) with pattern recognition for accurate lifecycle tracking.	Very High: Rapid real-time inference enables active, tactical flight rerouting.	"Black-box" interpretability issues; predictions degrade sharply if flight enters unrepresented atmospheric conditions.

1282

7.2 Appendix B: Dataset Catalog

1283

TABLE B1. Dataset for contrail prediction models

Dataset Name	Source/Agency	Type	Purpose in Contrail Research	Temporal Coverage	Notes
--------------	---------------	------	------------------------------	-------------------	-------



MODIS	NASA (Terra/Aqua Satellites)	Satellite Imagery (VIS/IR)	Contrail detection, optical depth, cirrus classification	2000–Present	Used in many ML and empirical models
CALIOP (CALIPSO)	NASA & CNES	Active Lidar	Vertical profiling of contrails and cirrus clouds	2006–Present	High vertical resolution
AVHRR	NOAA/NASA	Satellite Imagery	Retrospective contrail climatology, pattern recognition	1978–Present	Legacy dataset for detection
GOES-16/17	NOAA	Geostationary Satellite	Real-time contrail detection in Western Hemisphere	2016–Present	High temporal resolution
ERA5	ECMWF	Reanalysis (Atmospheric Fields)	Provides humidity, wind, and temperature inputs for contrail models	1979–Present	Used in CoCiP and APCEMM
MERRA-2	NASA GMAO	Reanalysis	Atmospheric initialization for global-scale models	1980–Present	High compatibility with ECHAM, CESM
AIRS	NASA (Aqua)	IR Sounding	Retrieves temperature and humidity profiles at flight altitudes	2002–Present	Complements MODIS and ERA5
SUCCESS Campaign Data	NASA (1996)	Field Campaign (In-situ)	Contrail microphysics and plume chemistry calibration	1996	Used in Jensen (1998), Kärcher models
FAAM Aircraft Data	UK Met Office	In-Situ Aircraft Measurements	Provides aerosol and humidity data for contrail modeling	2004–Present (Campaigns)	Irregular temporal coverage
NOAA GFS Forecasts	NOAA	Operational Weather Model	Inputs for SAC, MM5, WRF-based contrail predictions	Real-time	Available for AI hybrid models
ADS-B Flight Data	OpenSky Network, FlightRadar24	Aircraft Trajectories	Contrail path mapping, emissions modeling, routing optimization	Varies	May require commercial license
CIRA Contrail Climatology	Cooperative Institute for Research in the Atmosphere (CIRA)	Remote Sensing	Long-term climatological analysis of persistent contrails	1980s–Present	Derived from satellite synthesis

1284

7.3 Appendix C: Abbreviations

1285

TABLE C1. Comprehensive List of Abbreviations

Abbreviation	Full Name / Description
ABI	Advanced Baseline Imager
ACSM	Ames Contrail Simulation Model
ADM	Automated Detection and Matching
ADS-B	Automatic Dependent Surveillance–Broadcast
AHI	Advanced Himawari Imager (on Himawari satellite)
AI	Artificial Intelligence
AIC	Aircraft-Induced Cloudiness
AIRS	Atmospheric Infrared Sounder
APCEMM	Aviation Particle and Chemical Emissions Model
ARPS	Advanced Regional Prediction System
ART	Aerosols and Reactive Trace gases
ATC	All Tests Consolidation
AVHRR	Advanced Very High Resolution Radiometer
BADA	Base of Aircraft Data



BTD	Brightness Temperature Difference
CALIOP	Cloud-Aerosol Lidar with Orthogonal Polarization
CALIPSO	Cloud-Aerosol Lidar and Infrared Pathfinder Satellite Observation
CAMS	Copernicus Atmosphere Monitoring Service
CC	Contrail Cirrus
CDA	Contrail Detection Algorithm
CESM	Community Earth System Model
CFI	Contrail Frequency Indices
CI	Cirrus
CLZ	Contrail Likely Zone
CNN	Convolutional Neural Network
CoAtSaC	Contrail Attribution Sample Consensus
CoCiP	Contrail Cirrus Prediction Model
COT	Cloud Optical Thickness
DLR	Deutsches Zentrum für Luft- und Raumfahrt (German Aerospace Center)
DMSP	Defense Meteorological Satellite Program
DNB	Day/Night Band (part of VIIRS)
DP	Dynamic Programming
DWD	Deutscher Wetterdienst (German Weather Service)
EASA	European Union Aviation Safety Agency
ECHAM	European Centre Hamburg Model
ECMWF	European Centre for Medium-Range Weather Forecasts
ERA5	ECMWF Reanalysis v5 (climate reanalysis dataset)
ERF	Effective Radiative Forcing
FAA	Federal Aviation Administration
FAR	False Alarm Rate
FK5D	Flightkeys 5D
GAIA	Global AI Aviation
GEFS	Global Ensemble Forecast System
GEOS-5	Goddard Earth Observing System Model, Version 5
GFS	Global Forecast System
GHG	Greenhouse Gas
GISS	Goddard Institute for Space Studies
GOES	Geostationary Operational Environmental Satellite
HC	Hydrocarbons
ICAO	International Civil Aviation Organization
ICS	Invariant Coordinate System
IFS	Integrated Forecasting System (ECMWF)
IPCC	Intergovernmental Panel on Climate Change
ISSR	Ice-Supersaturated Region
IUP	Institute of Environmental Physics
IWC	Ice Water Content
KIT	Karlsruhe Institute of Technology
LCM	Lagrangian Cloud Model
LES	Large Eddy Simulation
LUT	Look-Up Table
MERRA	Modern-Era Retrospective analysis for Research and Applications
MISR	Multi-angle Imaging SpectroRadiometer
MIT	Massachusetts Institute of Technology
ML	Machine Learning
MM5	Fifth-Generation Penn State/NCAR Mesoscale Model
MODIS	Moderate Resolution Imaging Spectroradiometer
MODTRAN	Moderate Resolution Atmospheric Transmission
MPI-M	Max Planck Institute for Meteorology
MSG	Meteosat Second Generation



NASA	National Aeronautics and Space Administration
NCAR	National Center for Atmospheric Research
NCEP	National Centers for Environmental Prediction
NOAA	National Oceanic and Atmospheric Administration
NWP	Numerical Weather Prediction
OCA	Optimal Cloud Analysis
PCC	Potential Contrail Cover
PCCC	Potential Contrail Cirrus Cover
PCM	Probabilistic Cloud Mask
PINNs	Physics-Informed Neural Networks
PM	Particulate Matter
POD	Probability of Detection
PPS	Polar Platform System
PRE-TRAILS	Pre-trained Radiative AI Layered System
RANSAC	Random Sample Consensus
RAP	Rapid Refresh
RF	Radiative Forcing
RHi	Relative Humidity with respect to Ice
RRTM	Rapid Radiative Transfer Model
RRTMG	Rapid Radiative Transfer Model for GCMs
RTE	Radiative Transfer Equation
RTMs	Radiative Transfer Models
RUC	Rapid Update Cycle
SAC	Schmidt-Appleman Criterion
SAF	Sustainable Aviation Fuel
SCIAMACHY	Scanning Imaging Absorption Spectrometer for Atmospheric Chartography
SEVIRI	Spinning Enhanced Visible and Infrared Imager
SIPs	Simulation Ice Particles
SST	Supersonic Transport
STFM	Strategic Traffic Flow Management
SUCCESS	Subsonic Aircraft: Contrail and Cloud Effects Special Study
TOMS	Total Ozone Mapping Spectrometer
TUV	Tropospheric Ultraviolet and Visible Radiation Model
UKCA	UK Chemistry and Aerosols
UKMO	UK Met Office Unified Model
VIIRS	Visible Infrared Imaging Radiometer Suite
vPM	Volatile Particulate Matter
WAWFOR	World Aviation Weather Forecast
WFM-DOAS	Weighting Function Modified Differential Optical Absorption Spectroscopy
WRF	Weather Research and Forecasting Model
WRF-Chem	Weather Research and Forecasting model coupled with Chemistry
WV	Water Vapor

1286

1287 **Code availability**

1288 No original code was developed for this review article. Details, algorithms, and source code availability for the various contrail
 1289 prediction models discussed in this manuscript can be found within their respective cited literature.

1290 **Data availability**



1291 No new primary datasets were generated or analysed in this study. All data, literature metadata, and model information
1292 synthesized in this review are publicly available and properly cited in the reference list.

1293 **Author's contributions**

1294 Najeeb Ullah conducted the primary literature investigation, performed the core research synthesis, and wrote the original draft
1295 of the manuscript. Meiyin Zhu and Liuyong Chang provided overall supervision for the project. Meiyin Zhu acquired the
1296 research funding and contributed to the conceptualization and critical review. Hongwei Deng and Shengnan Yang contributed
1297 to the formal analysis and methodology of the reviewed models. Aman Ullah and Jiaqi Yin assisted with data curation
1298 (literature selection) and visualization. Muhammad Owais Ghani and Tianxu Huang contributed to the investigation. All
1299 authors participated in the critical review and editing of the final manuscript.

1300 **Declaration of competing interest**

1301 The authors declare that they have no known competing financial interests or personal relationships that could have appeared
1302 to influence the work reported in this paper.

1303 **Acknowledgments**

1304 The authors gratefully acknowledge the institutional support and research infrastructure provided by the Hangzhou
1305 International Innovation Institute of Beihang University, the AECC Shenyang Engine Research Institute, and the Institute for
1306 Aero Engine at Tsinghua University. We extend our gratitude to Meiyin Zhu for efforts in acquiring the funding that made
1307 this review possible. The authors also appreciate the access to institutional literature databases, computational resources, and
1308 academic networking platforms that facilitated the comprehensive synthesis of contrail prediction models.

1309 **Financial support**

1310 This research has been supported by the National Natural Science Foundation of China (grant nos. 52306208, U2433215, and
1311 52306184), the Beijing Natural Science Foundation (grant no. 3262018), the National Key Lab of Aerospace Power System
1312 and Plasma Technology (grant no. 110329JC36025060002), and the Research Start-up Funds of the Hangzhou International
1313 Innovation Institute of Beihang University (grant no. 2024KQ004).

1314 **References**

1315 Aamaas, B., Lund, M. T., Fuglestedt, J. S., Totterdill, A., Owen, B., Skowron, A., and Lee, D. S.: Continued global warming
1316 from aviation even under high-ambition mitigation scenarios, *One Earth*, 8, 101451-101466,
1317 <https://doi.org/10.1016/j.oneear.2025.101451>, 2025.
1318 Alsante, A. N. and Cheng, M. D.: Aerosol-Cloud Interactions From Aviation Soot Emissions, *Journal of Geophysical*
1319 *Research: Atmospheres*, 129, 1-18, <https://doi.org/10.1029/2023jd040277>, 2024.



- 1320 Anfossi, D., Physick, W., Degrazia, G., Ferrero, E., Hibberd, M., Hurley, P., Luhar, A., Trini Castelli, S., and van Dop, H.,
1321 Zannetti, P. (Ed.): Air Quality Modeling: Theories, Methodologies, Computational Techniques, and Available Databases and
1322 Software, Vol. II: Advanced Topics, Air Quality Modeling (Volume 2), EnviroComp / Air & Waste Management Association
1323 (A&WMA)2005.
- 1324 Bier, A., Unterstrasser, S., and Vancassel, X.: Box model trajectory studies of contrail formation using a particle-based cloud
1325 microphysics scheme, *Atmospheric Chemistry and Physics*, 22, 823-845, <https://doi.org/10.5194/acp-22-823-2022>, 2022.
- 1326 Bier, A., Unterstrasser, S., Zink, J., Hillenbrand, D., Jurkat-Witschas, T., and Lottemoser, A.: Contrail formation on ambient
1327 aerosol particles for aircraft with hydrogen combustion: a box model trajectory study, *Atmospheric Chemistry and Physics*,
1328 24, 2319-2344, <https://doi.org/10.5194/acp-24-2319-2024>, 2024.
- 1329 Bock, D. P. d.: Contrails Mitigation Federal Outreach Meeting, ARPA-E, ARPA-E Headquarters offices located at 950
1330 L'Enfant Plaza SW, suite 8000, in Washington, D.C, October 28th,
- 1331 Bock, L. and Burkhardt, U.: The temporal evolution of a long-lived contrail cirrus cluster: Simulations with a global climate
1332 model, *Journal of Geophysical Research: Atmospheres*, 121, 3548-3565, <https://doi.org/10.1002/2015jd024475>, 2016.
- 1333 Brasseur, G. P., Gupta, M., Anderson, B. E., Balasubramanian, S., Barrett, S., Duda, D., Fleming, G., Forster, P. M.,
1334 Fuglestvedt, J., Gettelman, A., Halthore, R. N., Jacob, S. D., Jacobson, M. Z., Khodayari, A., Liou, K.-N., Lund, M. T., Miake-
1335 Lye, R. C., Minnis, P., Olsen, S., Penner, J. E., Prinn, R., Schumann, U., Selkirk, H. B., Sokolov, A., Unger, N., Wolfe, P.,
1336 Wong, H.-W., Wuebbles, D. W., Yi, B., Yang, P., and Zhou, C.: Impact of Aviation on Climate: FAA's Aviation Climate
1337 Change Research Initiative (ACCRI) Phase II, *Bulletin of the American Meteorological Society*, 97, 561-583,
1338 <https://doi.org/10.1175/bams-d-13-00089.1>, 2016.
- 1339 Burkhardt, U. and Kärcher, B.: Process-based simulation of contrail cirrus in a global climate model, *Journal of Geophysical*
1340 *Research: Atmospheres*, 114, <https://doi.org/10.1029/2008jd011491>, 2009.
- 1341 Burkhardt, U. and Kärcher, B.: Global radiative forcing from contrail cirrus, *Nature Climate Change*, 1, 54-58,
1342 <https://doi.org/10.1038/nclimate1068>, 2011.
- 1343 Burkhardt, U., Kärcher, B., and Schumann, U.: Global Modeling of the Contrail and Contrail Cirrus Climate Impact, *Bulletin*
1344 *of the American Meteorological Society*, 91, 479-484, <https://doi.org/10.1175/2009bams2656.1>, 2010.
- 1345 Cannon, T., Hagan, T., Kramer, T., Schafer, D., Meeks, S., Medlin, R., Roland, D., Vasel-Be-Hagh, A., and Roberts, R.:
1346 Thermodynamic evaluation of contrail formation from a conventional jet fuel and an ammonia-based aviation propulsion
1347 system, *Commun Eng*, 3, 165, <https://doi.org/10.1038/s44172-024-00312-2>, 2024.
- 1348 Carleton, A. M., Travis, D. J., Master, K., and Vezhapparambu, S.: Composite Atmospheric Environments of Jet Contrail
1349 Outbreaks for the United States, *Journal of Applied Meteorology and Climatology*, 47, 641-667,
1350 <https://doi.org/10.1175/2007jamc1481.1>, 2008.
- 1351 Chen, C. C. and Gettelman, A.: Simulated radiative forcing from contrails and contrail cirrus, *Atmospheric Chemistry and*
1352 *Physics*, 13, 12525-12536, <https://doi.org/10.5194/acp-13-12525-2013>, 2013.



- 1353 Choi, J.-Y., Choi, J.-W., and Kim, H.-M.: Development of a Basic Contrail Prediction Model for the Contrail Reduction
1354 Certification of Commercial Aircraft, *Journal of Aerospace System Engineering*, 15, 11-19,
1355 <https://doi.org/10.20910/JASE.2021.15.3.11>, 2021.
- 1356 Coleman, R. F.: A New Formulation for the Critical Temperature for Contrail Formation, *Journal of Applied Meteorology*,
1357 35, 2270-2282, [https://doi.org/10.1175/1520-0450\(1996\)035<2270:Anfftc>2.0.Co;2](https://doi.org/10.1175/1520-0450(1996)035<2270:Anfftc>2.0.Co;2), 1996.
- 1358 Comstock, J. M., Lin, R. F., Starr, D. O. C., and Yang, P.: Understanding ice supersaturation, particle growth, and number
1359 concentration in cirrus clouds, *Journal of Geophysical Research: Atmospheres*, 113, D23211,
1360 <https://doi.org/10.1029/2008jd010332>, 2008.
- 1361 Corbosiero, K. L. and Molinari, J.: The Effects of Vertical Wind Shear on the Distribution of Convection in Tropical Cyclones,
1362 *Monthly Weather Review*, 130, 2110-2123, [https://doi.org/10.1175/1520-0493\(2002\)130<2110:Teovws>2.0.Co;2](https://doi.org/10.1175/1520-0493(2002)130<2110:Teovws>2.0.Co;2), 2002.
- 1363 DeGrand, J. Q., Carleton, A. M., Travis, D. J., and Lamb, P. J.: A Satellite-Based Climatic Description of Jet Aircraft Contrails
1364 and Associations with Atmospheric Conditions, 1977-79, *Journal of Applied Meteorology*, 39, 1434-1459,
1365 [https://doi.org/10.1175/1520-0450\(2000\)039<1434:Asbcdo>2.0.Co;2](https://doi.org/10.1175/1520-0450(2000)039<1434:Asbcdo>2.0.Co;2), 2000.
- 1366 Di Giusto, D., Boussu, G., Alix, S., Reverdy, C., Riou, M., and Petrisor, T.: Towards Contrail Mitigation through Robust and
1367 Frugal AI Driven Data Exploitation, ESANN 2024 proceedings, 32nd European Symposium on Artificial Neural Networks,
1368 Computational Intelligence and Machine Learning, Bruges (Belgium), 9-11 Oct,
1369 <https://doi.org/10.14428/esann/2024.ES2024-64>,
- 1370 Dimitropoulou, E., de Buyl, P., and Clerbaux, N.: Satellite-based estimation of high-altitude ice cloud radiative forcing derived
1371 through a Rapid Contrail-RF Estimation Approach, *Atmospheric Measurement Techniques*, 19, 437-459,
1372 <https://doi.org/10.5194/amt-19-437-2026>, 2026.
- 1373 Dischl, R., Kaufmann, S., and Voigt, C.: Regional and Seasonal Dependence of the Potential Contrail Cover and the Potential
1374 Contrail Cirrus Cover over Europe, *Aerospace*, 9, <https://doi.org/10.3390/aerospace9090485>, 2022.
- 1375 Dischl, R., Märkl, R., Sauer, D., Voigt, C., Harlaß, T., Scheibe, M., Hahn, V., Kaufmann, S., Marsing, A., Dörnbrack, A.,
1376 Roiger, A., Yu, F., Gauthier, M., Renard, C., Swann, P., Johnson, M., Ahrens, D., Sallinen, R., Eckel, G., and Le Clercq, P.:
1377 Fuel sulfur content can modulate contrail ice crystal numbers, *Communications Earth & Environment*, 6, 902,
1378 <https://doi.org/10.1038/s43247-025-02951-5>, 2025.
- 1379 Duda, D. P. and Minnis, P.: Basic Diagnosis and Prediction of Persistent Contrail Occurrence Using High-Resolution
1380 Numerical Weather Analyses/Forecasts and Logistic Regression. Part II: Evaluation of Sample Models, *Journal of Applied
1381 Meteorology and Climatology*, 48, 1790-1802, <https://doi.org/10.1175/2009jamc2057.1>, 2009.
- 1382 Duda, D. P., Minnis, P., and Nguyen, L.: Estimates of cloud radiative forcing in contrail clusters using GOES imagery, *Journal
1383 of Geophysical Research: Atmospheres*, 106, 4927-4937, <https://doi.org/10.1029/2000jd900393>, 2001.



- 1384 Duda, D. P., Minnis, P., and Palikonda, R.: Estimated contrail frequency and coverage over the contiguous United States from
1385 numerical weather prediction analyses and flight track data, *Meteorologische Zeitschrift*, 14, 537-548,
1386 <https://doi.org/10.1127/0941-2948/2005/0050>, 2005.
- 1387 Duda, D. P., Minnis, P., Nguyen, L., and Palikonda, R.: A Case Study of the Development of Contrail Clusters over the Great
1388 Lakes, *Journal of the Atmospheric Sciences*, 61, 1132-1146, [https://doi.org/10.1175/1520-0469\(2004\)061<1132:Acsofd>2.0.Co;2](https://doi.org/10.1175/1520-0469(2004)061<1132:Acsofd>2.0.Co;2), 2004.
- 1390 Duda, D. P., Minnis, P., Khlopenkov, K., Chee, T. L., and Boeke, R.: Estimation of 2006 Northern Hemisphere contrail
1391 coverage using MODIS data, *Geophysical Research Letters*, 40, 612-617, <https://doi.org/10.1002/grl.50097>, 2013.
- 1392 Engberg, Z., Teoh, R., Abbott, T., Dean, T., Stettler, M. E. J., and Shapiro, M. L.: Forecasting contrail climate forcing for
1393 flight planning and air traffic management applications: the CocipGrid model in pycontrails 0.51.0, *Geoscientific Model
1394 Development*, 18, 253-286, <https://doi.org/10.5194/gmd-18-253-2025>, 2025.
- 1395 EPA: Contrails fact sheet, 2025.
- 1396 Ernst, S.: Die Entstehung von Eisnebel aus den Auspuffgasen von Flugmotoren, *Institute of Atmospheric Physics*, 5, 1941.
- 1397 Euchenhofer, M. V., Prashanth, P., Parke, S. A., Eastham, S. D., and Waitz, I. A.: Contrail Observation Limitations Using
1398 Geostationary Satellites, *Geophysical Research Letters*, 52, <https://doi.org/10.1029/2025gl118386>, 2025.
- 1399 Filonchik, M., Peterson, M. P., Zhang, L., Hurynovich, V., and He, Y.: Greenhouse gases emissions and global climate change:
1400 Examining the influence of CO₂, CH₄, and N₂O, *Sci Total Environ*, 935, 173359,
1401 <https://doi.org/10.1016/j.scitotenv.2024.173359>, 2024.
- 1402 Forbes, R. M., Tompkins, A. M., and Untch, A.: A new prognostic bulk microphysics scheme for the IFS, 2011.
- 1403 Freudenthaler, V., Homburg, F., and Jäger, H.: Optical parameters of contrails from lidar measurements: Linear depolarization,
1404 *Geophysical Research Letters*, 23, 3715-3718, <https://doi.org/10.1029/96gl03646>, 1996.
- 1405 Fritz, T. M., Eastham, S. D., Speth, R. L., and Barrett, S. R. H.: The role of plume-scale processes in long-term impacts of
1406 aircraft emissions, *Atmospheric Chemistry and Physics*, 20, 5697-5727, <https://doi.org/10.5194/acp-20-5697-2020>, 2020.
- 1407 Gaillot, T., Beauchet, S., Lorne, D., and Krim, L.: The impact of fossil jet fuel emissions at altitude on climate change: A life
1408 cycle assessment study of a long-haul flight at different time horizons, *Atmospheric Environment*, 311, 119983-119995,
1409 <https://doi.org/10.1016/j.atmosenv.2023.119983>, 2023.
- 1410 Geraedts, S., Brand, E., Dean, T. R., Eastham, S., Elkin, C., Engberg, Z., Hager, U., Langmore, I., McCloskey, K., Yue-Hei
1411 Ng, J., Platt, J. C., Sankar, T., Sarna, A., Shapiro, M., and Goyal, N.: A scalable system to measure contrail formation on a
1412 per-flight basis, *Environmental Research Communications*, 6, 015008-015020, <https://doi.org/10.1088/2515-7620/ad11ab>,
1413 2024.
- 1414 Gierens, K. and Schumann, U.: Colors of contrails from fuels with different sulfur contents, *Journal of Geophysical Research:
1415 Atmospheres*, 101, 16731-16736, <https://doi.org/10.1029/96jd01169>, 1996.



- 1416 Grewe, V., Dahlmann, K., Flink, J., Frömming, C., Ghosh, R., Gierens, K., Heller, R., Hendricks, J., Jöckel, P., Kaufmann, S.,
1417 Kölker, K., Linke, F., Luchkova, T., Lührs, B., Van Manen, J., Matthes, S., Minikin, A., Niklaß, M., Plohr, M., Righi, M.,
1418 Rosanka, S., Schmitt, A., Schumann, U., Terekhov, I., Unterstrasser, S., Vázquez-Navarro, M., Voigt, C., Wicke, K.,
1419 Yamashita, H., Zahn, A., and Ziereis, H.: Mitigating the Climate Impact from Aviation: Achievements and Results of the DLR
1420 WeCare Project, *Aerospace*, 4, 34-38, <https://doi.org/10.3390/aerospace4030034>, 2017.
- 1421 Gruber, S., Unterstrasser, S., Bechtold, J., Vogel, H., Jung, M., Pak, H., and Vogel, B.: Contrails and their impact on shortwave
1422 radiation and photovoltaic power production – a regional model study, *Atmospheric Chemistry and Physics*, 18, 6393-6411,
1423 <https://doi.org/10.5194/acp-18-6393-2018>, 2018.
- 1424 Hansen, J., Sato, M., Ruedy, R., Nazarenko, L., Lacis, A., Schmidt, G. A., Russell, G., Aleinov, I., Bauer, M., Bauer, S., Bell,
1425 N., Cairns, B., Canuto, V., Chandler, M., Cheng, Y., Del Genio, A., Faluvegi, G., Fleming, E., Friend, A., Hall, T., Jackman,
1426 C., Kelley, M., Kiang, N., Koch, D., Lean, J., Lerner, J., Lo, K., Menon, S., Miller, R., Minnis, P., Novakov, T., Oinas, V.,
1427 Perlwitz, J., Perlwitz, J., Rind, D., Romanou, A., Shindell, D., Stone, P., Sun, S., Tausnev, N., Thresher, D., Wielicki, B.,
1428 Wong, T., Yao, M., and Zhang, S.: Efficacy of climate forcings, *Journal of Geophysical Research: Atmospheres*, 110, 1–45,
1429 <https://doi.org/10.1029/2005jd005776>, 2005.
- 1430 Hashemi, Z., Gholampour, M., Su, H.-H., Chiang, C.-Y., Chang, H.-H., and Wang, C.-C.: Hybrid physics-informed neural
1431 networks for airflow and thermal modeling in data center environments, *International Communications in Heat and Mass*
1432 *Transfer*, 168, 109511-109525, <https://doi.org/10.1016/j.icheatmasstransfer.2025.109511>, 2025.
- 1433 Heni, N., Akhiat, Y., Kinard, K., and Daw, Z.: Towards Deep Learning-Based Estimation of Contrail Environmental Impact:
1434 Transatlantic Flights as a Case Study, 2025 AIAA DATC/IEEE 44th Digital Avionics Systems Conference (DASC), Montreal,
1435 QC, Canada, <https://doi.org/10.1109/dasc66011.2025.11257398>, 2025.
- 1436 Heymann, J., Schneising, O., Reuter, M., Buchwitz, M., Rozanov, V. V., Velazco, V. A., Bovensmann, H., and Burrows, J.
1437 P.: SCIAMACHY WFM-DOAS XCO₂: comparison with CarbonTracker XCO₂ focusing on aerosols and thin clouds,
1438 *Atmospheric Measurement Techniques*, 5, 1935-1952, <https://doi.org/10.5194/amt-5-1935-2012>, 2012.
- 1439 Heymsfield, A., Baumgardner, D., DeMott, P., Forster, P., Gierens, K., and Kärcher, B.: Contrail Microphysics, *Bulletin of*
1440 *the American Meteorological Society*, 91, 465-472, <https://doi.org/10.1175/2009bams2839.1>, 2010.
- 1441 Hofer, S., Gierens, K., and Rohs, S.: How well can persistent contrails be predicted? An update, *Atmospheric Chemistry and*
1442 *Physics*, 24, 7911-7925, <https://doi.org/10.5194/acp-24-7911-2024>, 2024.
- 1443 Huebsch, W. W., Meza, O., and Lewellen, D. C.: Persistent Contrails and Contrail Cirrus. Part I: Large-Eddy Simulations
1444 from Inception to Demise, *Journal of the Atmospheric Sciences*, 71, 4399-4419, <https://doi.org/10.1175/jas-d-13-0316.1>, 2014.
- 1445 Hurrell, J. W., Holland, M. M., Gent, P. R., Ghan, S., Kay, J. E., Kushner, P. J., Lamarque, J. F., Large, W. G., Lawrence, D.,
1446 Lindsay, K., Lipscomb, W. H., Long, M. C., Mahowald, N., Marsh, D. R., Neale, R. B., Rasch, P., Vavrus, S., Vertenstein,
1447 M., Bader, D., Collins, W. D., Hack, J. J., Kiehl, J., and Marshall, S.: The Community Earth System Model: A Framework for



- 1448 Collaborative Research, *Bulletin of the American Meteorological Society*, 94, 1339-1360, [https://doi.org/10.1175/bams-d-12-](https://doi.org/10.1175/bams-d-12-00121.1)
1449 [00121.1](https://doi.org/10.1175/bams-d-12-00121.1), 2013.
- 1450 Jackson, A.: Statistical Contrail Forecasting, *Journal of Applied Meteorology and Climatology*, 40,
1451 [https://doi.org/10.1175/1520-0450\(2001\)040%3C0269:SCF%3E2.0.CO;2](https://doi.org/10.1175/1520-0450(2001)040%3C0269:SCF%3E2.0.CO;2), 2001.
- 1452 Jackson, A., Newton, B., Hahn, D., and Bussey, A.: Statistical Contrail Forecasting, *Journal of Applied Meteorology*, 40, 269-
1453 279, [https://doi.org/10.1175/1520-0450\(2001\)040<0269:Scf>2.0.Co;2](https://doi.org/10.1175/1520-0450(2001)040<0269:Scf>2.0.Co;2), 2001.
- 1454 Jansen, J. and Heymsfield, A. J.: Microphysics of Aerodynamic Contrail Formation Processes, *Journal of the Atmospheric*
1455 *Sciences*, 72, 3293-3308, <https://doi.org/10.1175/jas-d-14-0362.1>, 2015.
- 1456 Jarry, G., Dalmau, R., Very, P., Ballerini, F., and Bocu, S.-D.: GVCCS: a dataset for contrail identification and tracking on
1457 visible whole sky camera sequences, *Earth System Science Data*, 18, 1037-1059, <https://doi.org/10.5194/essd-18-1037-2026>,
1458 2026.
- 1459 Jensen, E. J., van den Heever, S. C., and Grant, L. D.: The Life Cycles of Ice Crystals Detrained From the Tops of Deep
1460 Convection, *Journal of Geophysical Research: Atmospheres*, 123, 9624-9634, <https://doi.org/10.1029/2018jd028832>, 2018.
- 1461 Jensen, E. J., Ueyama, R., Pfister, L., and Atlas, R. L.: The Impacts of Gravity Waves and Wind Shear on the Lifecycle of
1462 Cirrus Clouds in the Tropical Tropopause Layer, *Journal of Geophysical Research: Atmospheres*, 130,
1463 <https://doi.org/10.1029/2024jd042308>, 2025.
- 1464 Jensen, E. J., Toon, O. B., Kinne, S., Sachse, G. W., Anderson, B. E., Chan, K. R., Twohy, C. H., Gandrud, B., Heymsfield,
1465 A., and Miake-Lye, R. C.: Environmental conditions required for contrail formation and persistence, *Journal of Geophysical*
1466 *Research: Atmospheres*, 103, 3929-3936, <https://doi.org/10.1029/97jd02808>, 1998.
- 1467 Kalluri, S., Cao, C., Heidinger, A., Ignatov, A., Key, J., and Smith, T.: The Advanced Very High Resolution Radiometer:
1468 Contributing to Earth Observations for over 40 Years, *Bulletin of the American Meteorological Society*, 102, E351-E366,
1469 <https://doi.org/10.1175/bams-d-20-0088.1>, 2021.
- 1470 Kameníková, I., Nagy, I., and Hospodka, J.: Contrails and Their Dependence on Meteorological Situations, *Applied Sciences*,
1471 14, <https://doi.org/10.3390/app14083199>, 2024.
- 1472 Karcher, B.: Formation and radiative forcing of contrail cirrus, *Nat Commun*, 9, 1824, [https://doi.org/10.1038/s41467-018-](https://doi.org/10.1038/s41467-018-04068-0)
1473 [04068-0](https://doi.org/10.1038/s41467-018-04068-0), 2018.
- 1474 Kärcher, B. and Corcos, M.: On the Lifetimes of Persistent Contrails and Contrail Cirrus, *Journal of Geophysical Research:*
1475 *Atmospheres*, 130, e2025JD044488 (044481–044428), <https://doi.org/10.1029/2025jd044488>, 2025.
- 1476 Kärcher, B. and Yu, F.: Role of aircraft soot emissions in contrail formation, *Geophysical Research Letters*, 36, L01804,
1477 <https://doi.org/10.1029/2008gl036649>, 2009.
- 1478 Kärcher, B., Burkhardt, U., Unterstrasser, S., and Minnis, P.: Factors controlling contrail cirrus optical depth, *Atmospheric*
1479 *Chemistry and Physics*, 9, 6229-6254, <https://doi.org/10.5194/acp-9-6229-2009>, 2009.



- 1480 Kärcher, B., Kleine, J., Sauer, D., and Voigt, C.: Contrail Formation: Analysis of Sublimation Mechanisms, *Geophysical*
1481 *Research Letters*, 45, 13547–13552, <https://doi.org/10.1029/2018gl079391>, 2018.
- 1482 Kärcher, B., Burkhardt, U., Bier, A., Bock, L., and Ford, I. J.: The microphysical pathway to contrail formation, *Journal of*
1483 *Geophysical Research: Atmospheres*, 120, 7893-7927, <https://doi.org/10.1002/2015jd023491>, 2015.
- 1484 Kärcher, B., Busen, R., Petzold, A., Schröder, F. P., Schumann, U., and Jensen, E. J.: Physicochemistry of aircraft-generated
1485 liquid aerosols, soot, and ice particles: 2. Comparison with observations and sensitivity studies, *Journal of Geophysical*
1486 *Research: Atmospheres*, 103, 17129-17147, <https://doi.org/10.1029/98jd01045>, 1998.
- 1487 Khangaonkar, T., Premathilake, L., Cope, B., Knightes, C., and Tseng, A.: PLUMES2.0 – Dilution Model, Center for Urban
1488 Waters, University of Washington, TacomaEPA/600/B-24/339, 2024.
- 1489 Kleine, J., Voigt, C., Sauer, D., Schlager, H., Scheibe, M., Jurkat-Witschas, T., Kaufmann, S., Kärcher, B., and Anderson, B.
1490 E.: In Situ Observations of Ice Particle Losses in a Young Persistent Contrail, *Geophysical Research Letters*, 45,
1491 <https://doi.org/10.1029/2018gl079390>, 2018.
- 1492 Konopka, P. and Vogelsberger, W.: Köhler equation for finite systems: A simple estimation of possible condensation
1493 mechanisms in aircraft contrails, *Journal of Geophysical Research: Atmospheres*, 102, 16057-16064,
1494 <https://doi.org/10.1029/97jd00899>, 1997.
- 1495 Korhonen, K., Kristensen, T. B., Falk, J., Malmborg, V. B., Eriksson, A., Gren, L., Novakovic, M., Shamun, S., Karjalainen,
1496 P., Markkula, L., Pagels, J., Svenningsson, B., Tunér, M., Komppula, M., Laaksonen, A., and Virtanen, A.: Particle emissions
1497 from a modern heavy-duty diesel engine as ice nuclei in immersion freezing mode: a laboratory study on fossil and renewable
1498 fuels, *Atmospheric Chemistry and Physics*, 22, 1615-1631, <https://doi.org/10.5194/acp-22-1615-2022>, 2022.
- 1499 Kundgol, C. B., Wrase, J., Larsson, L., Rytter, D., and Josefsson, B.: Aircraft Contrail Prediction for Commercial Flights,
1500 2025 Integrated Communications, Navigation and Surveillance Conference (ICNS),
1501 <https://doi.org/10.1109/icns65417.2025.10976888>, 2025.
- 1502 Laaksonen, A. and Malila, J.: Ice nucleation, in: *Nucleation of Water*, 209-248, [https://doi.org/10.1016/b978-0-12-814321-](https://doi.org/10.1016/b978-0-12-814321-6.00018-x)
1503 [6.00018-x](https://doi.org/10.1016/b978-0-12-814321-6.00018-x), 2022.
- 1504 Lee, D. S., Fahey, D. W., Forster, P. M., Newton, P. J., Wit, R. C. N., Lim, L. L., Owen, B., and Sausen, R.: Aviation and
1505 global climate change in the 21st century, *Atmos Environ* (1994), 43, 3520-3537,
1506 <https://doi.org/10.1016/j.atmosenv.2009.04.024>, 2009.
- 1507 Lee, D. S., Fahey, D. W., Skowron, A., Allen, M. R., Burkhardt, U., Chen, Q., Doherty, S. J., Freeman, S., Forster, P. M.,
1508 Fuglestedt, J., Gettelman, A., De Leon, R. R., Lim, L. L., Lund, M. T., Millar, R. J., Owen, B., Penner, J. E., Pitari, G.,
1509 Prather, M. J., Sausen, R., and Wilcox, L. J.: The contribution of global aviation to anthropogenic climate forcing for 2000 to
1510 2018, *Atmos Environ* (1994), 244, 117834, <https://doi.org/10.1016/j.atmosenv.2020.117834>, 2021.
- 1511 Lee, T. F.: Jet Contrail Identification Using the AVHRR Infrared Split Window, *Notes and Correspondence*, 28, 1988.



- 1512 Lewellen, D. C.: Persistent Contrails and Contrail Cirrus. Part II: Full Lifetime Behavior, *Journal of the Atmospheric Sciences*,
1513 71, 4420-4438, <https://doi.org/10.1175/jas-d-13-0317.1>, 2014.
- 1514 Li, J., Kim, J.-H., Sridhar, B., and Ng, H. K.: Ames Contrail Simulation Model: Modeling Aviation Induced Contrails and the
1515 Computation of Contrail Radiative Forcing Using Air Traffic Data, Technical Memorandum (TM) NASA/TM-20230014633,
1516 1-48, 2023a.
- 1517 Li, J., Kim, J.-H., Sridhar, B., and Ng, H. K.: Review of Past Decade of Aviation Contrail Research: Insights and Future
1518 Directions for Operational Mitigation, National Aeronautics and Space Administration NASA/TM-20250007272, 2025.
- 1519 Li, Y., Mahnke, C., Rohs, S., Bundke, U., Spelten, N., Dekoutsidis, G., Groß, S., Voigt, C., Schumann, U., Petzold, A., and
1520 Krämer, M.: Upper-tropospheric slightly ice-subsaturated regions: frequency of occurrence and statistical evidence for the
1521 appearance of contrail cirrus, *Atmospheric Chemistry and Physics*, 23, 2251-2271, <https://doi.org/10.5194/acp-23-2251-2023>,
1522 2023b.
- 1523 Libbrecht, K. G.: Physical Dynamics of Ice Crystal Growth, *Annual Review of Materials Research*, 47, 271-295,
1524 <https://doi.org/10.1146/annurev-matsci-070616-124135>, 2017.
- 1525 Libbrecht, K. G. and Rickerby, M. E.: Measurements of Growth Rates of (0001) Ice Crystal Surfaces, arXiv preprint
1526 <https://doi.org/10.48550/arXiv.1110.5828>, 2011.
- 1527 Lin, Q., Leng, Q., Ding, Z., Yan, C., and Xu, X.: Optimizing Contrail Detection: A Deep Learning Approach with EfficientNet-
1528 b4 Encoding, 2024 IEEE 4th International Conference on Electronic Technology, Communication and Information (ICETCI),
1529 <https://doi.org/10.1109/icetci61221.2024.10594699>, 2024.
- 1530 Lu, Z., Zhang, Q., and Streets, D. G.: Sulfur dioxide and primary carbonaceous aerosol emissions in China and India, 1996–
1531 2010, *Atmospheric Chemistry and Physics*, 11, 9839-9864, <https://doi.org/10.5194/acp-11-9839-2011>, 2011.
- 1532 M. Ponater, S. B., R. Sausen, U. Schumann: Simulating the Global Atmospheric Response to Aircraft Water Vapour Emissions
1533 and Contrails - A First Approach Using a GCM *Annales Geophysicae*, 1996.
- 1534 M. Bjornson, C. B.: SAC Contrail Formation Study, USAF Environmental Technical Applications Center
1535 (USAFETAC/DNO), Scott AFB, IL 62225-5458, 1992.
- 1536 Magee, N. B., Miller, A., Amaral, M., and Cumiskey, A.: Mesoscopic surface roughness of ice crystals pervasive across a
1537 wide range of ice crystal conditions, *Atmospheric Chemistry and Physics*, 14, 12357-12371, [https://doi.org/10.5194/acp-14-
1538 12357-2014](https://doi.org/10.5194/acp-14-12357-2014), 2014.
- 1539 Mahowald, N., Albani, S., Kok, J. F., Engelstaeder, S., Scanza, R., Ward, D. S., and Flanner, M. G.: The size distribution of
1540 desert dust aerosols and its impact on the Earth system, *Aeolian Research*, 15, 53-71,
1541 <https://doi.org/10.1016/j.aeolia.2013.09.002>, 2014.
- 1542 Mahrt, F., Marcolli, C., David, R. O., Grönquist, P., Barthazy Meier, E. J., Lohmann, U., and Kanji, Z. A.: Ice nucleation
1543 abilities of soot particles determined with the Horizontal Ice Nucleation Chamber, *Atmospheric Chemistry and Physics*, 18,
1544 13363-13392, <https://doi.org/10.5194/acp-18-13363-2018>, 2018.



- 1545 Mannstein, H., Meyer, R., and Wendling, P.: Operational detection of contrails from NOAA-AVHRR-data, International
1546 Journal of Remote Sensing, 20, 1641-1660, <https://doi.org/10.1080/014311699212650>, 2010.
- 1547 Martin Frias, A., Shapiro, M. L., Engberg, Z., Zopp, R., Soler, M., and Stettler, M. E. J.: Feasibility of contrail avoidance in a
1548 commercial flight planning system: an operational analysis, Environmental Research: Infrastructure and Sustainability, 4,
1549 <https://doi.org/10.1088/2634-4505/ad310c>, 2024.
- 1550 Martin Stuffer, X. M., Gerd Wendler: MM5 contrail forecasting in Alaska, Monthly Weather Review - Special Selection,
1551 2004.
- 1552 Mazon, J. and Pino, D.: A WRF Simulation of an Episode of Contrails Covering the Entire Sky, Atmosphere, 7,
1553 <https://doi.org/10.3390/atmos7070095>, 2016.
- 1554 Meijer, V. R., Eastham, S. D., Waitz, I. A., and Barrett, S. R. H.: Contrail altitude estimation using GOES-16 ABI data and
1555 deep learning, Atmospheric Measurement Techniques, 17, 6145-6162, <https://doi.org/10.5194/amt-17-6145-2024>, 2024.
- 1556 Meyer, K., Platnick, S., Arnold, G. T., Amarasinghe, N., Miller, D., Small-Griswold, J., Witte, M., Cairns, B., Gupta, S.,
1557 McFarquhar, G., and O'Brien, J.: Evaluating spectral cloud effective radius retrievals from the Enhanced MODIS Airborne
1558 Simulator (eMAS) during ORACLES, Atmospheric Measurement Techniques, 18, 981-1011, [https://doi.org/10.5194/amt-18-](https://doi.org/10.5194/amt-18-981-2025)
1559 [981-2025](https://doi.org/10.5194/amt-18-981-2025) 2025.
- 1560 Minnis, P., Ayers, J. K., Palikonda, R., and Phan, D.: Contrails, Cirrus Trends, and Climate, Journal of Climate, 17, 1671-
1561 1685, [https://doi.org/10.1175/1520-0442\(2004\)017<1671:Cctac>2.0.Co;2](https://doi.org/10.1175/1520-0442(2004)017<1671:Cctac>2.0.Co;2), 2004.
- 1562 Minnis, P., Young, D. F., Garber, D. P., Nguyen, L., Smith, W. L., and Palikonda, R.: Transformation of contrails into cirrus
1563 during SUCCESS, Geophysical Research Letters, 25, 1157-1160, <https://doi.org/10.1029/97gl03314>, 1998.
- 1564 Minnis, P., Bedka, S. T., Duda, D. P., Bedka, K. M., Chee, T., Ayers, J. K., Palikonda, R., Spangenberg, D. A., Khlopenkov,
1565 K. V., and Boeke, R.: Linear contrail and contrail cirrus properties determined from satellite data, Geophysical Research
1566 Letters, 40, 3220-3226, <https://doi.org/10.1002/grl.50569>, 2013.
- 1567 Musial, J. P., Hüsler, F., Sütterlin, M., Neuhaus, C., and Wunderle, S.: Probabilistic approach to cloud and snow detection on
1568 Advanced Very High Resolution Radiometer (AVHRR) imagery, Atmospheric Measurement Techniques, 7, 799-822,
1569 <https://doi.org/10.5194/amt-7-799-2014>, 2014.
- 1570 N, H. A.: The Formation of Exhaust Condensation Trails by Jet Aircraft, AMERICAN METEOROLOGICAL SOCIETY,
1571 1953.
- 1572 Ng, J. Y.-H., McCloskey, K., Cui, J., Meijer, V. R., Brand, E., Sarna, A., Goyal, N., Van Arsdale, C., and Geraedts, S.: Contrail
1573 Detection on GOES-16 ABI With the OpenContrails Dataset, IEEE Transactions on Geoscience and Remote Sensing, 62, 1-
1574 14, <https://doi.org/10.1109/tgrs.2023.3345226>, 2024.
- 1575 Nguyen Huu, Ž., Kotarba, A. Z., and Wypych, A.: Evaluation of the operational MODIS cloud mask product for detecting
1576 cirrus clouds, Atmospheric Measurement Techniques, 18, 3897-3915, <https://doi.org/10.5194/amt-18-3897-2025>, 2025.



- 1577 Ning, Z., Ma, Y., He, S., Li, G., Xu, Y., Wang, Z., Zhang, Y., Ma, E., Ma, C., and Wu, J.: High altitude air pollution and
1578 respiratory disease: Evaluating compounded exposure events and interactions, *Ecotoxicol Environ Saf*, 285, 117046,
1579 <https://doi.org/10.1016/j.ecoenv.2024.117046>, 2024.
- 1580 Oh, L. J.: Sensitivities of Atmospheric Composition to High Altitude vehicle Emissions, Department of Aeronautics and
1581 Astronautics, MASSACHUSETTS INSTITUTE OF TECHNOLOGY, 75 pp., 2020.
- 1582 P. Stier , J. F., S. Kinne1 , S. Kloster , E. Vignati , J. Wilson , L. Ganzeveld , I. Tegen , M. Werner , Y. Balkanski , M. Schulz
1583 , O. Boucher , A. Minikin , and A. Petzold: The aerosol-climate model ECHAM5-HAM, *Atmospheric Chemistry and Physics*,
1584 1125-1156, 2005.
- 1585 Pal, D., Hall, R., Nazarenko, Y., Barrie, L., and Ariya, P. A.: Microphysical detection of nano-ice nuclei to ice crystals: a
1586 platform for ice nucleation research, *npj Climate and Atmospheric Science*, 8, 2397-3722, [https://doi.org/10.1038/s41612-](https://doi.org/10.1038/s41612-025-01062-4)
1587 [025-01062-4](https://doi.org/10.1038/s41612-025-01062-4), 2025.
- 1588 Patrick Minnis, D., David P, Palikonda, Rabindra, Bedka, Sarah T , Boeke, Robyn, Khlopenkov, Konstantin Chee, Thad,
1589 Bedka, Kristopher T.: Estimating Contrail Climate Effects From Satellite Data, 3rd AIAA Atmospheric Space Environments
1590 Conference, Honolulu, HI, US2013.
- 1591 Peter, P., Matthes, S., Frömming, C., Jöckel, P., Bugliaro, L., Giez, A., Krämer, M., and Grewe, V.: Influence of temperature
1592 and humidity on contrail formation regions in the general circulation model EMAC: a spring case study, *Atmospheric*
1593 *Chemistry and Physics*, 25, 5911-5934, <https://doi.org/10.5194/acp-25-5911-2025>, 2025.
- 1594 Petzold, A., Khan, N. F., Li, Y., Spichtinger, P., Rohs, S., Crewell, S., Wahner, A., and Kramer, M.: Most long-lived contrails
1595 form within cirrus clouds with uncertain climate impact, *Nat Commun*, 16, 9695, [https://doi.org/10.1038/s41467-025-65532-](https://doi.org/10.1038/s41467-025-65532-2)
1596 [2](https://doi.org/10.1038/s41467-025-65532-2), 2025.
- 1597 Podglajen, A., Plougonven, R., Hertzog, A., and Jensen, E.: Impact of gravity waves on the motion and distribution of
1598 atmospheric ice particles, *Atmospheric Chemistry and Physics*, 18, 10799-10823, <https://doi.org/10.5194/acp-18-10799-2018>,
1599 2018.
- 1600 Ponsonby, J., King, L., Murray, B. J., and Stettler, M. E. J.: Jet aircraft lubrication oil droplets as contrail ice-forming particles,
1601 *Atmospheric Chemistry and Physics*, 24, 2045-2058, <https://doi.org/10.5194/acp-24-2045-2024>, 2024.
- 1602 Ponsonby, J., Teoh, R., Kärcher, B., and Stettler, M. E. J.: An updated microphysical model for particle activation in contrails:
1603 the role of volatile plume particles, *Atmospheric Chemistry and Physics*, 25, 18617-18637, [https://doi.org/10.5194/acp-25-](https://doi.org/10.5194/acp-25-18617-2025)
1604 [18617-2025](https://doi.org/10.5194/acp-25-18617-2025), 2025.
- 1605 R.Paoli, J. H., T. J. Poinsoot,S.Ghosal Contrail formation in aircraft wakes using large eddy simulations, Center for Turbulence
1606 Research, 2002.
- 1607 Rädcl, G. and Shine, K. P.: Radiative forcing by persistent contrails and its dependence on cruise altitudes, *Journal of*
1608 *Geophysical Research: Atmospheres*, 113, <https://doi.org/10.1029/2007jd009117>, 2008.



- 1609 Randall, D. A., Bitz, C. M., Danabasoglu, G., Denning, A. S., Gent, P. R., Gettelman, A., Griffies, S. M., Lynch, P., Morrison,
1610 H., Pincus, R., and Thuburn, J.: 100 Years of Earth System Model Development, *Meteorological Monographs*, 59, 12.11-
1611 12.66, <https://doi.org/10.1175/amsmonographs-d-18-0018.1>, 2019.
- 1612 Rap, A., Forster, P. M., Jones, A., Boucher, O., Haywood, J. M., Bellouin, N., and De Leon, R. R.: Parameterization of contrails
1613 in the UK Met Office Climate Model, *Journal of Geophysical Research: Atmospheres*, 115,
1614 <https://doi.org/10.1029/2009jd012443>, 2010.
- 1615 Raphael Alamu, S. K., Sazzad Hossain, Mahendra rishnapatnam, Ankur Aggarwal, Zarif Zahir, Harshad Vijay Pandhare,
1616 Varun Shah: Physics-Informed Neural Networks for Climate Modeling Bridging Machine Learning and Physical Laws, 2025.
1617 Airspace over Europe, last
1618 Simulation of all global air traffic within one day, last
- 1619 Rieger, D., Bangert, M., Bischoff-Gauss, I., Förstner, J., Lundgren, K., Reinert, D., Schröter, J., Vogel, H., Zängl, G., Ruhnke,
1620 R., and Vogel, B.: ICON-ART 1.0 – a new online-coupled model system from the global to regional scale, *Geoscientific
1621 Model Development*, 8, 1659-1676, <https://doi.org/10.5194/gmd-8-1659-2015>, 2015.
- 1622 Riggi-Carolo, E., Dubot, T., Sarrat, C., and Bedouet, J.: AI-Driven Identification of Contrail Sources: Integrating Satellite
1623 Observation and Air Traffic Data, *Journal of Open Aviation Science*, 1, <https://doi.org/10.59490/joas.2023.7209>, 2023.
- 1624 Rubin-Zuzic, M., Bugliaro, L., Marsing, A., Wang, Z., Voigt, C., Simson, C., Kaiser, S., and Ziegler, P.: Reduced contrail
1625 radiative effect for fleets with low soot and water vapour emissions, *Atmospheric Environment: X*, 27,
1626 <https://doi.org/10.1016/j.aeaoa.2025.100353>, 2025.
- 1627 S. Gruber, B. V., H. Vogel, J. Bechtold, M. Jung, H. Pak: Simulating Contrails with COSMO-ART Based on Real Time, TAC-
1628 4 Proceedings, Bad Kohlgrub
- 1629 S. Unterstrasser, K. G.: Numerical simulations of contrail-to-cirrus transition – Part 1- An extensive parametric study,
1630 *Atmospheric Chemistry and Physics*, 10, 2017-2036, 2009.
- 1631 Sama, A., Meijer, V., Chevallier, R., Duncan, A., McConnaughay, K., Geraedts, S., and McCloskey, K.: Benchmarking and
1632 improving algorithms for attributing satellite-observed contrails to flights, *Atmospheric Measurement Techniques*, 18, 3495-
1633 3532, <https://doi.org/10.5194/amt-18-3495-2025>, 2025.
- 1634 Saulgeot, P., Brion, V., Bonne, N., Dormy, E., and Jacquin, L.: Effects of atmospheric stratification and jet position on the
1635 properties of early aircraft contrails, *Physical Review Fluids*, 8, <https://doi.org/10.1103/PhysRevFluids.8.114702>, 2023.
- 1636 Schrader, M. L.: Calculations of Aircraft Contrail Formation Critical Temperatures, *Journal of Applied Meteorology and
1637 Climatology*, 36, 1725–1729, [https://doi.org/10.1175/1520-0450\(1997\)036%3C1725:COACFC%3E2.0.CO;2](https://doi.org/10.1175/1520-0450(1997)036%3C1725:COACFC%3E2.0.CO;2), 1997.
- 1638 Schumann, U.: A contrail cirrus prediction model, *Geoscientific Model Development*, 5, 543-580,
1639 <https://doi.org/10.5194/gmd-5-543-2012>, 2012.
- 1640 Schumann, U. and Heymsfield, A. J.: On the Life Cycle of Individual Contrails and Contrail Cirrus, *Meteorological
1641 Monographs*, 58, 3.1-3.24, <https://doi.org/10.1175/amsmonographs-d-16-0005.1>, 2017.



- 1642 Schumann, U., Ström, J., Busen, R., Baumann, R., Gierens, K., Krautstrunk, M., Schröder, F. P., and Stingl, J.: In situ
1643 observations of particles in jet aircraft exhausts and contrails for different sulfur-containing fuels, *Journal of Geophysical*
1644 *Research: Atmospheres*, 101, 6853-6869, <https://doi.org/10.1029/95jd03405>, 1996.
- 1645 Schumann, U., Kiemle, C., Schlager, H., Weigel, R., Borrmann, S., D'Amato, F., Krämer, M., Matthey, R., Protat, A., Voigt,
1646 C., and Volk, C. M.: Long-lived contrails and convective cirrus above the tropical tropopause, *Atmospheric Chemistry and*
1647 *Physics*, 17, 2311-2346, <https://doi.org/10.5194/acp-17-2311-2017>, 2017.
- 1648 Seelig, T., Wolf, K., Bellouin, N., and Tesche, M.: Quantification of the radiative forcing of contrails embedded in cirrus
1649 clouds, *Nat Commun*, 16, 10703, <https://doi.org/10.1038/s41467-025-66231-8>, 2025.
- 1650 Singh, D. K., Sanyal, S., and Wuebbles, D. J.: Understanding the role of contrails and contrail cirrus in climate change: a global
1651 perspective, *Atmospheric Chemistry and Physics*, 24, 9219-9262, <https://doi.org/10.5194/acp-24-9219-2024>, 2024.
- 1652 Spichtinger, P. and Gierens, K. M.: Modelling of cirrus clouds – Part 1a: Model description and validation, *Atmospheric*
1653 *Chemistry and Physics*, 9, 685-706, <https://doi.org/10.5194/acp-9-685-2009>, 2009.
- 1654 Spichtinger, P., Marschalik, P., and Baumgartner, M.: Impact of formulations of the homogeneous nucleation rate on ice
1655 nucleation events in cirrus, *Atmospheric Chemistry and Physics*, 23, 2035-2060, <https://doi.org/10.5194/acp-23-2035-2023>,
1656 2023.
- 1657 Steven L. Baughcum, S. C. H., Peter S. Hertel, Debra R. Maggiora, and Carlos A. Oncina Stratospheric Emissions Effects
1658 Database Development, 1994.
- 1659 Stevens, B., Giorgetta, M., Esch, M., Mauritsen, T., Crueger, T., Rast, S., Salzmann, M., Schmidt, H., Bader, J., Block, K.,
1660 Brokopf, R., Fast, I., Kinne, S., Kornblueh, L., Lohmann, U., Pincus, R., Reichler, T., and Roeckner, E.: Atmospheric
1661 component of the MPI-M Earth System Model: ECHAM6, *Journal of Advances in Modeling Earth Systems*, 5, 146-172,
1662 <https://doi.org/10.1002/jame.20015>, 2013.
- 1663 Sun, J. and Roosenbrand, E.: Fast contrail estimation with OpenSky data, *Journal of Open Aviation Science*, 1,
1664 <https://doi.org/10.59490/joas.2023.7264>, 2023.
- 1665 Teoh, R., Engberg, Z., Shapiro, M., Dray, L., and Stettler, M. E. J.: The high-resolution Global Aviation emissions Inventory
1666 based on ADS-B (GAIA) for 2019–2021, *Atmospheric Chemistry and Physics*, 24, 725-744, [https://doi.org/10.5194/acp-24-
1667 725-2024](https://doi.org/10.5194/acp-24-725-2024), 2024a.
- 1668 Teoh, R., Engberg, Z., Schumann, U., Voigt, C., Shapiro, M., Rohs, S., and Stettler, M. E. J.: Global aviation contrail climate
1669 effects from 2019 to 2021, *Atmospheric Chemistry and Physics*, 24, 6071-6093, <https://doi.org/10.5194/acp-24-6071-2024>,
1670 2024b.
- 1671 Testa, B., Durdina, L., Alpert, P. A., Mahrt, F., Dreimol, C. H., Edebeli, J., Spirig, C., Decker, Z. C. J., Anet, J., and Kanji, Z.
1672 A.: Soot aerosols from commercial aviation engines are poor ice-nucleating particles at cirrus cloud temperatures, *Atmospheric*
1673 *Chemistry and Physics*, 24, 4537-4567, <https://doi.org/10.5194/acp-24-4537-2024>, 2024.



- 1674 Timothy C. Lieuwen (Nae), S. B., Sean Bradshaw, Leticia Cuellar-Hengartner, Eric H. Ducharme (Nae), Andrew Gettelman,
1675 Robert J. Hansman, Jr. (Nae), Richard H. Moore, Joyce E. Penner, Michael J. Prather, : Developing a Research Agenda on
1676 Contrails and Their Climate Impacts, National Academies Press, <https://doi.org/10.17226/29073>, 2025.
- 1677 Travis, D. J., Carleton, A. M., and Changnon, S. A.: An Empirical Model to Predict Widespread Occurrences of Contrails,
1678 Journal of Applied Meteorology, 36, 1211-1220, [https://doi.org/10.1175/1520-0450\(1997\)036<1211:Aemptw>2.0.Co;2](https://doi.org/10.1175/1520-0450(1997)036<1211:Aemptw>2.0.Co;2),
1679 1997.
- 1680 U.Schumann, O.: On conditions for contrail formation from aircraft exhausts, Meteorol Zeitschrift, 4-23, 1996.
- 1681 Ulrich Schuman, O.: Contrails - a prototype of cirrus cloud studies since 80 years, Meteorol Zeitschrift, 304-305, 1997.
- 1682 Unterstrasser, S.: The Contrail Mitigation Potential of Aircraft Formation Flight Derived from High-Resolution Simulations,
1683 Aerospace, 7, <https://doi.org/10.3390/aerospace7120170>, 2020.
- 1684 Unterstrasser, S. and Gierens, K.: Numerical simulations of contrail-to-cirrus transition – Part 1: An extensive parametric
1685 study, Atmospheric Chemistry and Physics, 10, 2017-2036, <https://doi.org/10.5194/acp-10-2017-2010>, 2010a.
- 1686 Unterstrasser, S. and Gierens, K.: Numerical simulations of contrail-to-cirrus transition – Part 2: Impact of initial ice crystal
1687 number, radiation, stratification, secondary nucleation and layer depth, Atmospheric Chemistry and Physics, 10, 2037-2051,
1688 <https://doi.org/10.5194/acp-10-2037-2010>, 2010b.
- 1689 Unterstrasser, S. and Sölch, I.: Study of contrail microphysics in the vortex phase with a Lagrangian particle tracking model,
1690 Atmospheric Chemistry and Physics, 10, 10003-10015, <https://doi.org/10.5194/acp-10-10003-2010>, 2010.
- 1691 Unterstrasser, S. and Stephan, A.: Far field wake vortex evolution of two aircraft formation flight and implications on young
1692 contrails, The Aeronautical Journal, 124, 667-702, <https://doi.org/10.1017/aer.2020.3>, 2020.
- 1693 Verma, P. and Burkhardt, U.: Contrail formation within cirrus: ICON-LEM simulations of the impact of cirrus cloud properties
1694 on contrail formation, Atmospheric Chemistry and Physics, 22, 8819-8842, <https://doi.org/10.5194/acp-22-8819-2022>, 2022.
- 1695 Voigt, C., Markl, R., Sauer, D., Dischl, R., Renard, C., Seeliger, K., Yu, F., Kaufmann, S., Brauer, T., Jurkat-Witschas, T., Le
1696 Chenadec, G., Moreau, J., Requena-Esteban, E., Bonne, N., Vals, M., Roche, A., Zelina, J., Dornbrack, A., Eirenschmalz, L.,
1697 Heckl, C., Horst, E., Lichtenstern, M., Marsing, A., Neumann, G., Roiger, A., Scheibe, M., Stock, P., Giez, A., Eckel, G., and
1698 Le Clercq, P.: Substantial aircraft contrail formation at low soot emission levels, Nature, 652, 112-118,
1699 <https://doi.org/10.1038/s41586-026-10286-0>, 2026.
- 1700 von Bonhorst, G., Maizet, M., and Gierens, K.: On contrail prediction under realistic weather forecast uncertainty using the
1701 example of WAWFOR data, Meteorologische Zeitschrift, <https://doi.org/10.1127/metz/1251>, 2025.
- 1702 Wex, H., Augustin-Bauditz, S., Boose, Y., Budke, C., Curtius, J., Diehl, K., Dreyer, A., Frank, F., Hartmann, S., Hiranuma,
1703 N., Jantsch, E., Kanji, Z. A., Kiselev, A., Koop, T., Möhler, O., Niedermeier, D., Nillius, B., Rösch, M., Rose, D., Schmidt,
1704 C., Steinke, I., and Stratmann, F.: Intercomparing different devices for the investigation of ice nucleating particles using
1705 Snomax® as test substance, Atmospheric Chemistry and Physics, 15, 1463-1485, <https://doi.org/10.5194/acp-15-1463-2015>,
1706 2015.



- 1707 Whitby, K. T.: The Physical Characterist of Sulfur Aerosols, *Atmospheric Environment*, 12, 135, 1977.
- 1708 Winker, D. M., Hostetler, C. A., and Hunt, W. H.: Cloud-Aerosol LIDar with Orthogonal Polarization (CALIOPe), IGARSS
1709 2003. 2003 IEEE International Geoscience and Remote Sensing Symposium. Proceedings (IEEE Cat. No.03CH37477),
1710 Toulouse, France, 1514-1516, <https://doi.org/10.1109/IGARSS.2003.1294160>,
- 1711 Wolf, K., Bellouin, N., and Boucher, O.: Sensitivity of cirrus and contrail radiative effect on cloud microphysical and
1712 environmental parameters, *Atmospheric Chemistry and Physics*, 23, 14003-14037, [https://doi.org/10.5194/acp-23-14003-](https://doi.org/10.5194/acp-23-14003-2023)
1713 [2023](https://doi.org/10.5194/acp-23-14003-2023), 2023.
- 1714 Yoo, H. and Li, Z.: Evaluation of cloud properties in the NOAA/NCEP global forecast system using multiple satellite products,
1715 *Climate Dynamics*, 39, 2769-2787, <https://doi.org/10.1007/s00382-012-1430-0>, 2012.
- 1716 Yu, F. and Turco, R. P.: The role of ions in the formation and evolution of particles in aircraft plumes, *Geophysical Research*
1717 *Letters*, 24, 1927-1930, <https://doi.org/10.1029/97gl01822>, 1997.
- 1718 Yu, F. and Turco, R. P.: Contrail formation and impacts on aerosol properties in aircraft plumes: Effects of fuel sulfur content,
1719 *Geophysical Research Letters*, 25, 313-316, <https://doi.org/10.1029/97gl03695>, 1998.
- 1720 Yu, F., Karcher, B., and Anderson, B. E.: Revisiting Contrail Ice Formation: Impact of Primary Soot Particle Sizes and
1721 Contribution of Volatile Particles, *Environ Sci Technol*, 58, 17650-17660, <https://doi.org/10.1021/acs.est.4c04340>, 2024a.
- 1722 Yu, F., Turco, R. P., and Kärcher, B.: The possible role of organics in the formation and evolution of ultrafine aircraft particles,
1723 *Journal of Geophysical Research: Atmospheres*, 104, 4079-4087, <https://doi.org/10.1029/1998jd200062>, 1999.
- 1724 Yu, J., Zhou, X., Li, L., Gao, L., Li, X., Pan, W., Ni, X., Wang, Q., and Chen, F.: High-resolution thermal infrared contrails
1725 images identification and classification method based on SDGSAT-1, *International Journal of Applied Earth Observation and*
1726 *Geoinformation*, 131, <https://doi.org/10.1016/j.jag.2024.103980>, 2024b.
- 1727 Zebediah Engberg, R. T., Tristan Abbott, Thomas Dean, Marc E. J. Stettler, and Marc L. Shapiro: Forecasting contrail climate
1728 forcing for flight planning and air traffic management applications: the CocipGrid model in pycontrails 0.51.0, *Geoscientific*
1729 *Model Development*, 18, 253-286, 10.5194/gmd-18-253-2025, 2025.
- 1730 Zhang, G., Zhang, J., and Shang, J.: Contrail Recognition with Convolutional Neural Network and Contrail Parameterizations
1731 Evaluation, *Sola*, 14, 132-137, <https://doi.org/10.2151/sola.2018-023>, 2018.
- 1732 Zhang, W. F., Paul R. Van Weverberg, Kwinten Forster, Piers M. Morcrette, Cyril J. Rap, Alexandru: Modelling contrail cirrus
1733 using a double-moment cloud microphysics scheme in the UK Met Office Unified Model, *Atmospheric Chemistry and Physics*,
1734 25, 14153-14166, 10.5194/acp-25-14153-2025, 2025.
- 1735